GENERAL ATOMIC

GA-A13903
UC-77

SAFETY ANALYSIS REPORT FOR FORT ST. VRAIN TEST ELEMENTS FTE-1 THROUGH FTE-8

(Proposed Supplement to the Final Safety Analysis Report for Fort St. Vrain Nuclear Generating Station)

by
G. B. BRADSHAW, N. I. MARSH, and C. F. WALLROTH

Work supported in part by
Contract E(04-3)-167
Project Agreement No. 17
for the San Francisco Operations Office
U. S. Energy Research and Development Administration
and ORNL Subcontract No. 4354

GENERAL ATOMIC PROJECTS 3224 & 4041 DATE PUBLISHED: AUGUST 31, 1976

DISCLAIMER

ABSTRACT

This report describes the eight fuel test elements proposed for inclusion into Segment 7 (first reload) of the Fort St. Vrain Nuclear reactor. It also presents the results of the analysis of the effects of the test elements on plant normal operation and plant safety.

Since the eight test elements represent a very small percentage of the core (0.4%), the analysis confirms that the test elements have a very small effect on the operation of the core under all conditions.

The test elements will be manufactured from near-isotropic H-451 graphite in place of the needle-coke H-327 used in the reference reload elements. This results in structurally stronger and superior heat transfer and dimensional change characteristics over the standard reload elements.

One major difference between the test elements and the reference fuel is the use of "cured-in-place" fuel rods as opposed to the reference fuel rods which are cured prior to insertion into the fuel element. The new process has obvious manufacturing advantages, but also has performance advantages, e.g., improved thermal conductivity. Another difference is that several coated fuel variations which are potential alternatives for future FSV reloads or for application in large HTGRs have been included in the test. These include weak acid resin derived (WAR) TRISO fissile particles and TRISO and BISO oxide fertile particles.

The fuel test element program is an important step towards the full-scale demonstration of safe and economic fuel and fuel element manufacturing technologies for the HTGR and will greatly increase the experimental data on the performance of HTGR fuel and graphite candidate materials under realistic power reactor operating conditions.

GLOSSARY OF TERMS

AIPA	accident initiation and progression analysis
AVS	agglomeration voie seche (dry route agglomeration process)
BISO	two-coating fuel particle
BOC	beginning of cycle
CEA	Commissariat a l'Energie Atomique
CIB	cured-in-bed (green fuel rods cured in an alumina bed)
CIP	cured-in-place (green fuel rods cured in the fuel element)
DBDA	design basis depressurization accident (DBDA)
EOC	end of cycle
EPRI	Electric Power Research Institute
FEVER	a multigroup one-dimensional depletion program for analyzing a fuel region and subregion in the axial direction
FIMA	fissions per initial heavy atom
FSAR	final safety analysis report
FTE	fuel test element
FSV	Fort St. Vrain
GA	General Atomic Company
GASSAR	General Atomic Standard Safety Analysis Report
GAUGE	a two-dimensional few-group diffusion-depletion program for analyzing a fuel region layer
GSP	gel support precipitate (a sol-gel process)
KFA/HOBEG	Kernforchungsanlage Julich GMBH/Hoch Temperatur Brennelement GMBH, Hanau
LOFC	loss of forced cooling
MLC	mid-length-center
PSC	Public Service Company of Colorado
RTE	recycle test element
RWA	rod withdrawal accident
SG	sol-gel process

TRISO	four-coating fuel particle
UKAEA	United Kingdom Atomic Energy Authority
WAR	weak acid resin (a bead-loading process)
VSM	Vanek-Simnad-Meyer (a high-temperature melt process)
Driver fuel	UC_xO_y WAR TRISO & ThO_2 SG TRISO

CONTENTS

FIGURES

FIGURES (Continued)

TABLES

TABLES (Continued)

1. INTRODUCTION

This document presents the results of safety and performance analyses that have been carried out to support the planned insertion of eight fuel test elements (FTEs) of advanced fuel into the Fort St. Vrain (FSV) reactor during its first refueling. The report describes the proposed FTEs, their operational behavior, their effect on postulated accidents described in the FSAR, and irradiation test results on the fuel element materials. The technical evaluations presented are intended to form the basis for Public Service Company of Colorado (PSC) and Nuclear Regulatory Commission approval for loading the FTEs into the FSV reactor, and are intended to comply with 10CFR50, paragraph 50.59.

The test elements will be primarily fabricated and assembled by the General Atomic Company (GA) under specifications and quality inspection requirements comparable to those used for manufacture of the initial core and reload segment fuel. All of the test element fuel materials have undergone full irradiation exposure in test capsules under ERDA, ORNL, GA, and foreign fuel qualification programs.

Incentives for early demonstration of the safety and reliability of the test elements include:

1. Obtaining early irradiation experience on future reload materials under actual commercial reactor operating conditions, which cover a range of neutron fluence, burnup, and temperature.

2. Demonstration of the acceptability of FSV fuel manufactured by pilot production plant equipment and processes under development for the commercial plants.

3. Surveillance testing and integral system demonstration of the acceptability of fuel materials and processes planned for use in the large commercial HTGR.

4. Demonstration of the acceptability of materials and processes providing improved separability characteristics for efficient reprocessing and recycle of reclaimed material.

5. Evaluation of candidate reload fuel supplied by different fabricators.

Many of the goals and objectives of the test element program described herein are consistent with the existing FSV core surveillance program described in Ref. 1.

This report considers only those test elements planned for insertion during the Segment 7 (first) refueling. Future test elements, such as those described in the ERDA-sponsored fuel development program plan for the steam-cycle HTGR (Ref. 2), will be covered by separate report.

This report is divided into four major sections: (1) a technical description of the fuel elements and fuel, (2) performance analysis under normal steady-state conditions, (3) safety analysis of the effect of the test elements on selected accidents considered in the FSAR, and (4) status of research and development programs and experience on the proposed test element materials.

2. SUMMARY

The proposed FSV test elements FTE-1 through FTE-8 are described in Table 2-1. These elements are all standard fuel blocks without control rod channels. They are designed to operate within the limits of peak fuel temperature, neutron fluence, and burnup specified for the initial core and reload fuel elements. Instrumentation is included in the test elements to measure each of these parameters. Locations of the elements within the core have been selected to yield test results over a range of exposure conditions without violating any technical specification limit. One test element will be located in each of Segments 2 through 6, and three will be placed in Segment 7. The basic fuel materials (graphite, highly enriched uranium, and thorium) and the fuel block reactivity worth of the test elements are unchanged from the initial core fuel elements which are replaced. Thus the neutronic characteristics of the core are essentially identical to those presented in the FSAR. Furthermore, the fuel loadings for all of the test elements with a residence time greater than one year are less than elements which they replace in order to introduce an additional safety margin. The maximum power perturbation to the elements surrounding the test elements is limited to ±2% of their original power.

The physical properties of the test element materials are improved over the initial FSV core materials. For instance, the strength and dimensional stability of H-451 near-isotropic graphite specified for the test elements under HTGR operating conditions is approximately 50% greater than the reference fuel H-327 needle-coke (anisotropic) graphite; and the thermal stability of the UC_xO_y fissile kernel and ThO_2 fertile kernel used in some of the test elements is improved, over the range of critical HTGR operating conditions, relative to the reference $(Th,U)C_2$ and ThC_2 particles. Three of the eight test elements contain small amounts of BISO coated (buffer + PyC)

TABLE 2-1
DESCRIPTION OF FORT ST. VRAIN FUEL TEST ELEMENTS FTE-1 THROUGH FTE-8

	FTE-1	FTE-2	FTE-3	FTE-4	FTE-5	FTE-6	FTE-7	FTE-8
Graphite type	H-451	H-451	H-451	H-451	H-451	H-451	H-451	H-451
Fissile fuel type[a]	UC_xO_y TRISO	UC_xO_y TRISO plus test fuel[b]	UC_xO_y TRISO	UC_xO_y TRISO plus test fuel[b]	UC_xO_y TRISO	UC_xO_y TRISO plus test fuel[b]	$(Th,U)C_2$ TRISO	$(Th,U)_2$ TRISO
Fertile fuel type	ThO_2 TRISO	ThO_2 TRISO plus BISO	ThO_2 TRISO	ThO_2 TRISO plus BISO	ThO_2 TRISO	ThO_2 TRISO plus BISO	ThC_2 TRISO	ThC_2 TRISO
Method of fuel rod curing[c]	CIP	CIP	CIP	CIP	CIP	CIP	CIB	CIB
Residence time, year	0.5	1.5	2.5	3.5	4.5	5.5	5.5	5.5
Peak fluence x 10^{25} n/m^2	0.52	1.80	3.10	3.96	3.43	6.65	7.10	7.12
Peak fuel temperature, °C	1021	1029	1034	1083	1141	1256	1078	1093
Burnup, FIMA[d]								
Fissile, %	13.0	32.0	46	49	54	70	73	73
Fertile, %	0.30	0.92	2.4	3.3	3.6	5.5	6.2	6.2

[a] x and y represent the mean quantities of carbon and oxygen and do not signify a specific compound. These values will be explicit in the final fuel specification. All kernels of this type are derived from weak acid resin beads.

[b] Test fuel includes:
- (3.6 Th,U)C_2 TRISO/ThO_2 TRISO, 88 rods per element CIB
- UC_2 TRISO/ThO_2 BISO, 88 rods per element CIP
- UC_xO_y TRISO/ThO_2 BISO, 262 rods per element CIP
- UC_2 TRISO/ThO_2 TRISO, 88 rods per element CIP

[c] CIP = cure-in-place fuel rod carbonization, CIB = cure in alumina bed - reference FSV process.

[d] FIMA = fissions per initial heavy metal atom.

fertile fuel which exhibits a greater diffusive release of some metallic fission products at high temperature compared with the reference TRISO coated (buffer + PyC + SiC + PyC) particles. However, the contribution of the fuel test elements to the allowable 30-year plateout inventory of two of the more important isotopes, cesium-137 and strontium-90, is less than 10^{-3} and 10^{-6}, respectively. Table 2-2 summarizes the amounts of the different fuel types in the core. The quantity of BISO fertile fuel introduced into the core by these test elements represents only 0.02% of the total thorium present. Only 0.01% of the total core fissions will occur in the BISO particles over their lifetimes.

Detailed performance analysis of the test elements was conducted to establish the power distribution, temperature history, fission product retention capabilities, graphite element stresses and dimensional stability of each test element for verification of design margins. These results are described in Section 5. The steady-state performance results were incorporated into the accident analysis to establish that:

1. There is no increase in the probability of occurrence or the consequences of an accident or malfunction previously evaluated in the FSAR.

2. The possibility of an accident or malfunction of a different type than any previously evaluated in the FSAR has been considered.

3. The margin of safety as defined on the basis of the technical specifications has not been reduced.

Irradiation experience for BISO and TRISO HTGR fuel particles is presented in Appendix A of the FSV FSAR and is summarized in Section 7 of this report. Experience obtained on over 800 Peach Bottom Core 2 fuel and test element assemblies, over 200 BISO coated particle samples in irradiation test capsules, and over 100 fuel rods in test bodies, give a high

TABLE 2-2
QUANTITY OF DIFFERENT FUEL TYPES IN THE FSV FTE-1 THROUGH FTE-6

Fuel Rod Type	Number of Fuel Rods	Uranium Loading U Total Heavy Metal (kg)	Thorium Loading Th-232 Heavy Metal (kg)
$(Th,U)C_2$ TRISO ThO_2 TRISO	264	0.058	0.929
UC_xO_y TRISO ThO_2 TRISO	17,098	3.306	61.470
UC_2 TRISO ThO_2 TRISO	264	0.058	0.929
UC_xO_y TRISO ThO_2 BISO	786	0.172	2.775
UC_2 TRISO ThO_2 BISO	264	0.058	0.929
Total	18,676	3.652	67.032

degree of confidence in the performance predictions for these materials under the most severe combination of temperature, neutron fluence, and burnup expected for the FSV reactor. Experience at Oak Ridge National Laboratory and European Research and Development groups has also been applied to the design of test elements. Tables 2-3 and 2-4 from Ref. 3 present a summary of operating and proposed HTGR plants which employ HTGR fuel technology.

Based on the above and specific results presented in Section 5 and 6, it is concluded that the proposed insertion of eight FSV test elements during reload 1 operations will involve no increased hazard to the health and safety of either the plant personnel or the public.

TABLE 2-3
SUMMARY OF HIGH-TEMPERATURE GAS-COOLED REACTORS UTILIZING COATED-PARTICLE FUEL

	Proposed HTGR	Peach Bottom HTGR	FSV HTGR	Dragon Reactor	AVR	UHTREX	THTR
Reactor type	Power	Prototype	Power demonstration	Experimental	Prototype	Experimental	Power demonstration
Criticality date		March 1966 (electricity produced on January 27, 1967)	January 31, 1974	August 1964 (full power on April 24, 1966)	August 1966 (electricity produced since December 1967)	March 1969	Scheduled for 1978
Thermal power, MW	3000/2000	115	842	20	46	3	750
Net electric power, MW	1160/770	40	330	None	15	None	300
Coolant	Helium	Helium	Helium	Helium	Helium	Helium	Helium
Inlet temp, °F (°C)	628 (331)	650 (343)	760 (404)	662 (350)	392 (200)	1600 (871)	482 (250)
Outlet temp, °F (°C)	1359 (737)	1300 (704)	1444 (784)	1382 (750)	1562 & 1740 (850 & 950)	2400 (1316)	1382 (750)
Pressure, psi (kg/cm^2)	725 (51.0)	350 (24.6)	700 (49.2)	300 (21.1)	150 (10.5)	220 (15.5)	569 (40)
Moderator	Graphite	Graphite	Graphite	Graphite	Graphite	Graphite	Graphite
Fuel	Coated UC_2 and ThO_2 particles in bonded rods 0.625 in. diam. by 2.5 in. length.	Coated $(Th,U)C_2$ particles in hot-pressed, graphite-matrix compacts (2.75 in. o.d. by 1.75 in. i.d., by 3 in. long).	Coated $(Th,U)C_2$, ThC_2 particles in bonded rods 0.5 in. diameter by 2 in. length.	Coated (Zr,U)C, (Th,U) C_2 and UC-10 particles in warm-pressed, resin bonded, graphite matrix, annular fuel compacts (1.7 in. o.d. by 2.1 in. long).	Coated $(Th,U)C_2$ particles in graphite spheres (first charge). Reloads with $(Th,U)O_2$ fuel.	Coated UC_2 particles in graphite cylinders.	Coated $(Th,U)O_2$ particles in graphite spheres.
Fuel elements	Hexagonal graphite blocks (14 in. across flats by 31 in. long) containing bonded rods of fuel particles interspaced with coolant channels.	Low-permeability graphite tubes (3.5 in. o.d.) containing 7.5 ft columns of fuel compacts.	Hexagonal graphite blocks (14 in. across flats by 31 in. long) containing bonded rods of fuel particles interspaced with coolant channels	Seven-rod clusters of low-permeability graphite tubes containing 63.5 in. columns of fuel compacts.	Machined graphite spheres (6 cm o.d. by 4 cm i.d.) filled by injection molding with carbonaceous matrix containing dispersed coated particles. (UCC type.) Also "wallpaper" and moulded type.	Graphite cylinders (1 in. o.d. by 0.5 in. i.d. by 5.5 in. long).	Moulded spheres (6 cm o.d. with 0.5 cm fuel free matrix surrounding a 5-cm diameter fueled matrix zone).
Coated particle loadings in compacts or beds, vol %	35-60	22-28	60-65	12 (fissile) 24 (fertile)	≤22	8-27	11.2
Heat removal from fuel elements	Internal	External	Internal	External	External	Internal	External
Fission-product purge system	No	Yes	No	Yes (Charge I); driver fuel elements only (Charge II); experimental elements only (Charge III onwards)	No	No	No
Core power density, avg., MW/m^3	8.4/8.2	8.3	6.3	14	3	1.3	6
Fuel temperature							
Maximum, °F (°C)	2559 (1404)	2430 (1332)	2300 (1260)	2280 (1249)	2250 (1232)	2900 (1593)	2282 (1250)
Average, °F (°C)	1635 (891)	1800 (982)	1500 (816)		1470 (799)	2600 (1427)	
Minimum, °F (°C)	770 (371)	1050 (566)	890 (477)		480 (249)	1980 (1082)	
Fuel burnup, FIMA[(a)]							
Fissile, max.	75	14	20	Charge I: 4.5 (<1 avg) Charge II+: 35-70	14 (average)	13 in 1 year (100% plant factor)	14.1 (12.0 average)
Fertile, max.	7	7	7	Charge I: <1 Charge II: 3-6 Charge III+: No fertile	None	None	None
Fast flux exposure, n/cm^2 (E > 0.18 MeV)							
Maximum	8.0 x 10^{21}	4.7 x 10^{21}	8.0 x 10^{21}	<2.4 x 10^{21} per year	7.6 x 10^{21}	1 x 10^{21} in 2 years	5.5
Average	5.2 x 10^{21}	3.6 x 10^{21}	5.5 x 10^{21}	<1.7 x 10^{21} per year	--	--	4.1
Fuel lifetime, year	4	3	6	Various (experimental)	5.4	Not specified	3

(a) Fissions per initial metal atom, %.

TABLE 2-4
DATA ON COATED PARTICLE FUELS FOR HIGH TEMPERATURE REACTORS

	Proposed HTGR[a]	Peach Bottom HTGR		FSV HTGR[a]	Dragon Reactor		AVR		UHTREX	THTR
Fissile Particles	PyC/SiC-coated UC_2	PyC-coated $(Th,U)C_2$		PyC/SiC-coated $(Th,U)C_2$	Multilayer PyC-coated (Zr,U)C and UO_2/10C		PyC-coated $(Th,U)C_2$ (first charge); $(Th,U)O_2$ reloads		PyC-coated UC_2	PyC-coated $(Th,U)O_2$
					Charge I	Chg. II Onwards	Initial	Reload		
Kernel	Dense spherical UC_2	Dense spherical $(Th,U)C_2$		Dense spherical $(Th,U)C_2$	Porous rounded (Zr,U)C	Porous rounded UC-10	Dense spherical $(Th,U)C_2$	Dense spherical $(Th,U)O_2$	Dense spherical UC_2	Dense spherical $(Th,U)O_2$
		Core 1	Core 2							
Diameter, μ	200	100–500	300–400	175	250–420	420–570	200	400	150–200	400
Th:U ratio	(all U)	5:1	5.5:1	4.25:1	8:1 (Zr:U)	10:1 (C:U)	5:1	11.2:1	(all U)	11.2:1
U enrichment, %	93	93	93	93	93	93	93	93	93	93
Coating	TRISO[b]	Monolithic PyC BISO	BISO[c]	TRISO[b]	Interrupted laminar	PyC-SiC-PyC or TRISO	Laminar columnar PyC	Triplex BISO	Triplex BISO-granular PyC	Triplex BISO
Thickness, μ						Chg. II Chg. III+				
First layer	100	55	40/50	50	37	30 35	33	70	27	70
Second layer	25	--	60/85	20	63	35 65	74	30	35	30
Third layer	25	--	--	20	--	110 35	--	80	40	80
Fourth layer	35	--	--	30	--	-- 55	--	--	--	--
Total coating	185	55	100/135	120	100	175 190	107	180 / THTR fuel	102	180
					Charges I & II[d]					
Fertile Particles	PyC-coated ThO_2	PyC-coated $(Th,U)C_2$		PyC/SiC-coated ThC_2	PyC-SiC-PyC-coated $(Th,U)C_2$		None		None	None (may be revised for reloads)
Kernel	Dense spherical ThO_2	Dense spherical $(Th,U)C_2$		Dense spherical $(Th,U)C_2$	Porous rounded $(Th,U)C_2$					
		Core 1	Core 2							
Diameter, μ	500	100–500	350–450	450	350–500					
Th:U ratio	All Th	21:1	18.5:1	(All Th)	10					
U enrichment, %	0	93	93	--	93					
Coating	BISO[c]	Monolithic PyC BISO	BISO[c]	TRISO[b]	PyC-SiC-PyC					
Thickness, μ										
First layer	85	55	40/50	50	30					
Second layer	75	--	45/60	20	30					
Third layer	--	--	--	20	100					
Fourth layer	--	--	--	40	--					
Total coating	160	55	85/110	130	160					

[a] See 4-1 for additional information.

[b] TRISO = Buffer + PyC + SiC + PyC.

[c] BISO = Buffer + PyC.

[d] No fertile particles in driver fuel from Charge III onwards; however, varieties of fertile fuel in experimental arrangements.

3. TEST OBJECTIVES AND DESIGN CRITERIA

The major overall objective of FTE-1 through FTE-8 is to demonstrate acceptable performance and safety of proposed future FSV fuel product specifications and processes prior to full-scale application. It is further intended that the irradiation results will provide lead fuel experience on materials planned for use in the large commercial steam-cycle HTGR as described in GA's Standard Safety Analysis Report (GASSAR). This approach is analogous to that employed for many years in the LWR industry to demonstrate and verify acceptable behavior of new fuel bundle designs and mixed oxide fuel assemblies prior to full-scale use.

General objectives of the FSV fuel test element program are to test commercial HTGR fuel components in order to obtain statistically significant results on:

1. Geometrical stability of the graphite blocks.
2. Fuel particle and fuel rod integrity.
3. Residual stresses and stress margins in the graphite.
4. Uranium depletion, including local variations.
5. Corrosion and carbon transport produced by impurities.
6. Design margins on thermal and fission product performance.
7. Isotopic composition and other data affecting fuel cycle economics.

The specific objectives of FTE-1 through FTE-8 are as follows:

1. Demonstration testing of near-isotropic graphite fuel elements at up to six time intervals under high fluence, temperature, and stress conditions.

2. Demonstration of the acceptability of improved fuel materials planned for use in later FSV reloads and the large HTGR (fresh and recycle fuel).

3. Integral testing of a limited amount of large HTGR-type fuel and manufacturing processes.

4. Surveillance of Segment 7 fuel (FTE-7 and FTE-8) via additional fission gas release measurements and metrology on selected fuel rods.

To meet the above objectives, the following design criteria have been applied to test elements FTE-1 through FTE-8.

1. The test elements shall be designed to be interchangeable with a standard FSV element and shall be manufactured and documented to at least the same quality levels as the reload fuel.

2. There shall be no detrimental effect on core performance and no significant change in the inventory of released fission products.

3. The test elements shall be designed for a lifetime at least as long as the elements being replaced.

4. Uranium and thorium loadings for FTE-6, -7, and -8, fuel rods and total element, shall not exceed the corresponding loadings of Segment 7 reload elements. These elements shall experience near-maximum power, temperature, fluence, and burnup conditions available in Segment 7.

5. Core locations shall be chosen that will maximize fuel element stresses for at least three of the eight FTEs.

6. Core locations shall be selected to permit annual discharge of test elements over the following six years.

7. The amount of test fuel shall be limited to the logical and practical minimum.

8. The test fuel shall be manufactured to either large HTGR fresh or recycle fuel specifications or proposed FSV reload specifications.

9. The test elements shall contain monitors to obtain measurements of power distributions, temperature history, and burnup characteristics.

The above criteria form the basis for (1) the design and operation of the test elements and (2) the performance and safety analysis reported herein.

4. TECHNICAL DESCRIPTION OF TEST FUEL

This section discusses the test element configuration, fuel types, materials, processes, and unique characteristics of the eight test elements and provides comparisons of physical characteristics with the FSV Segment 7 reload fuel. A detailed design specification is given in Ref. 4. Table 4-1 presents the significant differences between the reference FSV fuel and the test element fuel. The changes incorporated into the test elements represent technology improvements developed over the past several years for application to the large HTGR. Some of these improvements, such as near-isotropic graphite, were not commercially available at the time of FSV initial core production.

4.1. FUEL ELEMENT ASSEMBLY AND LOCATION IN THE CORE

The FSV test elements are designed to the same envelope dimensions and structural criteria as the standard FSV fuel element shown in Fig. 4-1 and described in Section 3.4.1.1 of the FSAR. Consequently the test elements can be handled and inserted into the core without restriction or special handling provisions.

Major differences between the test elements (Table 2-1) and standard FSV elements are the selection of fuel kernel composition and process method (Section 4.2), fuel rod materials (Section 4.3), graphite (Section 4.4), assembly and rod curing processes (Section 4.5), and the identification of test arrays and control fuel columns.

Test arrays are defined as a group of six fuel rod columns surrounding a single coolant hole. Seven test arrays are located within the fuel element to improve control of irradiation conditions, and are defined as

TABLE 4-1
COMPARISON OF FSV REFERENCE, PROPOSED FSV, AND LHTGR TEST FUELS

Feature	FSV Fuel		Large HTGR Commercial Fuel
	Reference	Test Element	
Fissile particles			
Kernel type	$(4Th,U)C_2$	UC_2, UC_xO_y (WAR)	UC_2,[(a)] UC_xO_y (WAR)
Coating type	TRISO	TRISO	TRISO
Kernel diameter, μm	100-275	200, 305, & 365	200, 305 and 365
Total coating thickness, μm	110-205	185 and 135 150-210	150-210
Fertile particles			
Kernel type	ThC_2	ThO_2	ThO_2
Coating type	TRISO	TRISO & BISO	BISO
Kernel diameter, μm	300-500	450 and 500	500
Total coating thickness, μm	115-175	160 and 175	160 and 175
Fuel rod			
Diameter, in.	0.491	0.4895 and 0.491	0.619
Length, in.	1.94	1.94	2.476
Binder	Coal tar pitch	Petroleum pitch	Petroleum pitch
Filler	Natural flake graphite	Synthetic flake graphite	Synthetic flake graphite
Shim particle	None	Near-isotropic graphite	Near-isotropic graphite
Heat treatment	Cure-in Al_2O_3 powder	Cure-in fuel block and alternative	Cure-in fuel block
Graphite fuel block			
Graphite type	Needle-coke	Near-isotropic	Near-isotropic
Hole geometry (number of fuel holes/coolant holes)	210/108	210/108[(b)]	132/72
Coolant hole diameter, in.	0.625	0.625	0.826
Fuel hole diameter, in.	0.500	0.498 and 0.500	0.624

[(a)] UC_xO_y is the reference recycle fissile kernel and is a development goal for the large HTGR. It is derived from ion exchange resin beads that are loaded with uranium and then heat treated to obtain a controlled amount of conversion to carbide.

[(b)] Arrangement of each test fuel combination is six fuel holes surrounding one coolant channel.

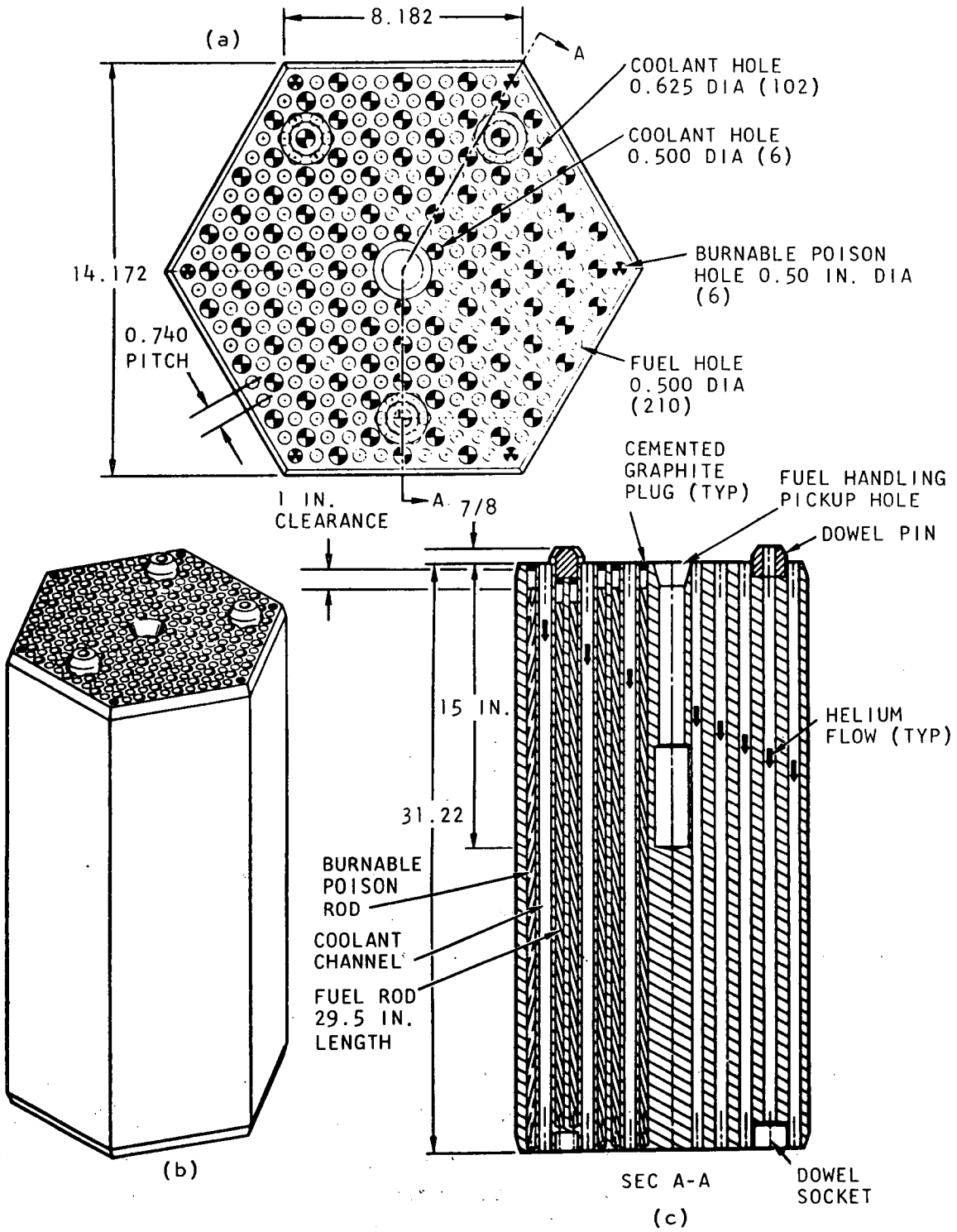

Fig. 4-1. Standard FSV fuel element configuration

shown in Fig. 4-2 for elements FTE-2, -4, and -6. These elements will be sequentially removed from the core after irradiation for approximately 1.5, 3.5, and 5.5 equivalent full-power years examination including gamma scans for isotopic distribution (Ref. 4).

FTE-1, -3, and -5 contain the same driver fuel as FTE-2, -4, and -6, but do not contain test fuel arrays or any BISO fertile particles. FTE-5 has the further distinction of being located at the core-reflector interface and thus contains a buffer area of heavy thorium loading as shown in Fig. 4-3. FTE-7 and -8 contain fuel particles and rods identical to Segment 7 reload fuel and differ from a reference FSV reload block only by the use of H-451 graphite and inclusion of instrumentation monitors. Inspection of FTE-1, -3, -5, -7, and -8 will be limited to visual examination of graphite fuel block integrity and dimensional checks. Detailed post-irradiation examination will be determined on an individual basis.

Core positions shown in Fig. 4-4 have been selected for the test elements based on the objectives outlined in Section 3. Locations for FTE-1, -2, and -4 were chosen to avoid rodded regions and regions near the reflector to minimize fuel block stresses, while locations for FTE-3, -5, and -6 were intentionally located in regions where fuel block stresses are expected to be high. FTE-7 and -8 were located to maximize both fast fluence and time-average temperature. All of the elements are located in the sixth layer from the top of the core (third fueled layer from the top). Table 4-2 gives the uranium and thorium loadings in each of the test elements, and compares these values to average loadings in the initial core and Segment 7.

Machining specifications for the test elements have been designed to control the gaps between the fuel rods and fuel block to simulate anticipated production conditions of tool wear, and to control coolant channel roughness (Ref. 5). These specifications take into account green rod shrinkage and the effects of the cure-in-place process to be employed for carbonizing the fuel rod matrix in FTE-1 through FTE-6.

NOTE:

CEA – COMMISSARIAT A L'ENERGIE ATOMIQUE

KFA/HOBEG – KERNFORCHUNGSANLAGE JULICH GMBH/HOCH TEMPERATUR BRENNELEMENT GMBH, HANAU

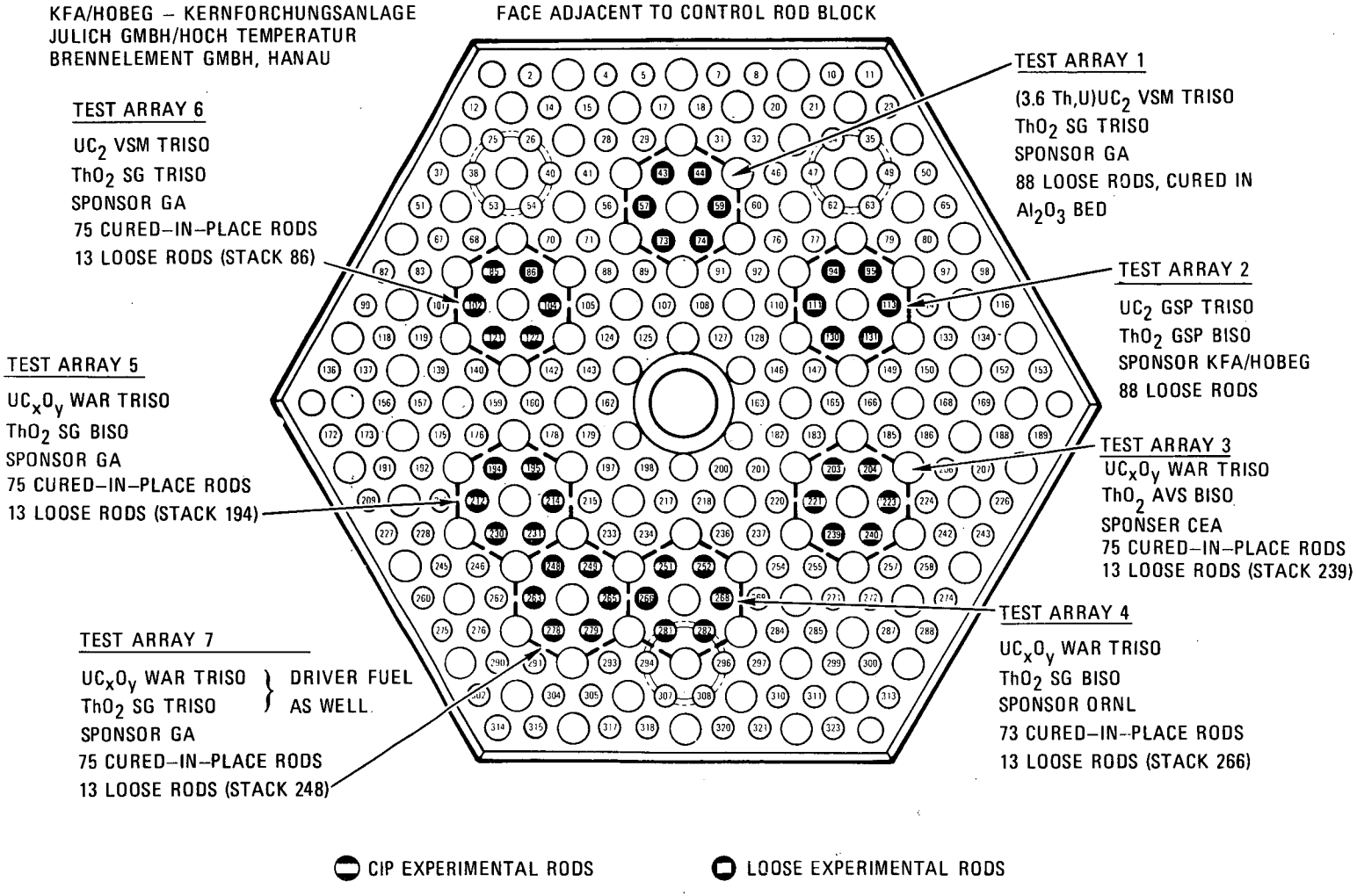

Fig. 4-2. Description of test arrays in FTE-2, FTE-4, and FTE-6

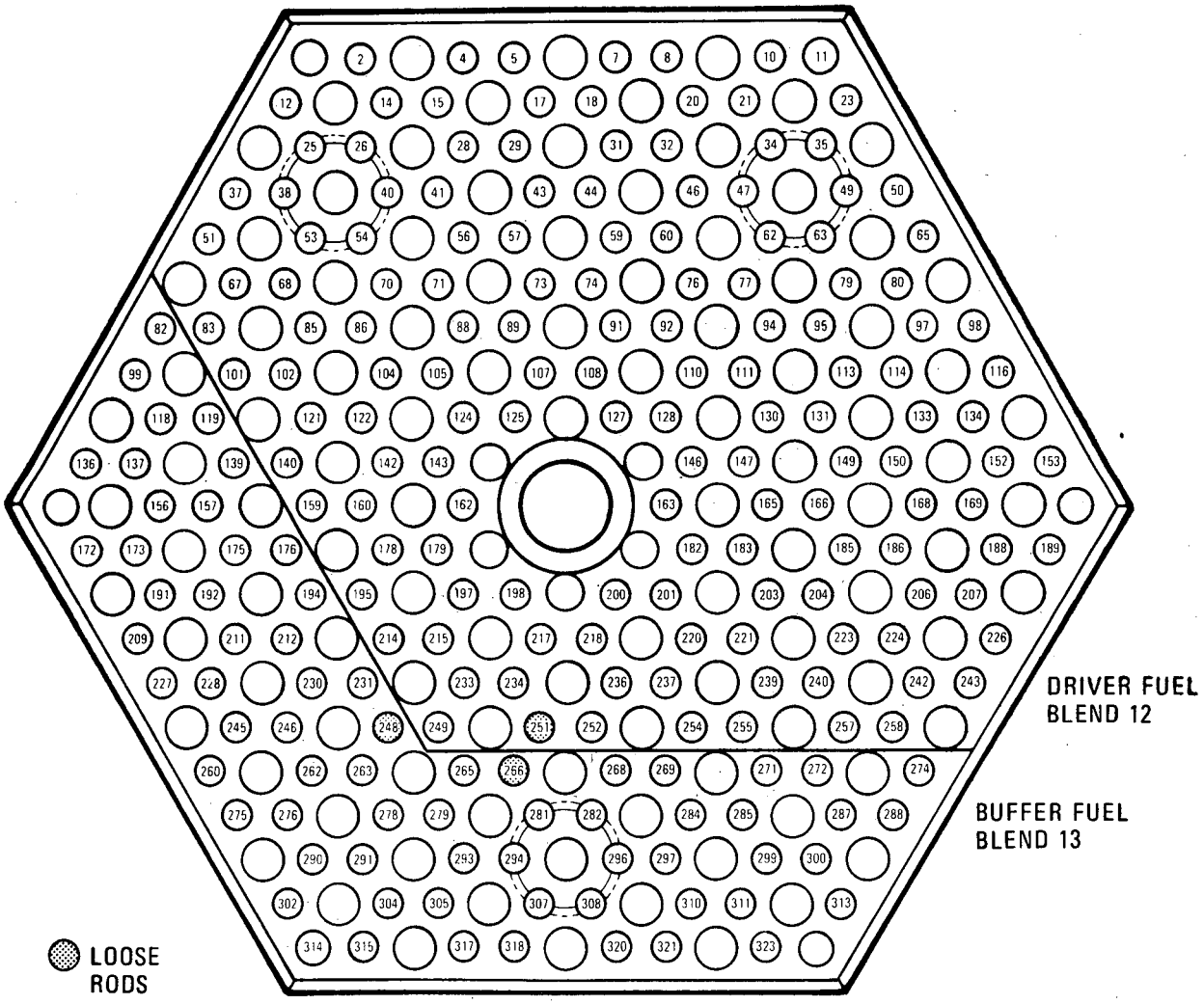

Fig. 4-3. FTE-5 element showing buffer fuel area

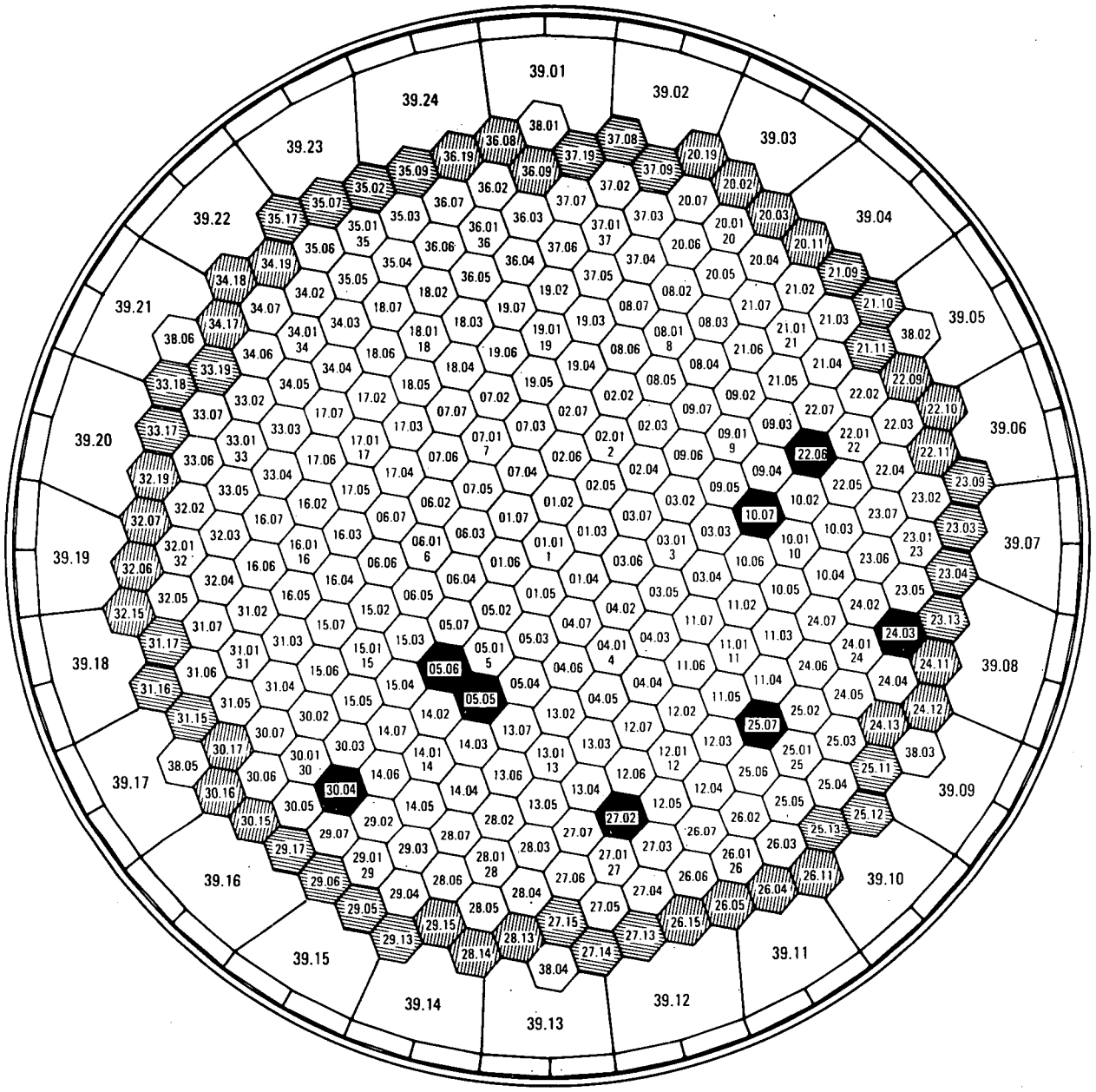

FTE-1	25.7.F.6	FTE-5	24.3.F.6
FTE-2	22.6.F.6	FTE-6	10.7.F.6
FTE-3	30.4.F.6	FTE-7	5.5.F.6
FTE-4	27.2.F.6	FTE-8	5.6.F.6

Fig. 4-4. Test element location (layer 6) showing location of eight test elements

TABLE 4-2
TEST ELEMENT HEAVY METAL LOADINGS

Element	Core Location	Segment	Uranium Loading U-Total Heavy Metal		Thorium Loading Th-Total Heavy Metal	
			g/rod	kg Total	g/rod	kg Total
FTE-1	25.7.F.6	2	0.176	0.548	3.52	10.968
FTE-2	22.6.F.6	3	0.176	0.547	3.52	10.947
FTE-3	30.4.F.6	4	0.176	0.548	3.52	10.968
FTE-4	27.2.F.6	5	0.176	0.547	3.52	10.947
FTE-5	24.3.F.6	6	0.176	0.371	3.52	7.413
	Buffer		0.137	0.138	4.71	4.748
Total FTE-5				0.509		12.161
FTE-6	10.7.F.6	7	0.306	0.952	3.55	11.041
FTE-7	5.5.F.6	7	0.3016	0.940	3.564	11.105
FTE-8	5.6.F.6	7	0.3016	0.940	3.564	11.105
Total FTE-1 through FTE-8				5.531		89.242
Segment 7 reload				220.0		2,400.0
Initial core				773.0		15,971.0

Extensive quality control procedures are applied during fuel fabrication to maintain well controlled conditions, and to insure dimensional accuracy and satisfaction of all manufacturing tolerances and specifications (Ref. 4). Special procedures have been developed for the test element fuel to assure that all of the test fuel and sampling plans, independent of manufacturer, meet the FSV fuel contamination limits and to assure accurate and consistent data on preirradiation characteristics. Each test element will be identified by a permanent three-digit type of number and a unique engraved serial number which will allow complete fabrication traceability.

Provisions exist to add boronated graphite burnable poison rods to the test elements; however, fuel loadings have been conservatively selected for FTE-1 through FTE-5 to obviate this requirement. Burnable poison materials for FTE-6 through FTE-8 will be the same as those used for Segment 7 reload fuel.

4.2. FUEL PARTICLES

4.2.1. Driver Fuel

The driver fissile fuel in FTE-1 through FTE-6 will be UC_xO_y TRISO fissile particles with kernels produced by the weak acid resin (WAR) process and ThO_2 TRISO fertile particles with kernels produced by a sol-gel process. A comparison of the kernel and coating properties for the test element driver fuel and FSV reload Segment 7 fuel was given in Table 4-1. The coating thicknesses and densities for the test element fuel are based on extensive irradiation experience (Section 7.3) and have been specified to limit the failure fraction of coatings to values below those expected for reference FSV Segment 7 fuel particles (Ref. 7). The coating design approach and dimensional stability of the coated particles are discussed extensively in the HTGR GASSAR licensing document (Ref. 8).

Driver fuel in FTE-7 and FTE-8 will consist of (3.6 Th,U)C_2 TRISO fissile and ThC_2 TRISO fertile particles derived from the same production batches as Segment 7 reload fuel.

4.2.2. Test Array Fuel

Several types of fuel particles will be contained in the test arrays of FTE-2, -4, and -6, as shown in Fig. 4-2 and further described in Table 4-3. The test arrays include both oxide and carbide fuel particles with BISO and TRISO coatings which differ as shown in Fig. 4-5. This fuel will consist of 176 rods with all TRISO particles and 350 rods with BISO fertile particles, and will occupy less than 20% of the fuel element. Table 4-4 provides a summary of the particle dimensional characteristics for the fertile fuel.

The BISO ThO_2 fertile fuel particles are the reference fuel for the large HTGR. In addition to a neutronic and fabrication advantage over TRISO fuel they also provide for more complete separation of the bred U-233 fuel from the spent U-235 during reprocessing operations. Test element BISO particles are designed for the maximum neutron exposure of 8×10^{25} n/m^2 ($E > 0.18$ MeV), 7.5% FIMA burnup, and peak temperatures of 1250° ± 100°C.

The experimental fuel in the test arrays will be subject to rigorous quality control inspection to verify coating properties and integrity, low contamination levels, and heavy metal loadings. Test fuel manufactured by sources other than GA will be required to meet specifications equivalent to the GA-produced fuel and will be subject to quality inspection by GA prior to fuel element assembly (Ref. 4).

4.3. FUEL RODS

The test element fuel particles and shim material will be bonded together with a matrix consisting of an organic binder and graphite filler

TABLE 4-3
TEST MATRIX FOR THE SIX FUEL HOLE TEST ARRAYS IN FTE-2, -4, AND -6

Test Array	Fissile Particle	Fertile Particle	Purpose
1	(3.6 Th,U)C_2 VSM TRISO	ThO_2 SG TRISO	Candidate FSV reload fuel
2	UC_2 GSP TRISO	ThO_2 GSP BISO	Commercial LHTGR
3	UC_xO_y WAR TRISO	ThO_2 AVS BISO	Commercial LHTGR
4	UC_xO_y WAR TRISO	ThO_2 SG BISO	Recycle HTGR
5	UC_xO_y WAR TRISO	ThO_2 SG BISO	Commercial LHTGR
6	UC_2 VSM TRISO	ThO_2 SG TRISO	Candidate FSV reload fuel
7	UC_xO_y WAR TRISO	ThO_2 SG TRISO	Candidate FSV reload fuel

Manufacturing processes:

VSM = Vanek-Simnad-Meyer, a high-temperature melt process.
GSP = Gel Support Precipitate, a sol-gel process.
WAR = Weak Acid Resin, a bead loading process.
SG = Sol-Gel process.
AVS = Agglomeration Voie Seche (dry route agglomeration process).

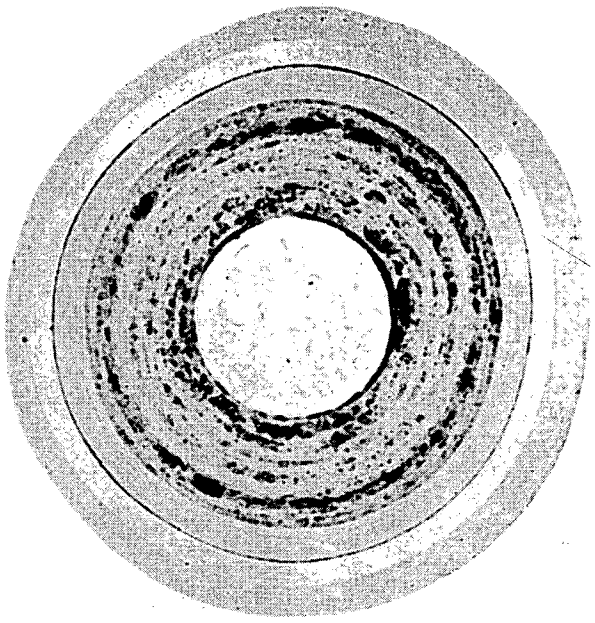

FISSILE PARTICLE

KERNEL-UC_2; 200 μM

COATING-TRISO

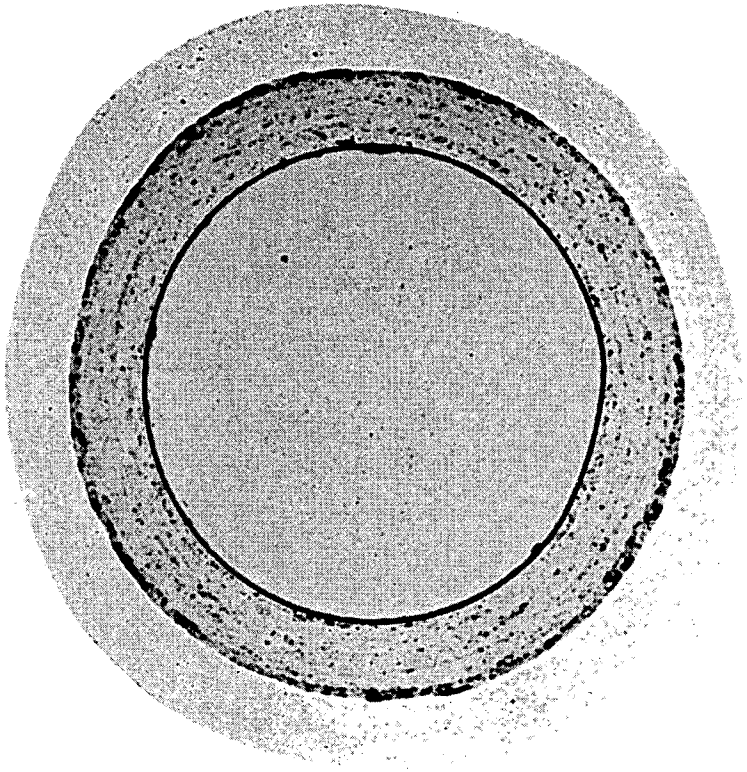

FERTILE PARTICLE

KERNEL-ThO_2; 500 μM

COATING-BISO

Fig. 4-5. Reference GA LHTGR coated fuel particles

TABLE 4-4
FERTILE FUEL PARTICLE CHARACTERISTICS COMPARISON

	ThC_2 (FSV Initial Core)		ThO_2 TRISO	ThO_2 BISO
	Type A	Type B		
Kernel diameter	355	455	450	500
Buffer thickness	55	55	60	95
Inner PyC	30	30	35	N/A
SiC	25	25	35	N/A
Outer PyC	$\geq$30	$\geq$40	45	80
Particle	635	755	800	850

which is heat treated to outgas and carbonize the binder to yield a structurally sound bonded fuel rod. Table 4-1 includes a comparison of fuel rod materials for the test elements and reference FSV fuel. The FTE fuel rod is very similar to that used in the FSV initial core with the exception of certain process and product improvements as described below.

The shim material consists of isotropic graphite granules about the same size as the coated fertile particle. The shim particles permit adjustment of fuel loading within the fixed volume of the fuel rod. The binder consists of a petroleum pitch into which is mixed a graphite flour. The binder-graphite mix makes up the matrix, which is melted and injected into molds containing the appropriate amount of fissile, fertile, and shim particles.

Bonding the fuel particles in this manner contains the particles on a well defined free standing body, and has the effect of increasing the thermal conductivity of the particle bed and decreasing the thermal gradients in the fuel particles by providing a relatively uniform heat flow path at the particle surface. The matrix formulation has been chosen to provide a rod with adequate strength to maintain integrity during irradiation without detrimental radiation-induced mechanical interaction between the fuel rod matrix and fuel particles (Ref. 9).

Heat treatment of most of the fuel rods in FTE-1 through FTE-6 will be performed in-situ by the cure-in-place (CIP) process developed at GA and described further in Section 4.5. The fuel rods in FTE-7 and -8 and those in selected locations of other test elements (Figs. 4-2 and 4-3) will be cured in alumina beds. The alumina bed curing process is identical to that used for the FSV initial core. The CIP process has been developed for LHTGR fuel as a process improvement. The product characteristics of fuel rods produced by the two carbonization techniques are identical.

Other loose rods in Figs. 4-2 and 4-3 will be of the cured-in-place type, but manufactured and taken out from graphite fixtures in order to allow dimensional measurements after firing and before and after irradiation.

The initial fuel element and fuel rod stack height dimensions provide sufficient axial void space to accommodate the relative axial dimensional changes of the graphite block and fuel rod stack expected during operation. Combustible spacers are used between pairs of fuel rods during the CIP process. One effect of these spacers is to lower the linear heat rate locally over that of loose stacked rods. This is accounted for in the thermal analysis. The thermal analysis also considers the effect of shim particles and BISO fuel particles on the dimensional stability of the fuel rods. The heat transfer characteristics of the FTE fuel rods compared with those of standard FSV fuel rods are discussed in Section 5.2.

4.4. FUEL ELEMENT GRAPHITE

The test element graphite blocks were manufactured by the Great Lakes Carbon Company from near-isotropic graphite, grade H-451, development lot 426. Grade H-451 is an extruded near-isotropic petroleum coke graphite produced in 17-in.-diameter by 34-in.-long logs (Ref. 10). Use of near-isotropic petroleum coke filler material produces a stronger, more isotropic graphite that is more dimensionally stable than the needle-coke type graphite grade H-327 currently used in the FSV reactor core. The essential advantage of H-451 graphite over H-327 is attributable to differences between the properties of the near-isotropic petroleum coke filler used in the manufacture of H-451 and those of the needle-coke filler used in H-327.

Unirradiated properties of H-451 (lot 426) and H-327 graphites are given in Table 4-5. Typical values are also presented for H-451 and H-327 graphite properties after irradiation at 900°C to 6 x 10^{25} n/m^2 (E > 0.18 MeV)$_{HTGR}$ (Ref. 11). Material properties listed in Table 4-5 illustrate

TABLE 4-5
COMPARISON OF H-451 and H-327 GRAPHITES

Property	Unirradiated Value		Values after Irradiation at 1173°K (900°C) to 6 x 10^{25} n/m^2	
	H-451	H-327	H-451	H-327
Density	1.72	1.77	--	--
Ultimate tensile strength, kPa (psi) (mean)				
Axial, MLC[a]	13,652 (1970)	11,239 (1630)	20,581 (2985)	16,927 (2455)
Radial, MLC	10,756 (1560)	6,480 (940)	16,200 (2350)	9,090 (1315)
Elastic modulus, 10^6 kPa (psi)				
Axial, MLC	7.95 (1.15)	10.34 (1.5)	17.93 (2.6)	23.44 (3.4)
Radial, MLC	6.9 (1.00)	4.14 (0.6)	15.65 (2.27)	9.65 (1.4)
Coefficient of thermal expansion, 10^{-6} K^{-1} (300-773 K)				
Axial, MLC	4.03	1.20	3.89	1.05
Radial, MLC	4.52	3.05	4.37	2.66
Thermal conductivity (radial), W/mK (cal/cm-sec-°C)				
@ 400°C	88.28 (0.211)	84.1 (0.201)	25.1 (0.06)	18.83 (0.045)
@ 800°C	62.8 (0.150)	62.8 (0.150)	31.4 (0.075)	20.9 (0.05)

[a] MLC = mid-length-center of a 432-mm (17-in.) diameter by 864-mm (34-in.) long log.

the basic differences between H-451 and H-327 graphite. Grade H-451 is more isotropic than H-327, especially in properties such as strength, elastic modulus, and thermal expansivity. In addition, the absolute strength of H-451 is higher than that of H-327 in both the axial and radial direction.

The irradiation-induced changes in thermal properties are less pronounced in H-451 than in H-327. Consequently, the thermal conductivity of irradiated H-451 is approximately 50% higher than that of H-327, which provides additional conservatism in the thermal analysis of the test elements, which assume H-327 values. Ultimate tensile strength and elastic modulus increase in both graphites (Ref. 12). Irradiation-induced dimensional changes for H-451 graphite are more isotropic and show no net expansion over the temperature and fluence ranges of FSV in comparison with H-327, as shown in Fig. 4-6. As a result, fuel elements made from H-451 graphite will be more dimensionally stable under normal reactor conditions.

Chemical impurities and oxidation reaction rates are approximately the same for H-451 and H-327 (Ref. 13).

4.5. CURE-IN-PLACE PROCESS

The cure-in-place process is a method of curing the green fuel rods to outgas and carbonize the binder while the rods are assembled within the fuel element. This is performed in a specially designed BTU walking beam furnace which provides good temperature and atmosphere control during heat treating. Figure 4-7 shows the steps involved in the process and Table 4-6 presents typical fuel properties that are obtained.

Axial gaps between fuel rods are controlled by the insertion of plastic spacers which volatilize during heat treatment. These spacers are used primarily to ease the manufacturing process. Figure 4-8 shows a typical fuel rod stacking arrangement for the CIP process.

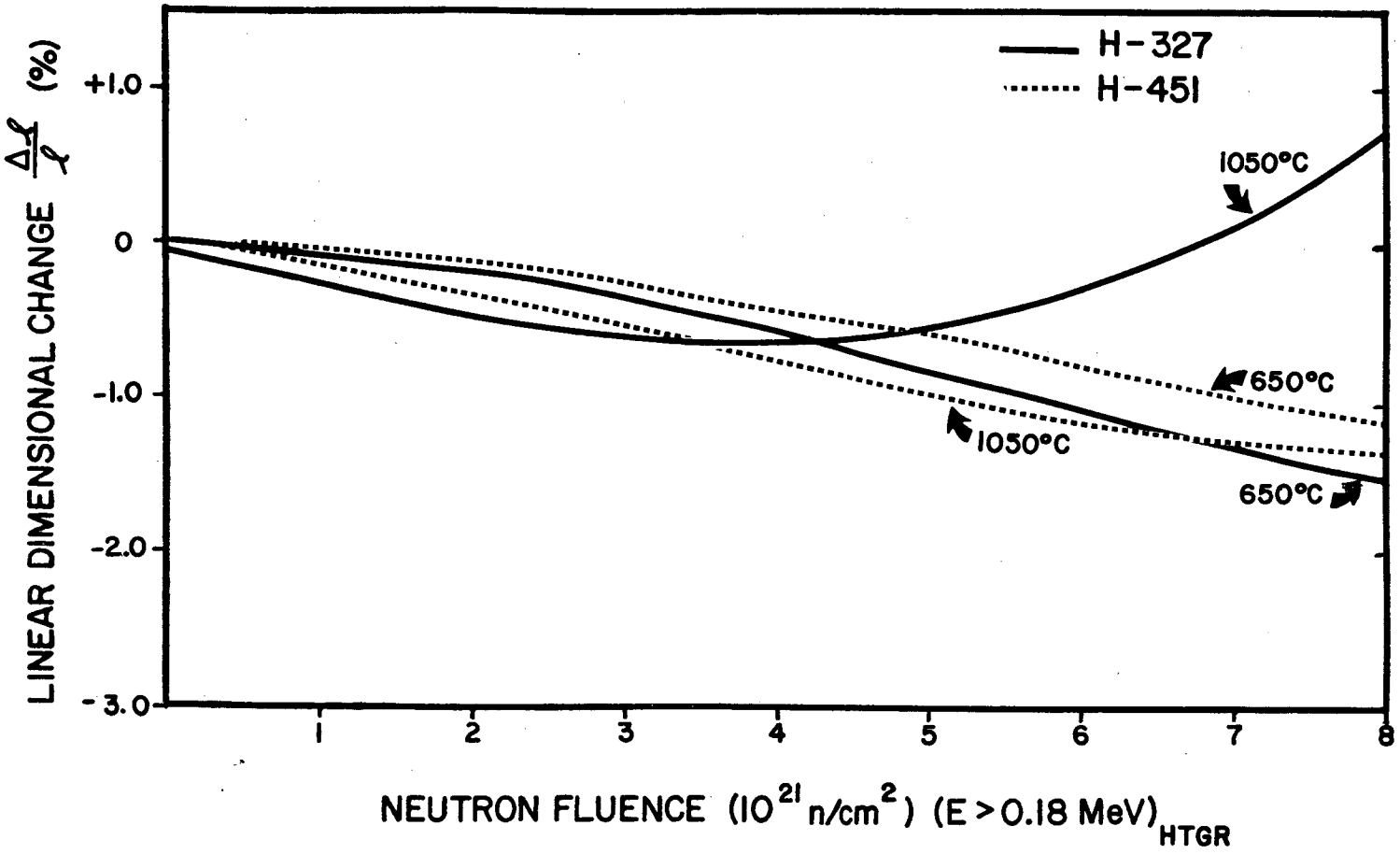

Fig. 4-6. Comparison of H-327 and H-451 graphite dimensional stability in the radial direction

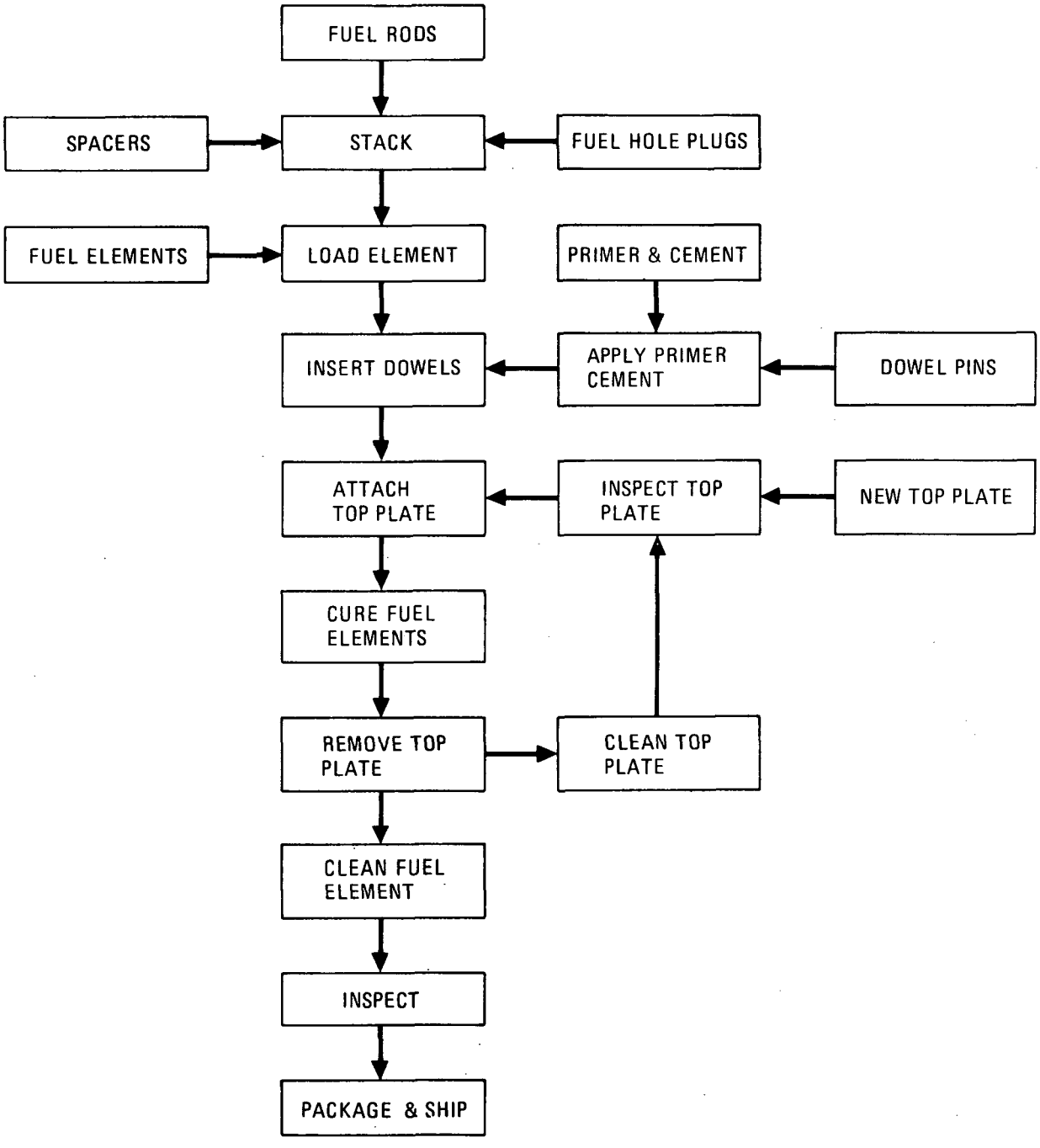

Fig. 4-7. Flowsheet for the cure-in-place fuel rod carbonization process

TABLE 4-6
TYPICAL FUEL CHARACTERISTICS OBTAINED DURING CURE-IN-PLACE PROCESSING

Property	Typical Mean Values
Pitch coke yield	27%
Macroporosity	33%
Fuel rod push out shear stress after curing	73.5 kPa
Fraction exposed heavy metal	5×10^{-5}
Friction factor at $7 \times 10^4 < Re\ 1.5 \times 10^5$	<0.0222
Radial gaps	0.089 mm (0.0035 in.)

Curing conditions require temperatures ranging from 1750° to 1850°C and duration of 75 to 90 minutes. A purge gas system is employed to remove volatile hydrocarbons, and cleaning steps remove any residual material from the block and coolant holes. Impurity analysis of fired fuel rod matrix shows that levels are approximately the same as for the FSV initial core. During the firing process the fuel rods shrink away from the graphite leaving a small gap. The fuel rods may be removed from the fuel element by applying sufficient force to overcome the friction between the fuel rod and the graphite.

All of the test elements except FTE-7 and -8 will undergo CIP processing of the fuel rods. Fuel rods in these two elements, and selected fuel stacks in the remaining test elements, will be cured in packed alumina beds, which was the reference process used for the FSV core. The cured rods are then loaded into the fuel blocks, without spacers, and sealed with a special end cap at the top of the fuel stack.

4.6. FLUENCE BURN-UP AND TEMPERATURE MONITORS

Each of the eight test elements will contain monitors for measuring the operating fluence, burn-up, and temperatures of the experimental fuel and overall fuel element. The monitor design selected includes SiC temperature monitors, neutron dosimetry wires, and fuel particles for burnup analysis, which are encased in an H-451 graphite crucible and are similar to devices used for FSV surveillance elements (Ref. 1). Figure 4-9 shows a sketch of the proposed monitors.

A sufficient number of monitors will be located across the block to allow measurement of in-block temperature and fluence tilts and conditions at each experimental fuel array in FTE-2, -4, and -6. Table 4-7 indicates the number of monitors for each of the test elements. These quantities assume that each test array will contain one column with four monitors, one at each end and the other two equally spaced along the fuel stack,

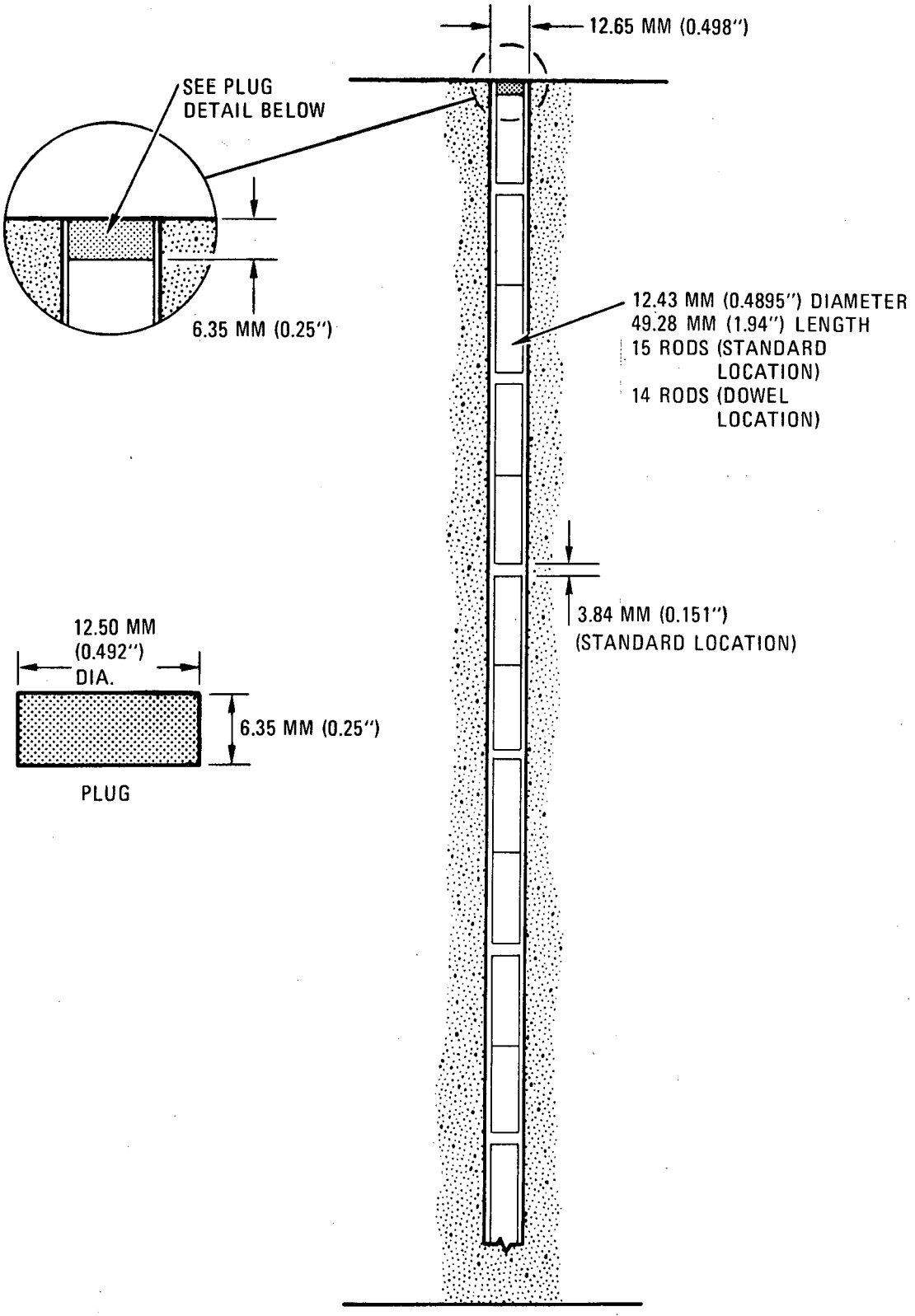

Fig. 4-8. Fuel rod configuration for cure-in-place assembly process

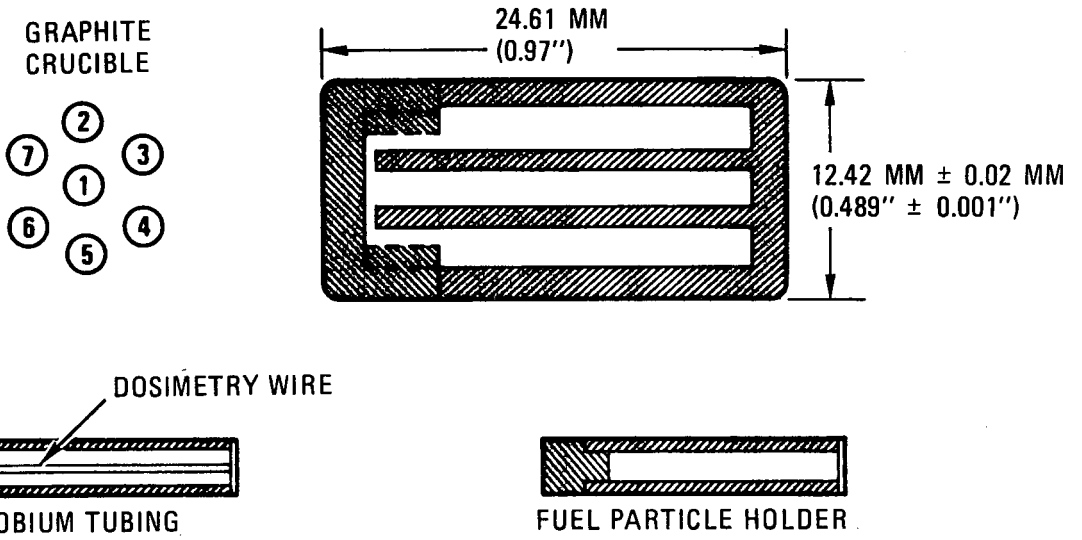

ITEM	MATERIAL	REACTION
1. SiC TEMPERATURE MONITOR		
2. FERTILE FUEL PARTICLES (< 20)		
3. THERMAL NEUTRON DOSIMETER	V–Co	Co–59 (n,γ)Co–60
4. FAST NEUTRON DOSIMETER	V–Ni (Ni–60 ENRICHED Ni)	Ni–60 (n,p)Co–60
5. FISSILE FUEL PARTICLES (< 20)		
6. THERMAL NEUTRON DOSIMETER	V	V–51(n,γ)V–52 $\xrightarrow{\beta^-}$ Cr–52
7. FAST NEUTRON DOSIMETER	V–Fe(Fe–54 ENRICHED Fe)	Fe–54(n,p)Mn–54

(MAY BE REPLACED BY ALTERNATE FOR FTE–4 THRU FTE–8 (3.5 YR–5.5 YR RESIDENCE TIMES)

Fig. 4-9. Schematic diagram of temperature and fluence monitor for use in FSV test elements

TABLE 4-7
QUANTITY OF INSTRUMENTATION MONITORS IN TEST ELEMENTS

Location Within Element	Total Quantity							
	FTE-1	FTE-2	FTE-3	FTE-4	FTE-5	FTE-6	FTE-7	FTE-8
Test array fuel columns or equivalent location	6	28	6	28	6	28	6	6
Element face - top only	6	6	6	6	6	6	6	6
Element center - top only	2	2	2	2	2	2	2	2
Control fuel column	4	--	4	--	4	--	4	4
Added buffer interface fuel column	--	--	--	--	4	--	--	--
Total	18	36	18	36	22	36	18	18

Note: All instrumentation monitors are located in fuel columns with fuel rods which have been individually cured in alumina beds or separate graphite crucibles or on top of fuel rod columns after curing in place.

plus six monitors located at each face of the element and two near the center. Additional monitors are required for the buffer element in order to measure interface effects between the two fuel loadings used (Fig. 4-3).

Because of the high temperatures required during curing, the fluence, burn-up, and temperature monitors must be assembled in test columns with loose rods after the curing process. The loose rods will be cured in place in separate graphite crucibles, then separated and measured for dimensions after firing. Fluence, burn-up, and temperature monitors will also be placed at the top of selected fuel columns that have been cured-in-place.

5. PERFORMANCE ANALYSIS - NORMAL OPERATION

5.1. NUCLEAR ANALYSIS

The effects of the test elements on the nuclear characteristics of the FSV core were evaluated using axial FEVER (Ref. 13a) and radial GAUGE (Ref. 13a) calculations. These calculations approximate three-dimensional results to within ±10%. They were performed to establish the axial and radial power correction factors for FTE-1 through FTE-5, which replace partially depleted elements, and to estimate possible effects of the test elements on control rod worths, excess reactivity, and other nuclear related parameters.

5.1.1. Fuel Loadings and Burnable Poisons

Uranium and thorium loadings for the test elements are given in Table 4-2. FTE-2 through FTE-5 contain uranium loadings which are lower than the uranium loadings for the elements which they replace. Consequently they require no lumped burnable poison. FTE-6, -7, and -8 use the same fuel loading as the Segment 7 elements they replace, and will contain the standard Segment 7 lumped burnable poison loadings.

5.1.2. Power Perturbations

The radial and axial power perturbations due to the test elements were computed with the FEVER and GAUGE computer programs and were combined to obtain a total power correction factor for the test elements. It is assumed that the radial power perturbation decreases at approximately the same rate

as the axial perturbation and will gradually disappear during the segment life cycle. These combined correction factors are given in Fig. 5-1. This correction is defined as:

$$F_p(t) = \frac{\text{power in test element at time (t)}}{\text{power in element replaced at time (t)}}$$

Time-dependent axial power correction factors were obtained using FEVER results for each of the test elements as shown in Fig. 5-2.

The FEVER calculations overestimate the power perturbation effect since the boundary conditions imply an infinite number of adjacent patches with test elements added.

Table 5-1 shows the beginning-of-cycle power perturbations in both the fuel column containing the test element and in the corresponding fuel region. The small power perturbations shown will be reduced further with burnup. There is no change for FTE-6, -7, and -8, which are located in Segment 7. These results emphasize that the test elements will have essentially no impact on region peaking factors specified in LCO 4.1.3 of the FSV Technical Specifications.

In summary, the power in test element FTE-1 will be greater than the power which would have been produced in the replaced element. Test elements FTE-2 through FTE-5 will produce less power than the elements which they replace. Test elements FTE-6 through FTE-8 produce no power perturbation. The test elements have less than a 2% effect on neighboring fuel elements or axial power distributions. Also, region and column peaking factors given in LCO 4.1.3 of the FSV FSAR are unchanged.

5.1.3. Fluence Perturbations

The FEVER and GAUGE calculations have shown that the fast flux is basically unchanged by the introduction of the test elements. Hence, the

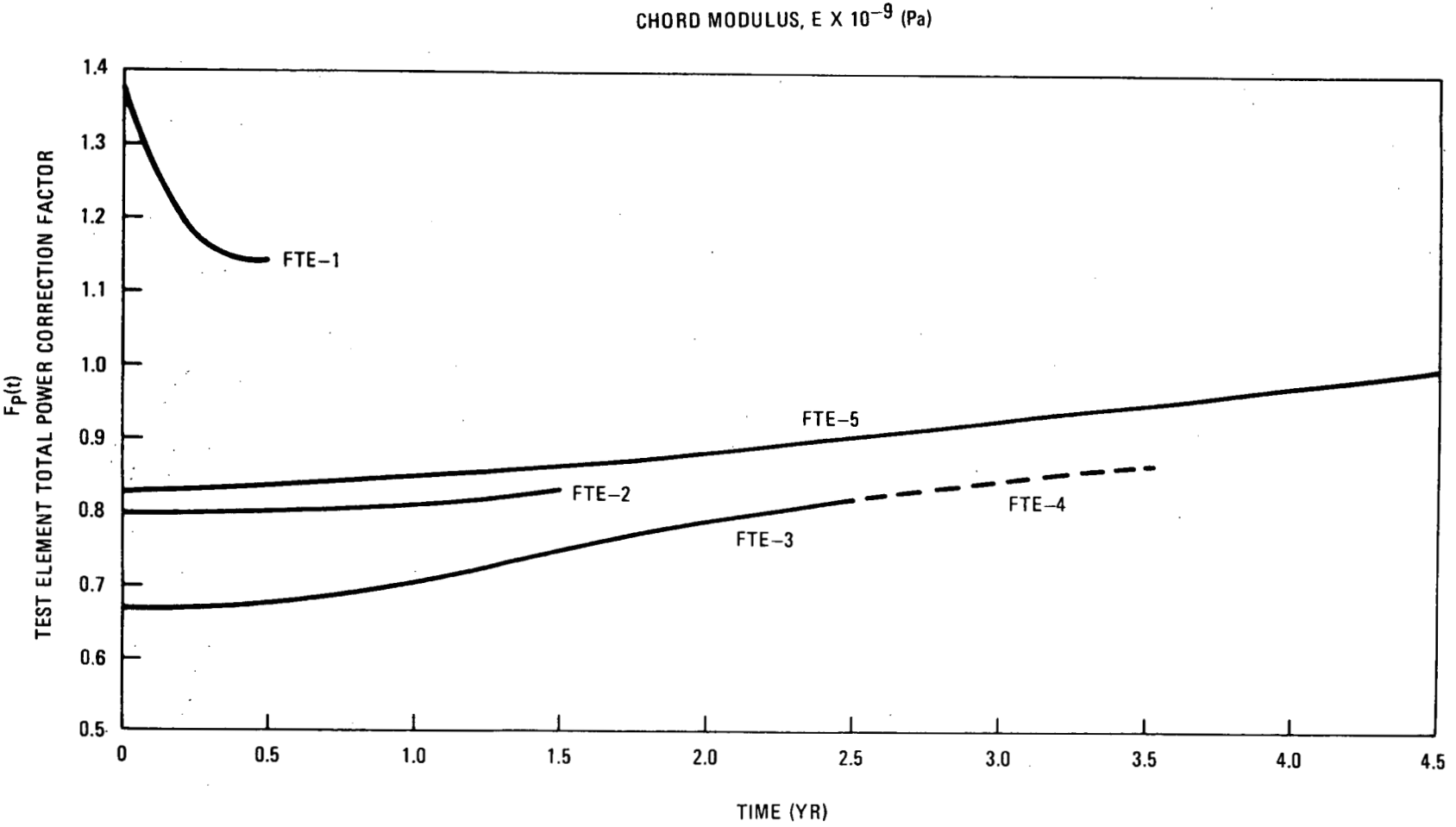

Fig. 5-1. FSV axial power correction factor for FSV test elements 1 through 5

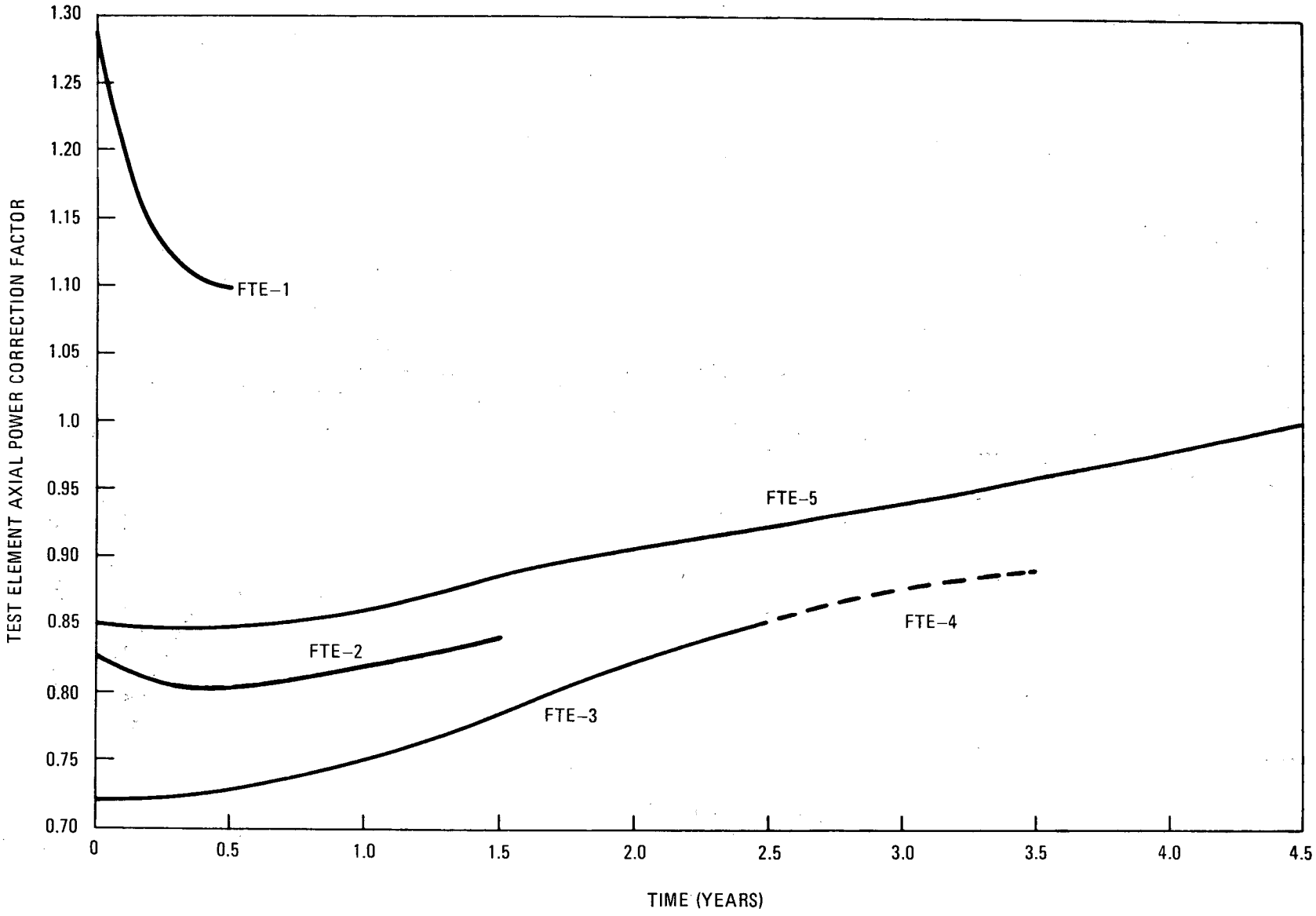

Fig. 5-2. FSV total (axial + radial) power correction factor for FSV test elements

TABLE 5-1
FUEL COLUMN AND REGION POWER PERTURBATIONS AT BOL

	FTE-1	FTE-2	FTE-3	FTE-4	FTE-5
Fuel column	+8%	-2%	-5%	-4%	-2%
Refueling region	+3%	∿0	-2%	-1%	∿0

fluence can be computed by integrating the fast flux from the original nuclear analysis over the residence time of the test elements.

5.1.4. Control Rod Worths and Reactivity Effects

The introduction of test elements into the core produced essentially zero ($<-5 \times 10^{-6}$ Δk) change in reactivity and only a very small change in the region power factors. Analysis has also shown that these test elements will have appreciably less than 0.001 Δk influence on any control rod worth. In addition, test elements will not affect the shutdown margin, excess reactivity, reactivity lifetime, temperature coefficients, and xenon worth.

5.1.5. Fuel Handling

The maximum k_∞ of the test elements is lower than the maximum k_∞ of the replaced elements. Since the fuel handling equipment and storage analysis is based on the most reactive FSV elements, there will be no special fuel handling problems (with respect to reactivity) for the test elements.

5.1.6. Decay Heat

Because of the lower power, or shorter residence time, of the test elements there will be no increase in the heat loads above those specified for standard FSV elements. However, since the test elements will be shipped in special casks, the maximum expected afterheat at 100 days after shutdown was determined and the values are given below (a 20% uncertainty has been included in these values for conservatism):

	FTE-1	FTE-2	FTE-3	FTE-4	FTE-5	FTE-6	FTE-7	FTE-8
Decay heat (watts)	384	552	684	684	720	816	912	912

5.2. THERMAL ANALYSIS

5.2.1. Analysis Procedure

Thermal analysis was performed for normal operating conditions using the TREVER code at all of the test element sites, for the FSV standard elements, to obtain the time histories of fast neutron fluence, fuel burnup, fuel temperature, and fuel performance (i.e., fission product retention). This analysis was repeated replacing the FSV standard elements with the corresponding test elements FTE-1 through FTE-8 to obtain comparative fuel performance results. The TREVER code description and the method of thermal and fuel performance analyses are described in Ref. 14.

The fuel particle performance models used in the analysis are described in Section 5.7 and are available for the following types of fuel particles:

1. TRISO - $(Th/U)C_2$ and TRISO - ThC_2 in Ref. 15.
2. TRISO - UC_2 and BISO - ThO_2 in Refs. 7 and 16.
3. TRISO - ThO_2 in Ref. 17.
4. TRISO - UC_xO_y - WAR (ref. 17).

The thermal analysis takes into account the differences in graphite thermal conductivity, thermal expansion and irradiation shrinkage, fuel rod dimensional change characteristics, and burnup calculations.

The proposed test elements (see Table 2-1) are of H-451 graphite, whereas the FSV standard elements are of H-327 graphite. As noted in Ref. 14, the H-451 graphite has a higher thermal conductivity, experiences lower irradiation contraction in the radial direction, and has a higher thermal expansion coefficient.

The presence of shim particles in many of the test fuel rods results in higher fuel rod thermal conductivity (Ref. 14). This has been conservatively neglected and a fuel rod thermal conductivity of four Btu/hr-ft-°F has been used in the analysis.

The test fuel rods containing BISO fuel particles experience higher irradiation contraction in the radial direction (Ref. 14) than fuel rods containing all TRISO fuel. This has been accounted for in the analysis.

5.2.2. Analysis Results

The fuel performance of test elements FTE-1 through FTE-8 has been compared individually with the corresponding FSV standard elements as a function of fast neutron fluence, burnup, and temperature under normal operating conditions.

The performances of all the test element fuel versus the FSV reference fuel are summarized in Table 5-2, where the most severe environment of fuel centerline temperature, fast neutron fluence and fuel particle burnup are compared. Also, the resultant 95% confidence values of end-of-life kernel migration distances and expected fuel failures are given. The test array 1 to 7 and driver fuel in test elements FTE-2, -4, and -6 (refer to Table 2-1) are formed into three groups as shown in Table 5-2, as they are expected to have similar particle burnup, fuel rod dimensional change characteristics, and kernel migration rates.

FTE-1 is expected to operate at higher power levels than the element it replaces, as shown in Fig. 5-2. The time history of the fuel centerline temperatures during its 6 months of core residency is shown in Fig. 5-3. The increase in average fuel temperature over the reference fuel element temperature is about 135°C. This increase in temperature results in a higher kernel migration rate, but the kernel migration distance at the end of 6 months is only a small fraction of the buffer coating thickness as seen in Table 5-2. The end-of-life fluence, burnup, and the expected fuel particle coating failure fraction is small in FTE-1.

FTE-2 through FTE-5 are expected to operate at lower power levels in comparison with the FSV reference elements they replace as shown in Fig. 5-2. The fuel temperatures as a function of time for the test elements FTE-2 through FTE-5 are shown in Figs. 5-4 and 5-5 during their respective

TABLE 5-2
MOST SEVERE ENVIRONMENT EXPERIENCED BY VARIOUS FUEL TEST ELEMENTS

Test Element No.	Test Array	Fuel ℄ Temperature (°C)		Max. Fluence ($\times 10^{25}$ n/m^2)	Max. Burnup FIMA		Max. Kernel Mig. Distance (microns)		Max. Fuel Particle Coating Failure (%)	
		Max.	Time Averaged		Fissile	Fertile	Fissile	Fertile	Fissile	Fertile
FTE-1		1253	1129	0.52	0.128	0.002	0.32	1.75	0.0	0.460
	Ref.[a]	1011	996	1.05	0.061	0.003	0.07	0.04	0.244	0.095
FTE-2	1	911	863	1.80	0.065	0.009	0.29	0.81	0.260	0.157
	2 to 5	912	864	1.80	0.300	0.009	0.08	0.82	0.0	0.126
	6,7 and Driver	904	857	1.80	0.300	0.009	0.08	0.77	0.0	0.157
	Ref.[a]	1046	1011	2.50	0.098	0.01	0.47	0.32	0.392	0.225
FTE-3		892	848	3.07	0.440	0.024	0.06	0.67	0.027	0.270
	Ref.[a]	1076	1042	3.80	0.140	0.025	1.03	0.72	0.544	0.440
FTE-4	1	987	891	3.96	0.110	0.033	0.55	1.50	0.456	0.346
	2 to 5	989	893	3.96	0.460	0.033	0.17	1.52	0.134	0.247
	6,7 and Driver	977	884	3.96	0.460	0.033	0.15	1.40	0.134	0.247
	Ref.[a]	1092	1019	4.85	0.150	0.034	1.32	1.02	0.610	0.598
FTE-5		1014	967	3.43	0.550	0.036	0.68	4.17	0.063	0.360
	Ref.[a]	1157	1031	3.94	0.170	0.037	3.66	3.50	0.670	0.650
FTE-6	1	1229	1043	6.65	0.180	0.056	5.70	12.06	0.720	0.580
	2 to 5	1232	1046	6.65	0.710	0.056	2.62	12.50	0.440	0.420
	6,7 and Driver	1222	1036	6.65	0.710	0.056	2.18	10.89	0.440	0.580
	Ref.[a]	1227	1043	6.65	0.180	0.056	5.70	6.54	0.720	0.986
FTE-7		1077	1012	6.48	0.190	0.062	1.27	0.88	0.750	1.100
	Ref.[a]	1072	1011	6.48	0.190	0.062	1.20	0.82	0.750	1.100
FTE-8		1081	1015	6.54	0.190	0.062	1.29	0.89	0.750	1.100
	Ref.[a]	1076	1014	6.54	0.190	0.062	1.23	0.83	0.750	1.100

[a] Reference FSV fuel in H-327 graphite block.

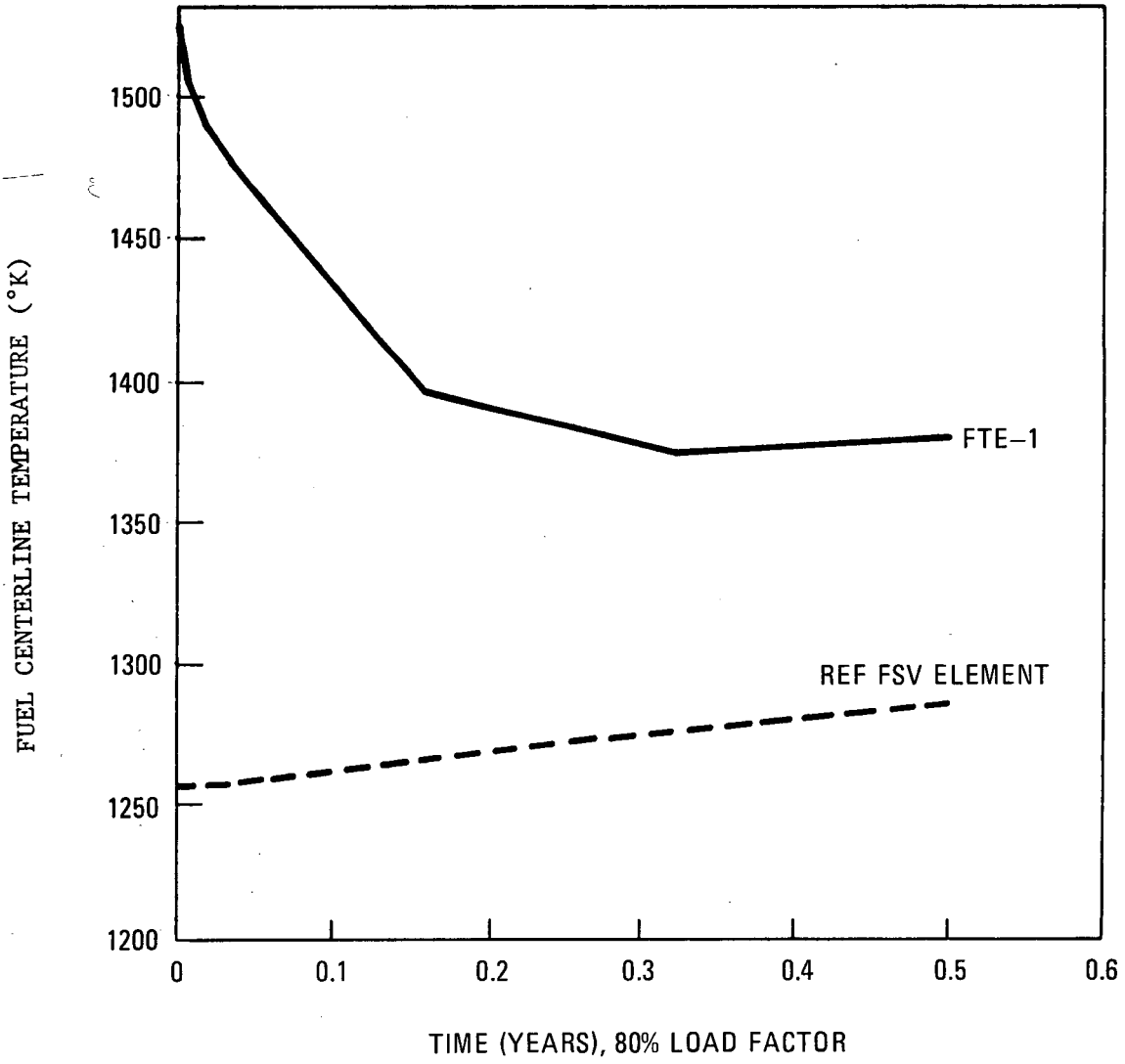

Fig. 5-3. Time history of maximum fuel centerline temperature in FTE-1

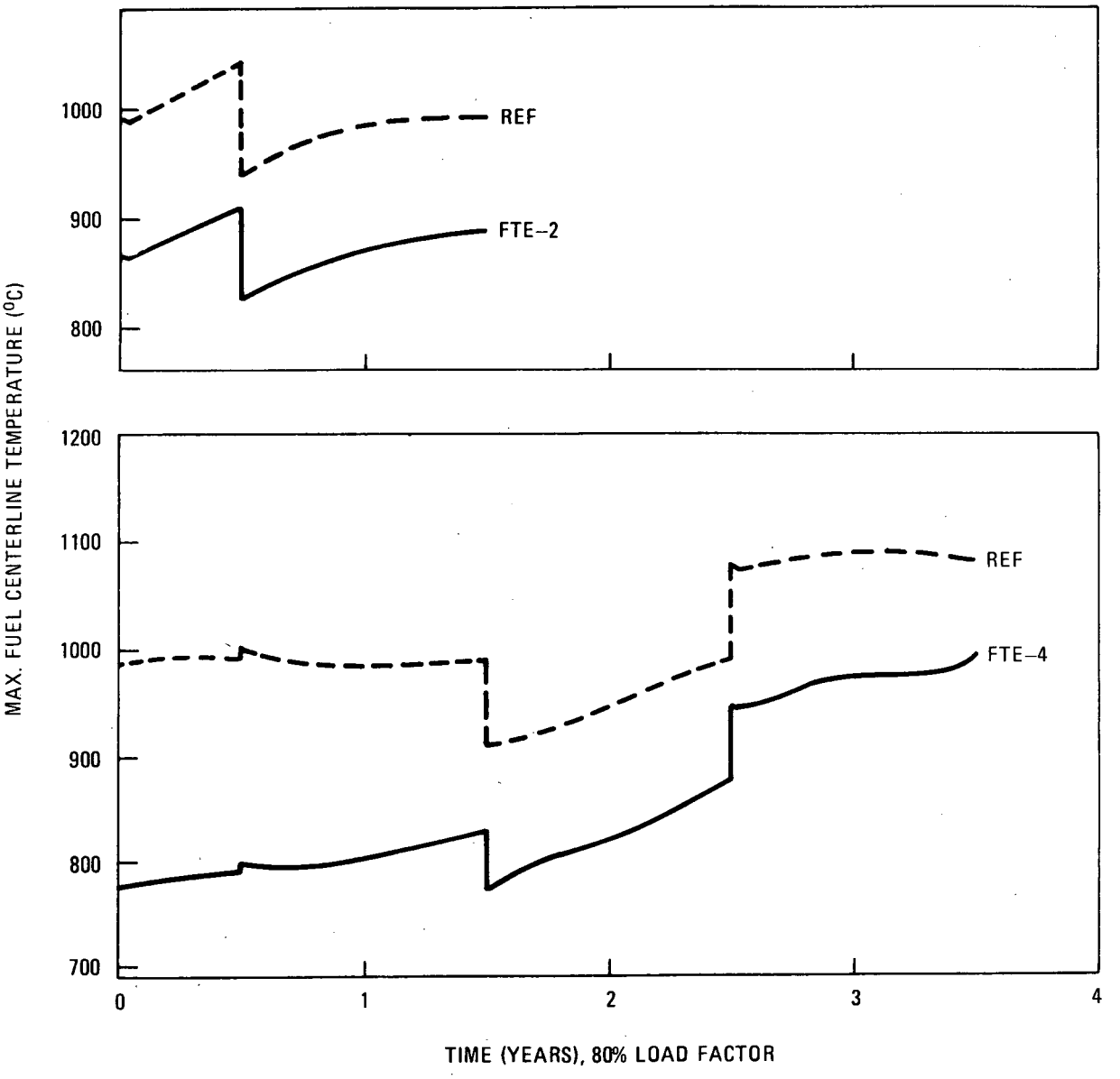

Fig. 5-4. Time history of maximum fuel centerline temperature in FTE-2 and FTE-4

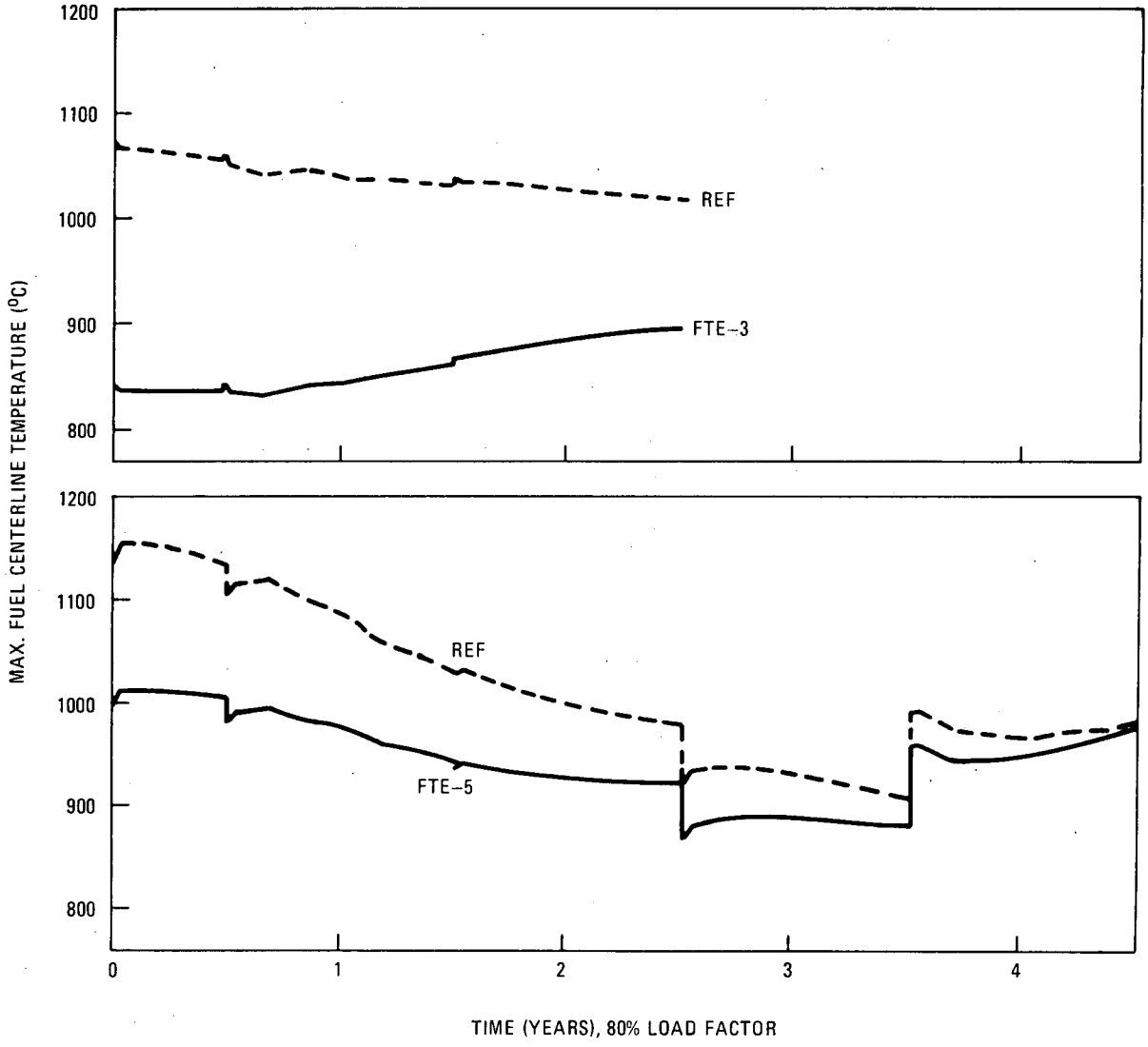

Fig. 5-5. Time history of maximum fuel centerline temperature in FTE-3 and FTE-5

core residency period. For FTE-2 and FTE-4, which contain test arrays 1 to 7 and driver fuel, representative fuel temperature time-histories are shown. The test elements experience significantly lower fuel temperatures; they also experience lower fuel burnup and fast neutron exposure, as their core residence time is 6 months shorter than the elements they replace. The kernel migration rates are different for the different kernel types, but the end-of-life kernel migration distances are very small. The fuel particle coating failure fractions in test elements FTE-2 through FTE-5 are expected to be substantially lower than those of the corresponding FSV reference elements, as shown in Table 5-2.

The test elements FTE-6 through FTE-8 are expected to operate at the same power as those of the corresponding FSV reference elements. As shown in Figs. 5-6 and 5-7, the temperatures experienced by these test elements are slightly higher than those of the FSV reference elements they replace. This is due to the combination of the differences in thermal properties of graphite and the fuel rod dimensional change characteristics.

FTE-7 and -8 have the same type of fuel as the FSV reference elements, whereas FTE-6 contains test fuel. These test elements experience the same fluence and burnup environment and FTE-7 and -8 are expected to have the same level of fuel performance as those of the FSV reference elements. Exceptions to this include the test fuel in FTE-6, which is expected to have significantly lower fuel particle coating failure rates than the FSV reference fuel.

5.3. FISSION PRODUCT RELEASE ANALYSIS

5.3.1. Gaseous Fission Product Release

Both pyrocarbon and silicon carbide coatings are effective barriers to the release of gaseous fission products (including iodine). Consequently, gaseous fission products released into the coolant are from fuel particles with failed coatings and from uranium and thorium contamination of the as-manufactured fuel. For this analysis, contamination is defined

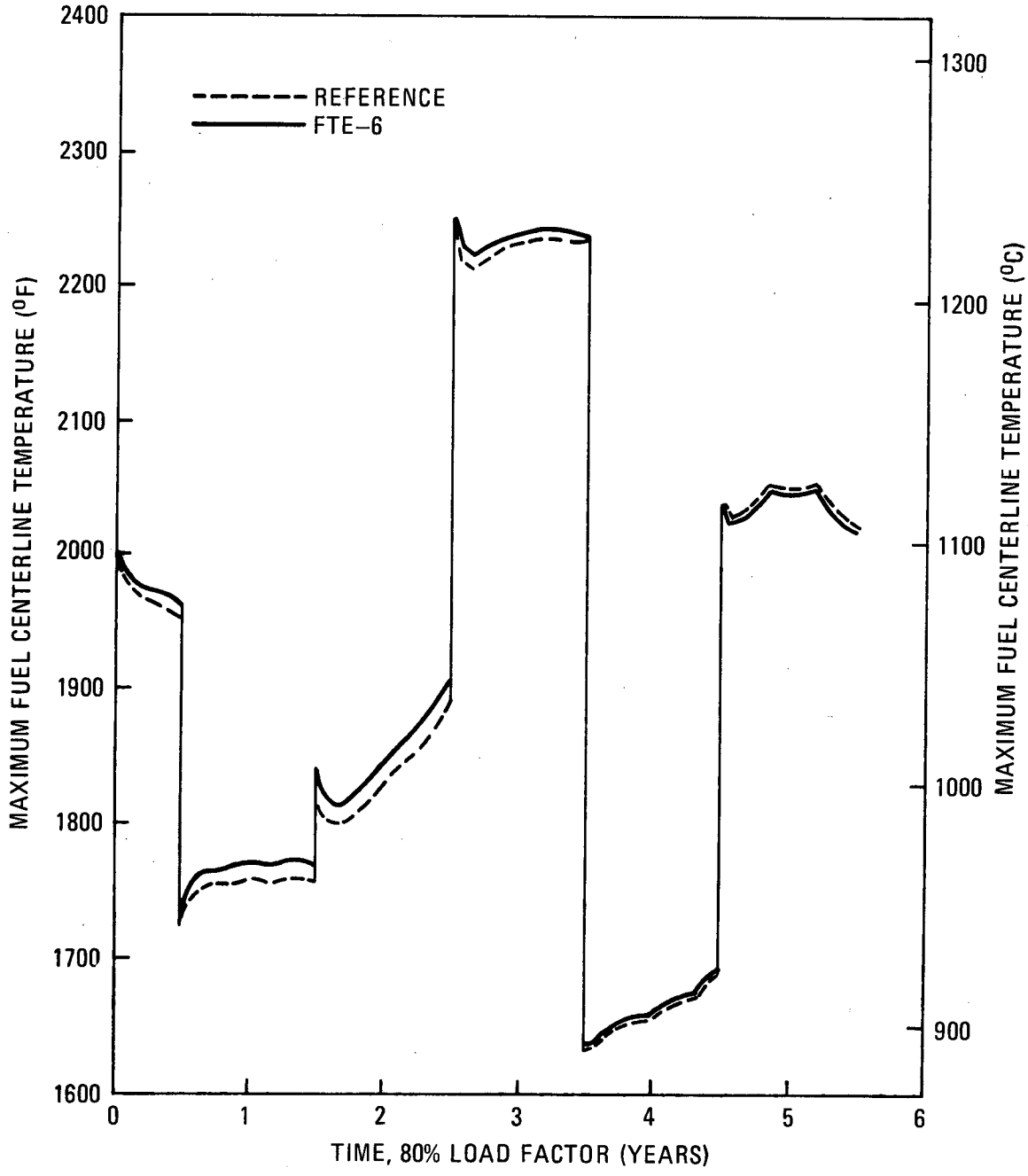

Fig. 5-6. Time history of maximum fuel centerline temperature in FTE-6

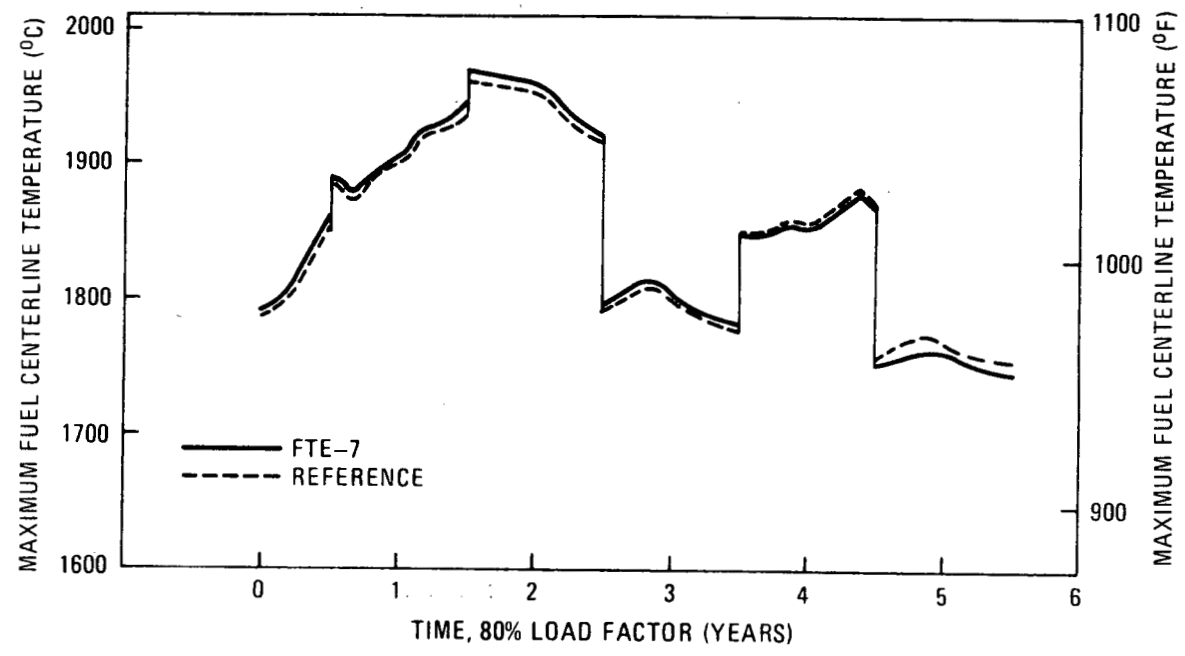

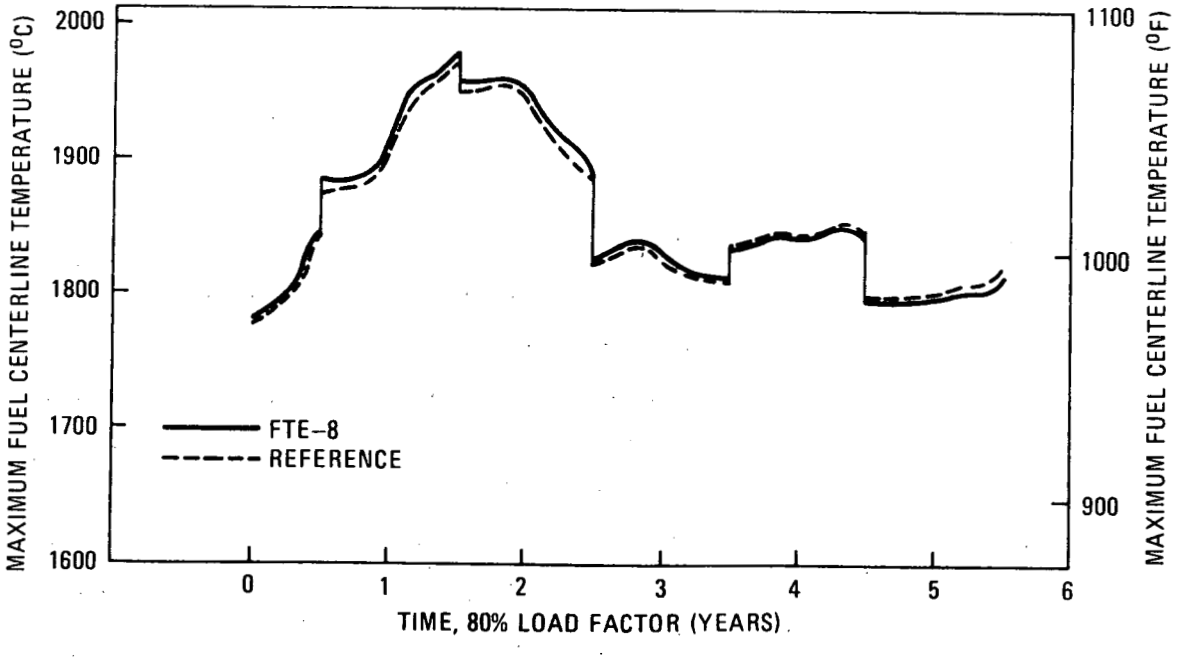

Fig. 5-7. Time history of maximum fuel centerline temperature in FTE-7 and FTE-8

as that heavy metal not contained within fuel particle coatings. In the manufacture of test element fuel for FSV, fuel manufacturing specifications will be set and rigorous quality control procedures followed to assure that heavy metal contamination levels for the test fuel are equal to or less than those for the regular FSV fuel. Hence, the fission product source due to heavy metal contamination in the fuel will be equal to or less than that from the corresponding FSV fuel.

Table 5-2 gives the irradiation temperature and predicted fuel particle coating failure fractions for each of the test elements. As shown in the table, these fissile and fertile coating failure fractions are always less than the corresponding reference FSV fissile and fertile failure fractions. The fraction of fissions occurring in failed test fissile fuel particles is therefore less than that occurring in reference FSV failed fissile fuel particles. Thus, if reference and test failed coatings have the same gaseous fission product release fractions, the test fuel will have a lower gaseous fission product release rate than the reference fuel. The variables which can influence the value of gaseous release fractions are discussed below.

Figure 4-2, in addition to showing the location for various test fuels in FTE-2, -4, and -6, gives the chemical composition of the seven fuel test arrays present in the test elements. The chemical composition of the test fuel particle kernels is sometimes different from that of FSV fuel: FSV fissile and fertile fuel is $(Th/U)C_2$ and ThC_2, respectively. Fuel test elements one through six contain advanced fuel types intended for future use in large HTGRs and for future FSV reload segments. As such, these fuel types have already undergone extensive irradiation testing. The results of these tests indicate that there is no discernable difference between carbide and oxide fuel kernel gaseous release fractions when both fuel kernels have approximately the same material density (Refs. 15 and 18). Regarding fission gas release, oxide fuel particle kernels have in fact some advantage over carbide fuel kernels in that the presence of very small amounts of water in the helium coolant over a prolonged period of time can cause hydrolysis of an exposed carbide fuel particle kernel. This leads to increased fission

gas release. Before an oxide fuel particle kernel can be hydrolyzed, it must first be converted to a carbide form. This occurs only at very high temperatures relative to nominal HTGR conditions. Irradiation test results indicate no fission gas release dependence upon fuel burnup (FIMA) or neutron fluence over the range of normal operating conditions experienced in an HTGR (Ref. 18).

Fission gas release from fuel is, of course, temperature dependent: the fission gas release rate increases with increasing temperature, assuming a constant fuel particle coating failure fraction. Table 5-2 indicates that, with the exception of FTE-1, the fuel test elements operate near or well below the temperatures of the reference FSV fuel they replace. Consequently, the operating temperatures of the test elements alone would cause the release of fission gases to be lower in the test fuel than in the fuel being replaced. Despite the higher operating fuel temperature of FTE-1, the gaseous release rate from the test fuel is substantially below that of the reference fuel because of the very much lower fuel particle coating failure fraction of the test fuel (Ref. 19).

It has been experimentally shown that fuel particles with WAR fuel kernels release fission gases at a rate about five times greater than the reference FSV VSM fuel particle kernel type upon failure of the fuel particle coating (Ref. 20). This is interpreted as being due to the lower material density of the WAR kernels. Although the release rate from failed fuel particles with WAR kernels is greater than that from failed particles with VSM kernels, the fuel particle design is more robust and coating performance for WAR kernels is therefore superior to that of TRISO coatings on FSV VSM kernels. Analyses which combine the lower fuel particle coating failure fractions of fuel particles with WAR kernels with the effects of higher gaseous release rate indicate that the gaseous release from FTE-5 and -6 is approximately 90 and 70% higher, respectively, than that from the FSV fuel it will replace. Test fuel particles with WAR fuel kernels are present in the first six test elements. When the six test elements are considered altogether, the release rate from the test fuel with WAR fuel kernels is about equal to that from the FSV fuel it will replace (Ref. 19).

Techniques for calculating primary coolant radioactivity levels are described in detail in Ref. 21.

5.3.2. Metallic Fission Product Release

The presence of BISO coated fuel particles in the test fuel causes an increase in the release of metallic fission products. Unlike TRISO coated fuel particles, which contain a silicon carbide coating that is impermeable to metallic fission products, BISO coated fuel particles have only pyrocarbon coatings. Irradiation tests have shown that some metallic fission products migrate through BISO fuel particle coatings when the fuel operates at a high temperature for a long period of time. Extensive calculations have been performed to determine the effect of placing BISO fuel particles in FSV fuel test elements (Ref. 19). The calculational methods and fundamental data input are discussed in detail in Refs. 22 and 23. Calculations were done for cesium and strontium, since their migration properties are representative of a large group of chemical elements and since Cs-137 and Sr-90 are two of the more important radionuclides.

Results of this analysis are given in Table 5-3. The releases of cesium and strontium from FTE-6 are approximately 3.6 and 9.8 times greater than that from the FSV reference element replaced by the test element. The contribution of the test element release to the 30-year cesium and strontium design curie levels is approximately 10^{-3} and 10^{-7}, respectively. The release of cesium and strontium from FTE-2 and -4, the only other test elements containing BISO fuel particles, is at least an order of magnitude less than the release from FTE-6.

TABLE 5-3
CESIUM AND STRONTIUM RELEASE FROM FTE-6
(curies)

	Cs-137	Sr-90
FTE-6	4.5	4×10^{-5}
FSAR 30-yr value (FSAR Table 3.7-2)	4560	324

5.3.3. Conclusion

It is concluded that the increase in metallic fission product release due to the presence of BISO coated fuel particles will be almost imperceptible.

Results from the thermal analysis (Table 5-2) indicate that fuel test element in-pile operating temperatures are essentially equal to, or are substantially less than, the standard fuel elements being replaced, with the exception of FTE-1, which operates at a higher temperature than the fuel element it replaces, but only for a six-month irradiation period. Analyses also indicate that fuel particle coating failure fractions for the test fuel are substantially less than those for the elements they replace. Analyses also show that gaseous fission product release (i.e., Kr, Xe, I) from the test elements is approximately equal to that from the elements they replace and that the increased metallic fission product release (i.e. Cs, Sr) will be imperceptibly small.

5.4. GRAPHITE STRUCTURAL ANALYSIS

The most significant structural difference between reload fuel elements and proposed test elements is the use of near-isotropic H-451 graphite used in place of the needle coke H-327 which is being used in the initial core and reload elements. The tensile strengths of these two types of graphite are given in Table 5-4. It can be seen that except for the end center location, the strength of H-451 graphite in both radial and axial direction is substantially higher than that of H-327 graphite. Other parameters that affect the structural analysis of test elements consist of mainly thermal and mechanical properties.

The important graphite thermal property in the calculation of temperature distribution in fuel elements is the thermal conductivity of graphite.

TABLE 5-4
COMPARISON OF MEAN ULTIMATE TENSILE STRENGTHS OF UNIRRADIATED H-327 AND H-451 GRAPHITES

Log Position	H-327 Strength kPa (psi)	H-451 Strength kPa (psi)
	Axial Direction	
End center	15,030 (2180)	15,270 (2215)
End edge	16,510 (2395)	18,030 (2615)
Mid-length center	11,240 (1630)	13,580 (1970)
Mid-length edge	16,510 (2395)	19,170 (2780)
	Radial Direction	
End center	9,310 (1350)	13,930 (2020)
End edge	9,310 (1350)	15,170 (2200)
Mid-length center	6,480 (940)	10,760 (1560)
Mid-length edge	8,900 (1290)	13,960 (2025)

The thermal conductivity of both types of graphite as a function of irradiation temperature and fluence is shown in Fig. 5-8. As can be seen, the thermal conductivity of H-451 graphite is higher than that of H-327 graphite at all temperatures and fluences.

The calculation of fuel element stresses and deformation involves the following mechanical properties of which a comparison for the two types of graphites is given below:

1. Elastic modulus: A comparison of chord modulus of both H-327 and and H-451 graphite as a function of neutron fluence is shown in Fig. 5-9. The modulus of H-451 graphite is 30 to 40% lower than that of H-327 graphite and therefore, for a given strain, the stresses in H-451 graphite element are significantly lower than in H-327 graphite.

2. Creep properties: Figs. 5-10, 5-11, and 5-12 present the comparisons of creep properties of the two types of graphites. These properties indicate that the creep behavior of both graphites is similar.

3. Irradiation-induced dimensional change: Operating stresses are produced within the graphite elements by strains due to differential irradiation-induced dimensional changes across the element. Figs. 5-13 and 5-14 show the irradiation-induced dimensional changes of H-327 and H-451 graphite in both axial and radial directions. A comparison of these two figures shows that, at peak temperatures and fluences, the irradiation-induced dimensional change of H-451 graphite in the axial direction is about 50% lower than that of H-327 graphite. As a result of this behavior, the stresses in fuel elements made from H-451 graphite are lower than those in the H-327 graphite elements they replace.

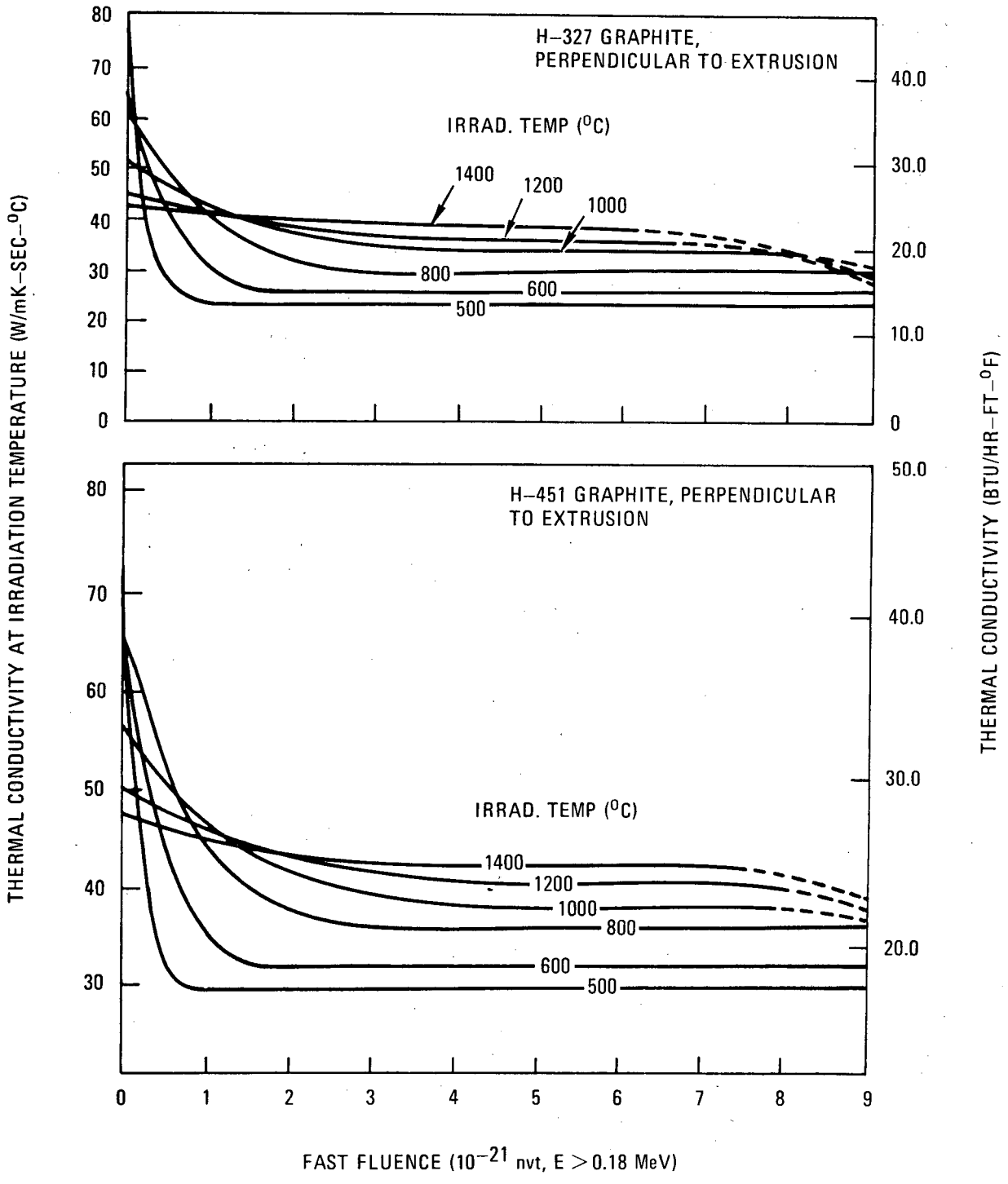

Fig. 5-8. Thermal conductivity of H-327 and H-451 graphite as a function of irradiation temperature and fluence

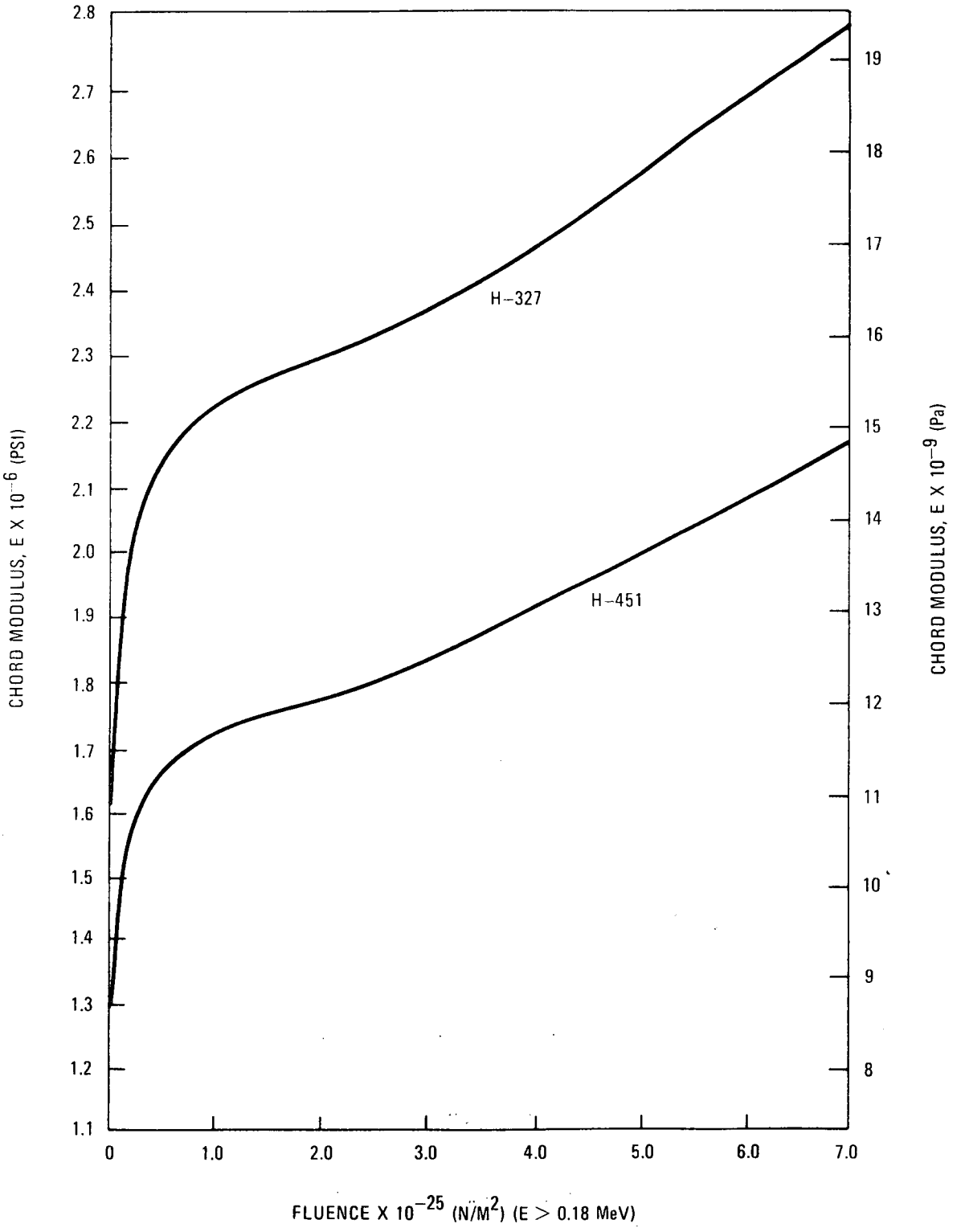

Fig. 5-9. Chord modulus for H-327 and H-451 graphite, axial direction

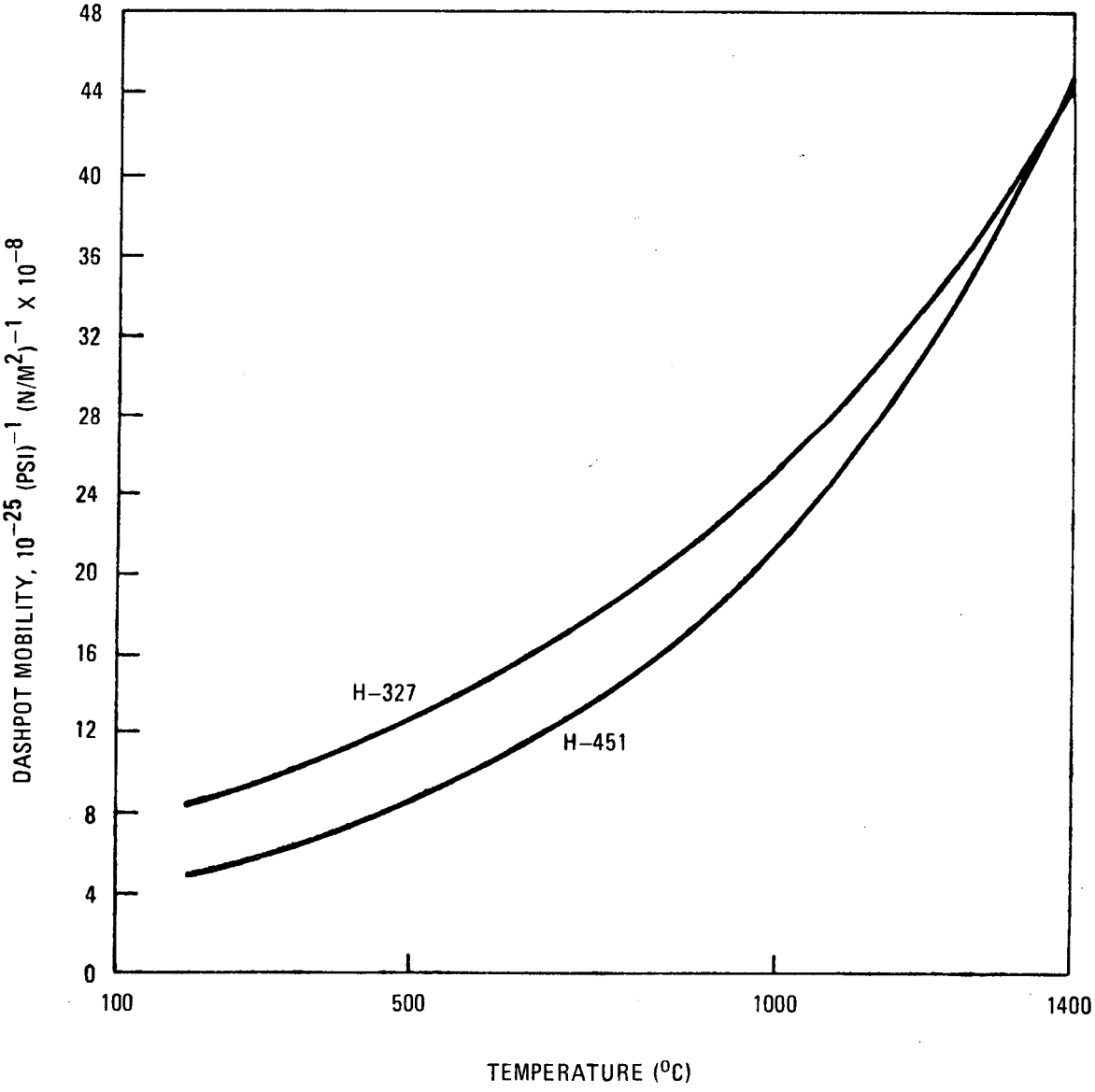

Fig. 5-10. Steady-state creep dashpot mobility for H-327 and H-451 graphite

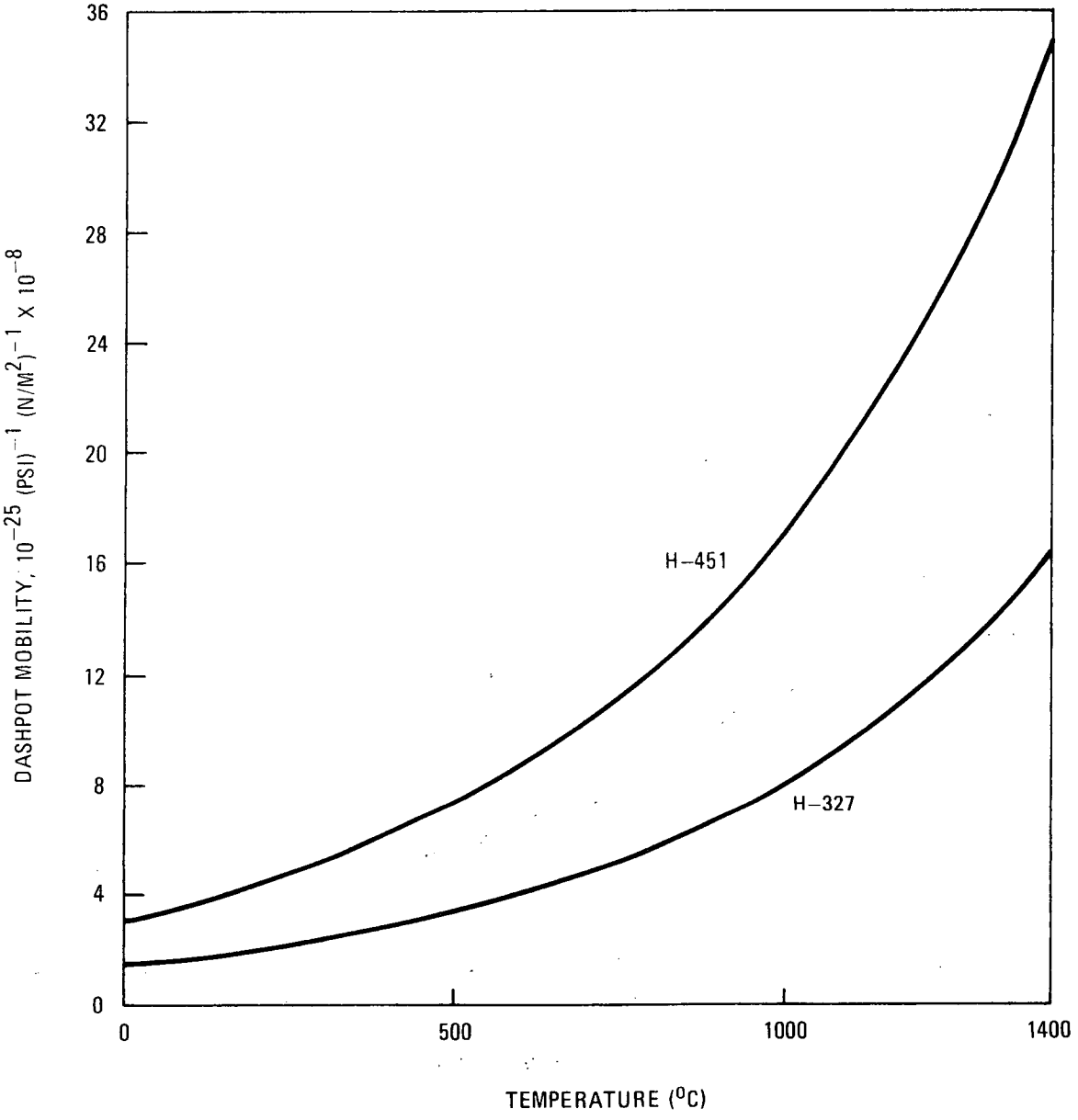

Fig. 5-11. Transient creep dashpot mobility for H-327 and H-451 graphite

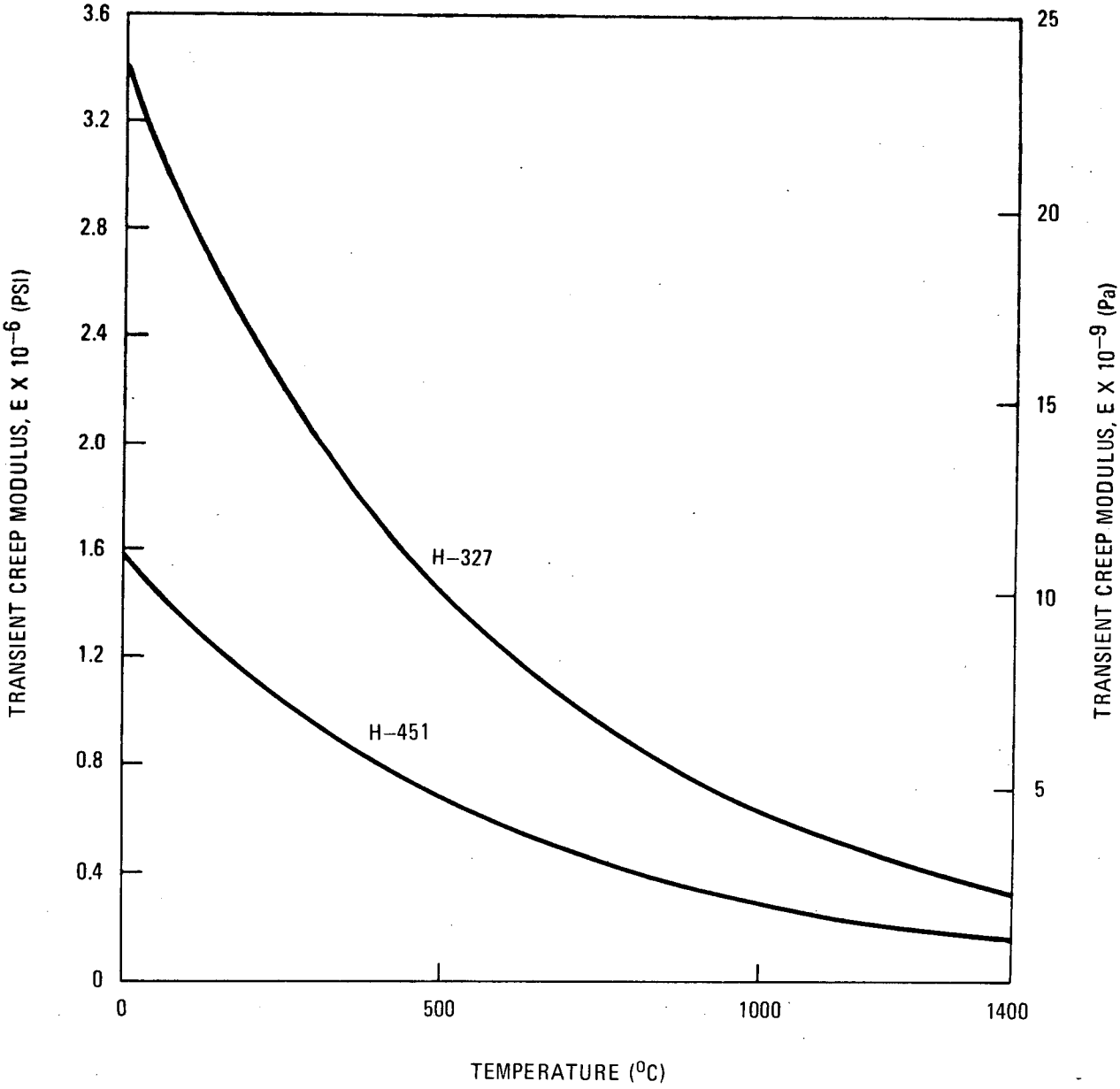

Fig. 5-12. Transient creep spring modulus (axial) for H-327 and H-451 graphite

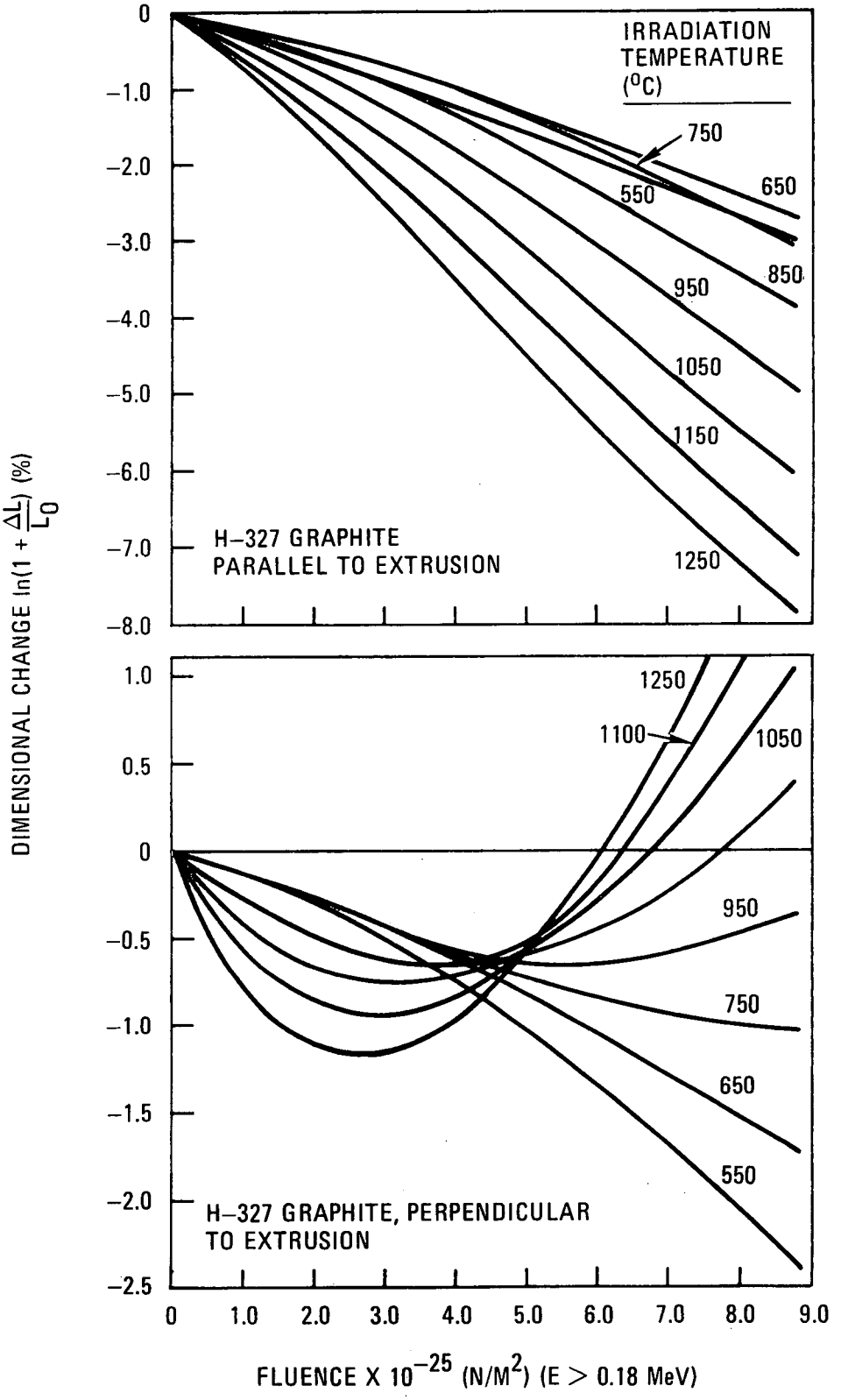

Fig. 5-13. Needle-coke graphite (H-327) dimensional change in parallel and perpendicular directions

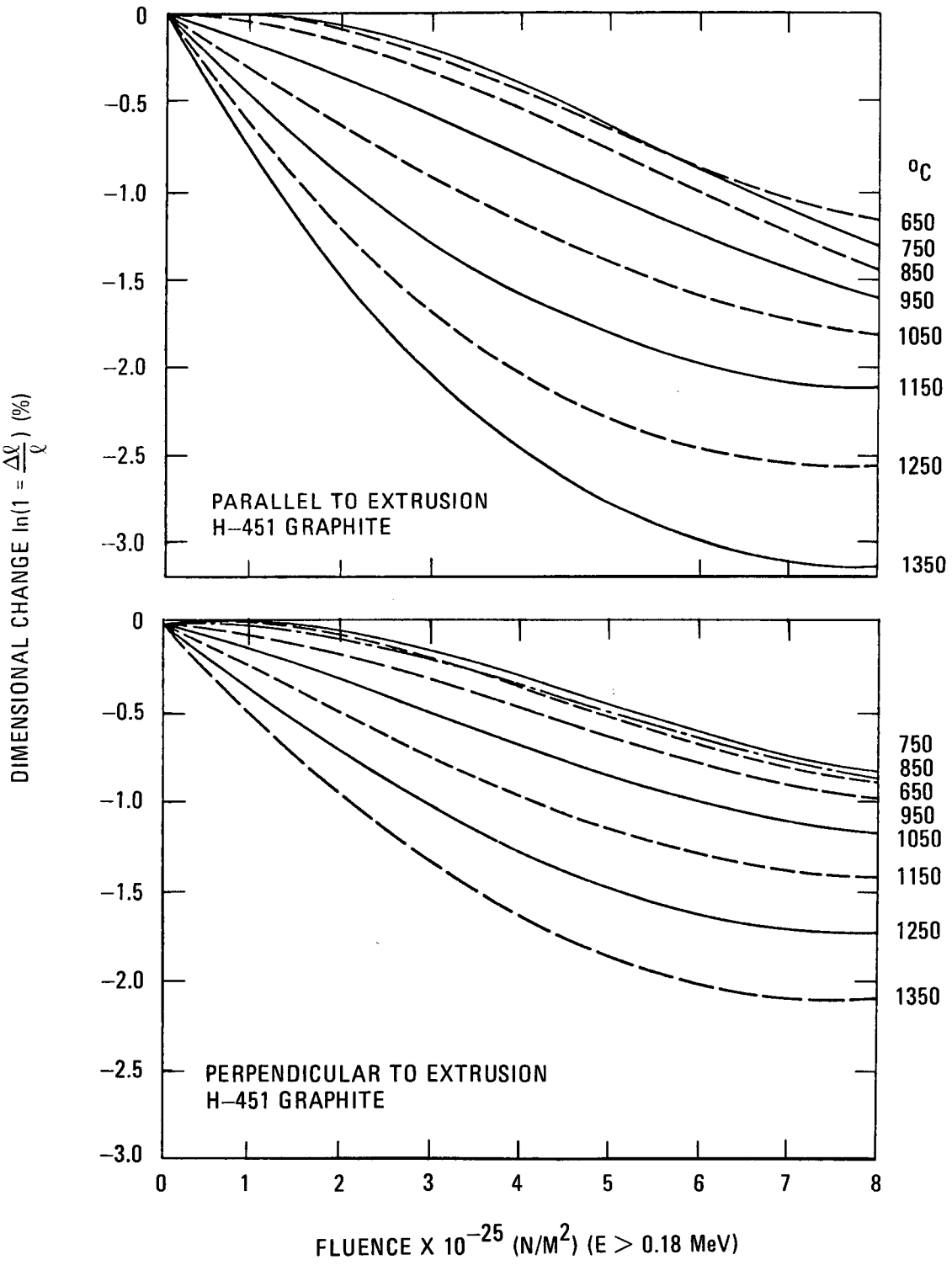

Fig. 5-14. Near-isotropic graphite (H-451) dimensional change in parallel and perpendicular directions

4. Thermal strains: While the irradiation-induced strains make the major contributions to the operating stresses within the graphite elements, the thermal strains contribute strongly to the shutdown stresses. A comparison of the thermal strains of H-327 and H-451 graphite in both the radial and axial directions as a function of temperatures is given in Fig. 5-15. The thermal expansion of H-451 graphite is about 30% and 100% higher than that of H-327 graphite in the radial and axial directions.

Using the above thermal and mechanical properties, stress and dimensional change analyses were performed for H-451 graphite test elements and the results were compared with similar analyses performed for the H-327 graphite fuel elements the test elements are to replace. The analyses were performed using the SURVEY-STRESS computer code which calculates stresses, strains, and deformations using the viscoelastic beam theory.

Stress analyses of fuel elements indicate that the stress distribution across the elements changes significantly with time. The initial operating stresses in a previously unirradiated fuel element are compressive in hotter portions of the element and tensile in cooler portions. Under irradiation by fast neutrons, the hotter graphite shrinks faster than the colder graphite. After a period of operation varying from a few months to about a year, the irradiation-induced dimensional changes overcome the thermal strains in magnitude and the colder portion of the graphite which was originally in tension goes into compression while the hotter portion goes into tension. As a result, the location of the maximum tensile stress within the element changes during irradiation.

The strength of graphite varies spatially within a fuel element; the minimum strength values are found near the center of the element and the higher strength values are found near the edges. In addition, the local strength of graphite changes with irradiation according to the temperature and fluence history at each location.

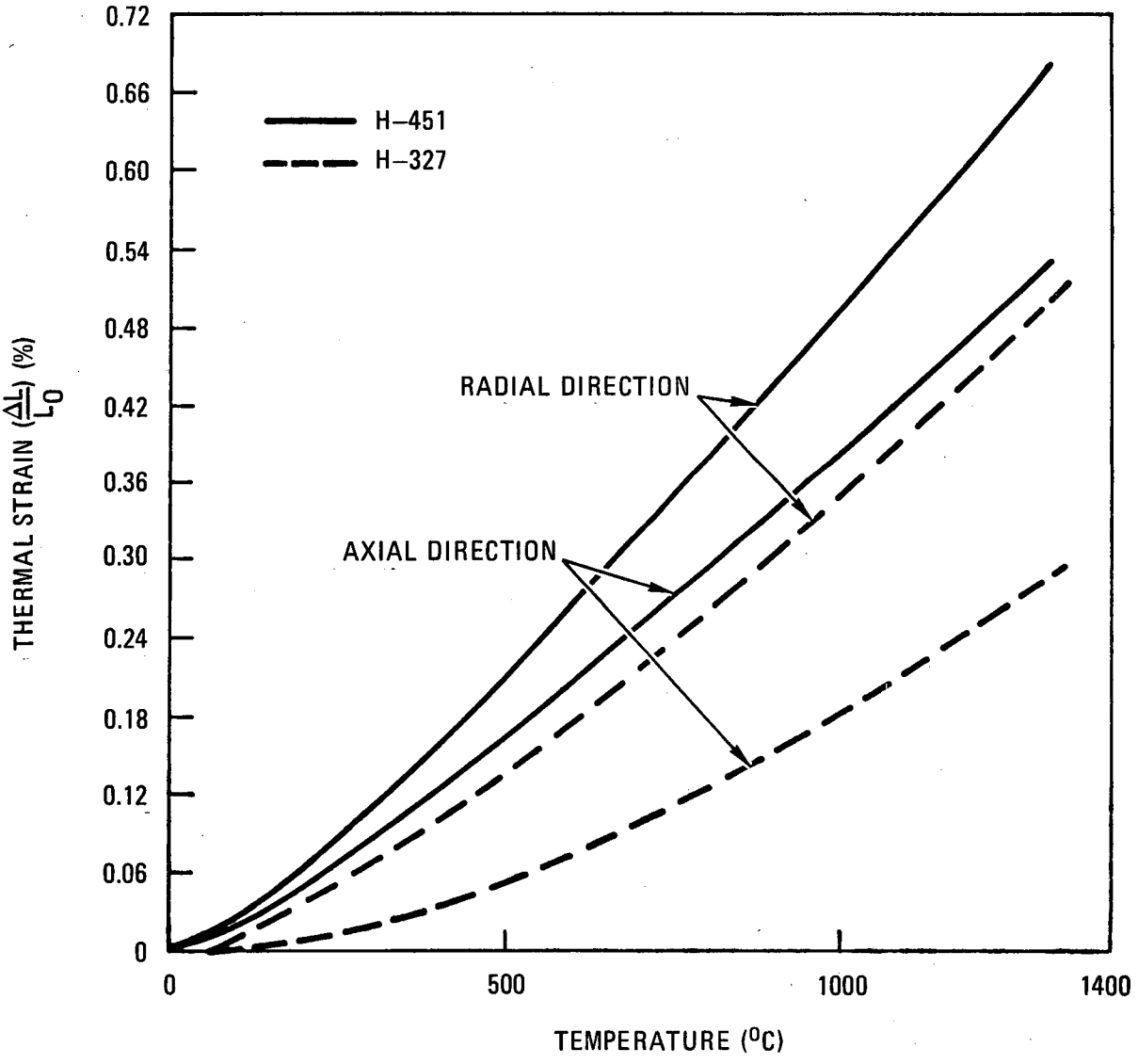

Fig. 5-15. Thermal strains in unirradiated H-327 and H-451 graphite

In structural analysis of a fuel element, the stress and strength are calculated at several spatial locations within the fuel element throughout its lifetime. The ratio of the local stress to the local strength of the graphite, called the "stress ratio," is used as a measure of the structural performance of the fuel element.

A comparison is shown in Table 5-5 of the operating tensile stress ratio in test element FTE-1 (made from H-451 graphite) with the stress ratio in the reference fuel element (made up of H-327 graphite) to be replaced by FTE-1. As can be seen, the peak operating stress ratio in FTE-1 is about the same as that in the corresponding reference fuel element.

The FSV plant is expected to operate continuously between refueling operations. However, shutdowns can occur frequently and these shutdowns cause large changes in temperature distributions and, hence, elastic stresses in the fuel elements. In the absence of creep and irradiation strain, a shutdown to a state of uniform temperature would simply remove the operating thermal stress and reduce the stress to zero. The influence of creep and irradiation strain, however, causes maximum shutdown stresses higher than maximum normal operating stresses.

Shutdown stresses are calculated periodically for test elements by superimposing a shutdown on the normal continuous operating history. The shutdown stress ratios were calculated for test element FTE-1 at several time points during its residency in the core. As can be seen in Table 5-5, the maximum shutdown stress ratios in the test element are lower than those in the element it replaced. Similar time histories of operating and shutdown stress ratios for test elements FTE-2 through FTE-8 were calculated; the expected maximum operating and shutdown stress ratios for each test element and the element it replaces are summarized in Table 5-6. These results indicate that the use of H-451 graphite improves the stress margin as compared to original FSV elements.

TABLE 5-5
COMPARISON OF OPERATING AND SHUTDOWN STRESS-TO-STRENGTH RATIOS IN TEST ELEMENT FTE-1 AND THE REPLACED REFERENCE ELEMENT

Time (days)	Operating Stress Ratio		Shutdown Stress Ratio	
	Ref. Elements	Test Elements	Ref. Elements	Test Elements
0	0.053	0.056	0.055	0.000
1	0.040	0.036	0.035	0.011
3	0.026	0.020	0.042	0.022
7	0.023	0.016	0.045	0.026
30	0.022	0.015	0.052	0.030
75	0.020	0.012	0.068	0.038
127	0.020	0.009	0.086	0.042
155	0.022	0.009	0.099	0.068

TABLE 5-6
COMPARISON OF MAXIMUM OPERATING AND SHUTDOWN STRESS-TO-STRENGTH RATIOS IN TEST ELEMENTS AND THE REPLACED REFERENCE ELEMENTS

Test Element Identification	Operating Stress Ratio		Shutdown Stress Ratio	
	Ref. Elements	Test Elements	Ref. Elements	Test Elements
1	0.053	0.056	0.099	0.068
2	0.129	0.097	0.184	0.111
3	0.080	0.065	0.155	0.101
4	0.140	0.042	0.172	0.127
5	0.076	0.098	0.338	0.232
6	0.170	0.083	0.259	0.176
7	0.094	0.082	0.204	0.099
8	0.094	0.092	0.191	0.092

Based on the above analysis it is concluded that the inclusion of the above test elements in the FSV core does not cause any safety problems and significantly improves the stress margin in these elements.

5.5. GRAPHITE DIMENSIONAL CHANGE

During core operation, the graphite test elements will be exposed to fast neutron irradiation which will induce dimensional changes in the graphite. Because of the differences in dimensional change behavior between H-451 and H-327 graphite, an analysis was performed to calculate the expected axial and radial dimensional changes of new test elements, and the results were compared with the changes expected in the elements being replaced. Analysis was performed to calculate the time history of expected axial and radial contraction of the fuel test elements and of the fuel elements they replace. Table 5-7 shows the maximum axial and radial shrinkage for all of the eight test elements and the shrinkage of the elements they replace. The maximum axial shrinkages of all test elements are less than those of the corresponding elements they replace. The maximum radial shrinkage rates for H-451 become greater than for H-327. When H-327 graphite is exposed to higher fluence at temperatures greater than 850°C, it ceases to shrink and begins to expand. Consequently, FTEs 1 through 5 will shrink less than the H-327 elements they replace and FTEs 6, 7, and 8 will finish life with a resultant greater radial shrinkage than the elements they replace would have exhibited. The maximum test element expansions at reactor operation for the radial and axial directions are calculated to be 0.5% and 0.4%, respectively. This is primarily a result of thermal expansion. The maximum corresponding expansions at reactor shutdown are smaller and calculated to be 0.06% and 0.01% (Table 5-7).

Because of the differential axial dimensional change within each element, the fuel elements adjacent to the side reflector and near rodded regions will experience a small amount of bowing in addition to the normal axial and radial contraction. The bowing is a result of the large radial fast neutron flux gradient across the element. Table 5-8 shows the maximum

TABLE 5-7
COMPARISON OF AXIAL AND RADIAL SHRINKAGES (PERCENTAGE) OF TEST ELEMENTS AND THE REFERENCE ELEMENTS THEY REPLACE AT EOL

Test Element Identification	Reference Elements		Test Elements	
	Axial	Radial	Axial	Radial
FTE-1	0.06	0.12	0.01[a]	0.06[a]
FTE-2	0.51	0.34	0.21	0.05
FTE-3	0.98	0.43	0.51	0.22
FTE-4	1.71	0.44	0.87	0.42
FTE-5	0.77	0.48	0.50	0.24
FTE-6	2.84	0.32	1.79	0.96
FTE-7	2.73	0.51	1.79	0.99
FTE-8	2.92	0.39	1.85	1.01

[a] Expansion. This only occurs at very low fluence levels at low operating temperatures. (See Fig. 5-12).

TABLE 5-8
COMPARISON OF END-OF-LIFE CENTERLINE BOWING IN TEST ELEMENTS AND THE REFERENCE ELEMENTS THEY REPLACE [mm (in.)]

Test Element Identification	Reference Elements	Test Elements
FTE-1	0.041 (0.0016)	0.056 (0.0022)
FTE-2	0.213 (0.0084)	0.086 (0.0034)
FTE-3	0.950 (0.0374)	0.488 (0.0192)
FTE-4	0.650 (0.0256)	0.442 (0.0174)
FTE-5	1.613 (0.0635)	1.295 (0.0510)
FTE-6	2.276 (0.0896)	1.463 (0.0576)
FTE-7	0.386 (0.0152)	0.251 (0.0099)
FTE-8	0.363 (0.0143)	0.345 (0.0136)

expected bow of the test elements and the bow of the elements they replace. The results show that the expected bowing of test elements is about the same as that of the elements they replace.

The eight test elements are proposed to be located in the third layer from the top of the active core. As a result, the top and bottom surfaces of the test elements will have to interface and align with partially irradiated fuel elements. The FSV dowel/socket system was designed such that an element irradiated to its full exposure can easily align with a fresh fuel element. To assure that these dowel/socket systems match with each other, an analysis was performed to calculate the dimensional changes of each test element and of the partially irradiated fuel elements at top and bottom of each test element. The result of this analysis indicates that the minimum clearance between dowel and socket at any face of any test element is about the same, but never worse, than that of the reference elements. Therefore, it is concluded that the alignment of fresh test elements with partially irradiated fuel elements will cause no problem.

5.6. FUEL ROD PERFORMANCE

5.6.1. Dimensional Stability

The fuel rods fabricated for the FSV-FTEs are of the LHTGR type with fissile, fertile, and graphite shim particles bonded together in a carbonaceous matrix. All components undergo dimensional changes during irradiation. It has been demonstrated during the FSV fuel development effort that the matrix component shrinks more rapidly than the fuel particles. Therefore, the bulk fuel rod shrinkages are controlled by the dimensional change of the close-packed constituent particles including shim (Refs. 24, 25, and 26). Using this premise, a computer code has been developed to calculate the irradiation-induced LHTGR fuel rod dimensional changes as a function of the irradiation conditions. The model assumes the particles in the rod are in point-to-point contact (close-packed array) and the rod dimensional change is isotropic. The percent dimensional change of a rod

during irradiation is assumed equal to one-third of the percent volume change of the constituent particle types and can be calculated using Eq. 5-1 if the dimensional change behavior of the various particle types as a function of the irradiation conditions is known:

$$\%\Delta\ell/\ell_o = 1/3 \sum_i^n x_i \, (\%\Delta V/V_o)_i \quad , \tag{5-1}$$

where $\%\Delta\ell/\ell_o$ = percent linear dimensional change of the fuel rod,
$\%\Delta V/V_o$ = percent volume change of the i^{th} particle type,
x_i = particle volume fraction of the i^{th} particle type,
n = number of fuel particle types.

The irradiation-induced volume change of each particle type is calculated using separate subroutines. For the BISO particles the same analytical stress model employed in design studies is used. TRISO particle dimensional changes are calculated assuming that only the outer pyrocarbon shrinks. Shim particle dimensional variations are calculated using Eq. 5-2,

$$\frac{\Delta V}{V_{o_{isotropic}}} = 2\left(\frac{\Delta\ell}{\ell_o}\right)_{radial} + \left(\frac{\Delta\ell}{\ell_o}\right)_{axial} \tag{5-2}$$

and irradiation data on bulk dimensional changes of similar graphite stock.

A comparison has been made between measured and predicted dimensional changes for rods containing LHTGR-type particles irradiated in capsules P13M, P13N, P13P, P13R, and P13S; HRB-4, -5, -6, and HT-24, -25 (Refs. 27, 28, 29). There are minor differences between calculated and observed dimensional change. These differences are related to the fact that the particle dimensional change data used in Eq. 5-1 is derived from readily available unrestrained PyC dimensional change measurements, but the PyC in the particles is restrained and exhibits a somewhat different dimensional change behavior.

In view of this systematic error in calculated dimensional change, the code calculations have been normalized to the empirical data using an experimentally derived correction factor. Data in Refs. 27, 28, and 29 show rods containing three different near-isotropic graphite shim materials have similar dimensional change profiles. This, plus the fact that the uncertainties fall into a relatively narrow band, justifies using a single correction factor for all rod compositions. This factor is defined as the average fractional difference between calculated and observed shrinkages; i.e.,

$$\left(\frac{D_{obs}}{D_{calc}}\right) \quad .$$

The resulting empirical correction factor is 0.64 ± 0.20; i.e.,

$$\Delta D/D_{o_{actual}} = (0.64 \pm 0.20) \quad \Delta D_o/D_{pred} \quad .$$

a fuel rod dimensional change correction factor is being used in current core design studies and in the safety analysis for the FSV FTEs.

5.6.2. Thermal Conductivity

The thermal conductivity of HTGR-type fuel rods has been studied to show the effect of the expected range of fuel and shim particle compositions on conductivity (Ref. 7). The thermal conductivity of unirradiated prototype HTGR fuel compacts containing four different shim contents was determined in the temperature range 950° to 1250°C, the thermal conductivity of each compact type decreased approximately 20%, as shown in Fig. 5-16.

The lowest thermal conductivities observed were for the unshimmed compact; the conductivity reached a minimum value of 0.0165 cal/cm-sec-°C (4 Btu/ft-hr-°F) at approximately 1250°C. The value of 0.0165 cal/cm-sec-°C was selected for the thermal analysis of FTE-1 through FTE-8 fuel temperatures as a conservative low estimate. This same value was used in the FSV

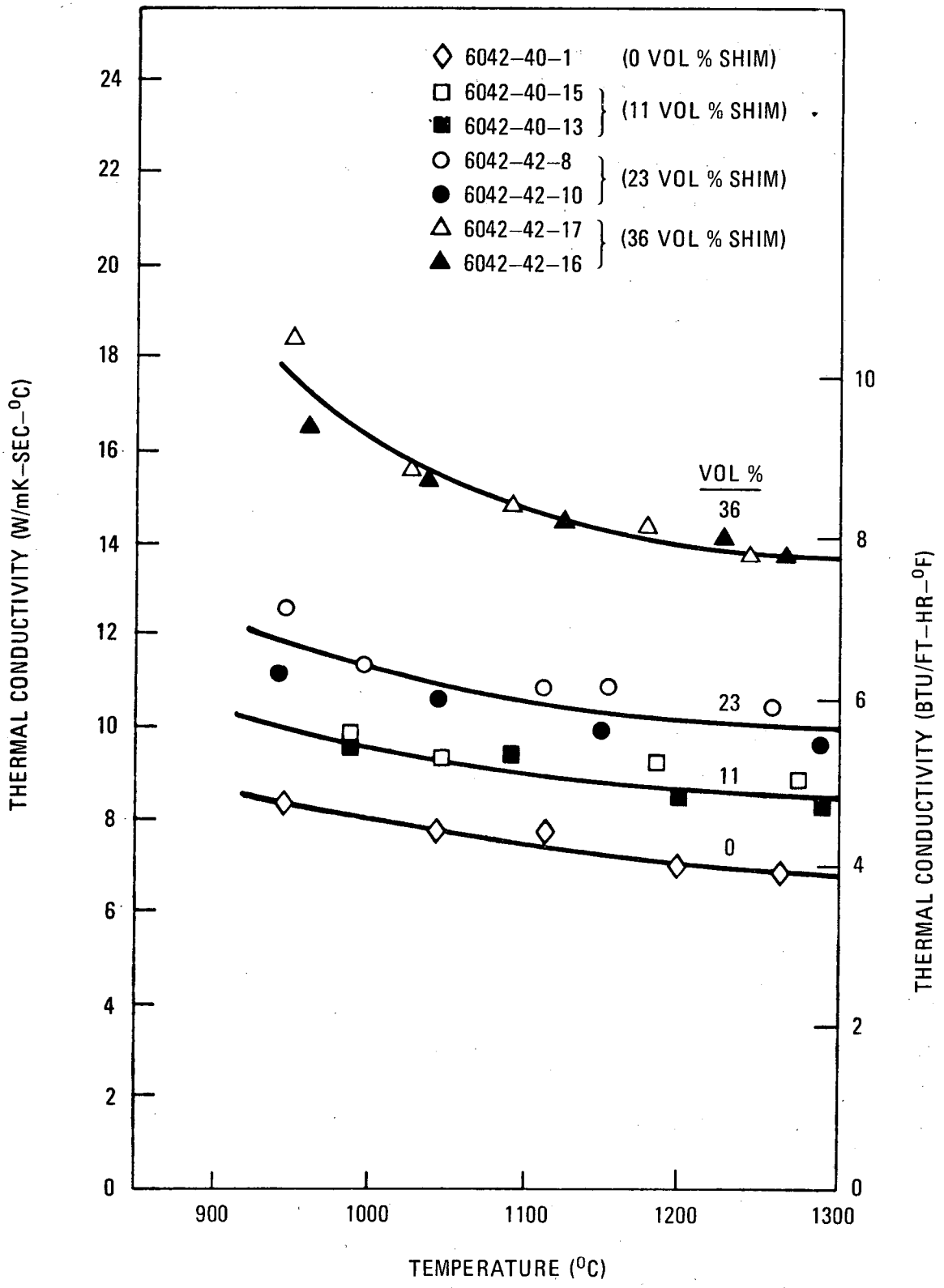

Fig. 5-16. Thermal conductivity of prototype LHTGR fuel rods versus temperature (Th/U = 20) (Ref. 30)

FSAR. The highest thermal conductivity observed was for the compact shimmed 36 vol %. These compacts reached a value of approximately 0.033 cal/cm-sec-°C (8 Btu/ft-hr-°F) at 1250°C. The lowest thermal conductivity observed for the 23 vol % shimmed compact, which represents the "average" fuel compact for an HTGR core, was nearly 0.025 cal/cm-sec-°C (6 Btu/ft-hr-°F).

The effect of irradiation on the thermal conductivity of fuel compacts was estimated by considering the irradiation effects on the individual components of fuel compacts (i.e., the PyC and SiC coatings on the fuel particles), the graphite shim particles, and the graphitic matrix (Ref. 30). The calculations indicate that the thermal conductivity may decrease with irradiation in the low-temperature range of operation of the fuel (600° to 1000°C) and increase or remain constant in the upper fuel temperature range (1000° to 1400°C).

In the upper temperature range, where high conductivity is of greatest importance to minimize peak fuel temperatures, the thermal conductivity of an average fuel rod of the type in FTE-1 through FTE-8 will remain well above the value of 0.0165 cal/cm-sec-°C (4 Btu/hr-ft-°F) used in thermal design as shown in Fig. 5-17 from Ref. 30. THis estimate is consistent with results from postirradiation measurement of thermal conductivity in fuel rods (Ref. 30).

5.7. FUEL PERFORMANCE MODELS

The coatings on individual fissile and fertile fuel particles are the primary barriers to the release of fission products from the fuel particles. Low fission product release rates therefore imply a high degree of particle coating integrity. An extensive irradiation and out-of-pile test program has shown that particle survival rates in excess of 99% can be expected from similar fuel operating in an HTGR environment. The test programs have identified four phenomena that control UC_2 and ThO_2 fuel particle performance in the thermal/nuclear environment of an HTGR core (Refs. 8, 9, and 16).

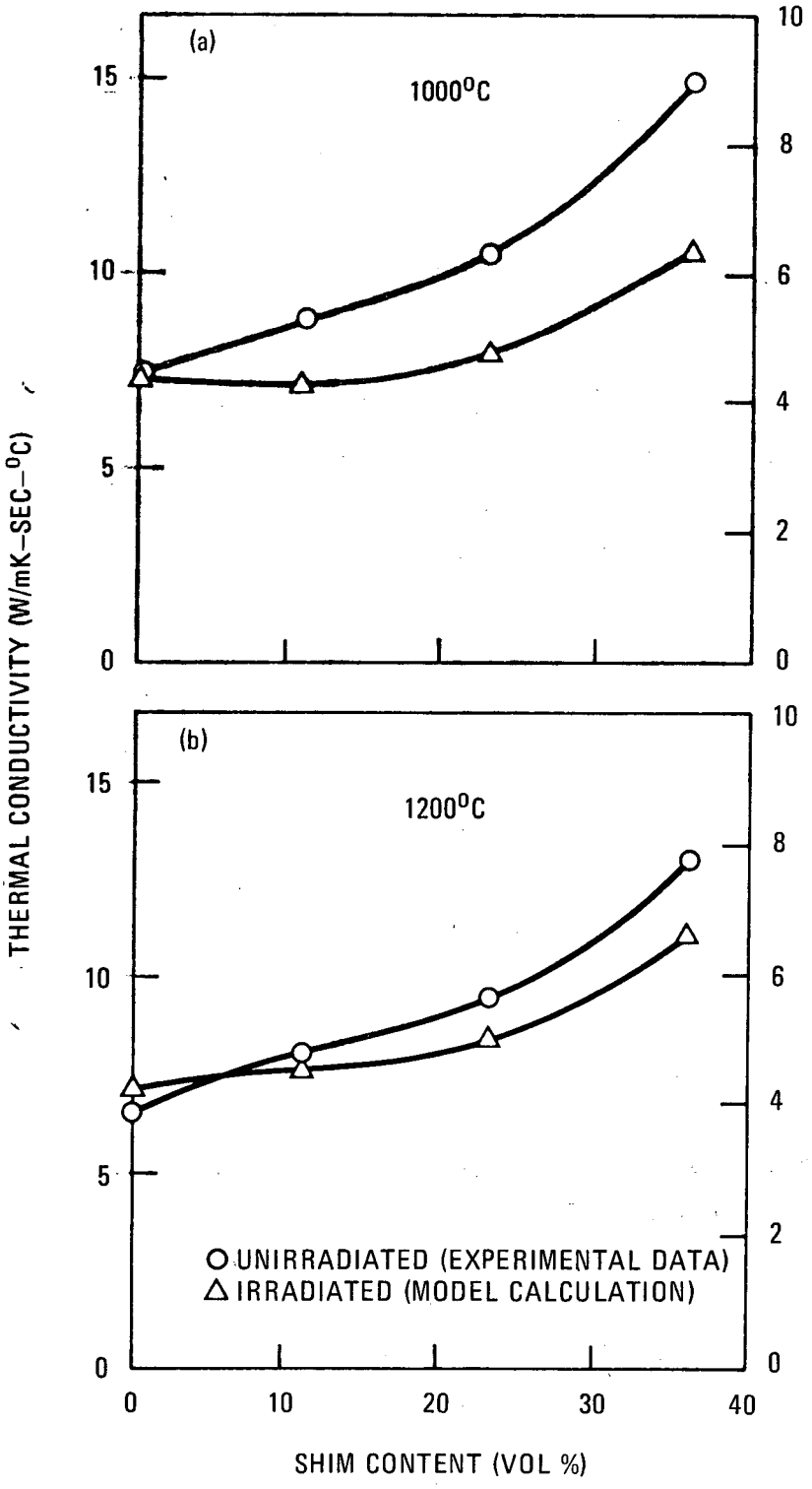

Fig. 5-17. Thermal conductivity curves for unirradiated and irradiated LHTGR fuel rods, irradiation fluence = ∿3 x 10^{21} n/cm^2, irradiation and measurement temperature = (a) 1000°C and (b) 1200°C (Ref. 30)

The first phenomenon, kernel migration (amoeba), occurs in both the TRISO UC_2 fissile fuel and the BISO ThO_2 fertile fuel. Kernel migration is primarily a function of temperature and temperature gradient and can result in fuel coating failure as kernels migrate completely through the outer structural layers.

The second phenomenon, pressure vessel rupture of both the BISO and TRISO coatings, can occur as increasing fission gas pressures cause the coatings to be stressed beyond failure limits. The particles most susceptible to pressure vessel failure have large kernels and thin coatings. Particle design criteria are established to essentially eliminate pressure vessel failure in fuel meeting HTGR specifications during steady-state reactor operation.

A third phenomenon that limits fuel performance is the high temperature chemical behavior of TRISO fuel. At temperatures in the range 1600° to 2000°C, the SiC coating layer on TRISO fuel is subject to attack by rare earth fission products. The SiC layer degradation can lead to premature pressure vessel failure of the TRISO coatings.

The fourth phenomenon that contributes to fuel failure is the presence of occasional fabrication defects (missing and defective coating layers) which are allowed by the fuel specifications. Table 5-9 compares the defective coating limits for FSV and LHTGR fuel particles.

TABLE 5-9
SPECIFICATION LIMITS FOR MISSING OR DEFECTIVE COATING

Defective Coating	$(Th,U)C_2$ TRISO (FSV) (%)	UC_2 and WAR UC_xO_y TRISO (LHTGR) (%)	ThO_2 and ThC_2 TRISO (FSV) (%)	ThO_2 BISO (LHTGR) (%)
Inner PyC	0.1	0.3 Total	0.1	0.2 Total
SiC	0.3		1.0	
Outer PyC	0.1		0.1	

The test elements will contain four types of fissile fuel and two types of fertile fuel as shown in Table 4-3. Specifications used to evaluate test fuels assumed kernel and coating properties that were acceptable for either FSV or LHTGR fuel. Additionally, the same set of specifications were assumed for fuel evaluation whenever there were multiple suppliers for a single fuel type. Consequently, fuels acceptable for the test arrays in FTE-2, -4, and -6 were considered to be identical, and a single set of performance models were used for each particle type independent of fuel supplier.

Fissile fuel performance models developed for the VSM UC_2 TRISO particle, which are described in Ref. 17, were also applied for the GSP UC_2 and WAR UC_xO_y TRISO particles. The models in Ref. 17 will give a conservative estimate of TRISO WAR fuel performance because of two advantages of the WAR fuel kernels relative to VSM kernels. The first advantage is that the WAR kernels are porous and less subject to kernel migration than dense VSM kernels. It has been shown that unirradiated WAR kernels do not migrate in a thermal gradient (Ref. 31). Although tests designed to define the kernel migration behavior of irradiated WAR fuel kernels are in progress, it will be conservatively assumed that they migrate at the same rate as unirradiated VSM UC_2 kernels. Migration of UC_2 relative to other fuel compositions is shown in Fig. 5-18. The second performance advantage of the WAR particles is related to reactions between rare earth and lanthanide fission products and the SiC layer of TRISO fuels. These fission products escape from VSM UC_2 kernels and react with the SiC layer of TRISO coatings at temperatures exceeding 1500°-1600°C. The small quantity of oxygen in the WAR kernels ties up the rare earths and lanthanides as oxides, thereby reducing or eliminating reactions between SiC and rare earth or lanthanide fission products. Both in-pile and out-of-pile tests have qualitatively demonstrated this improved feature of WAR performance. Until the kinetics of the reaction have been defined, it will be conservatively assumed that failure by SiC-fission product reactions occurs at the same rate in WAR UC_xO_y and VSM UC_2 TRISO fissile fuel.

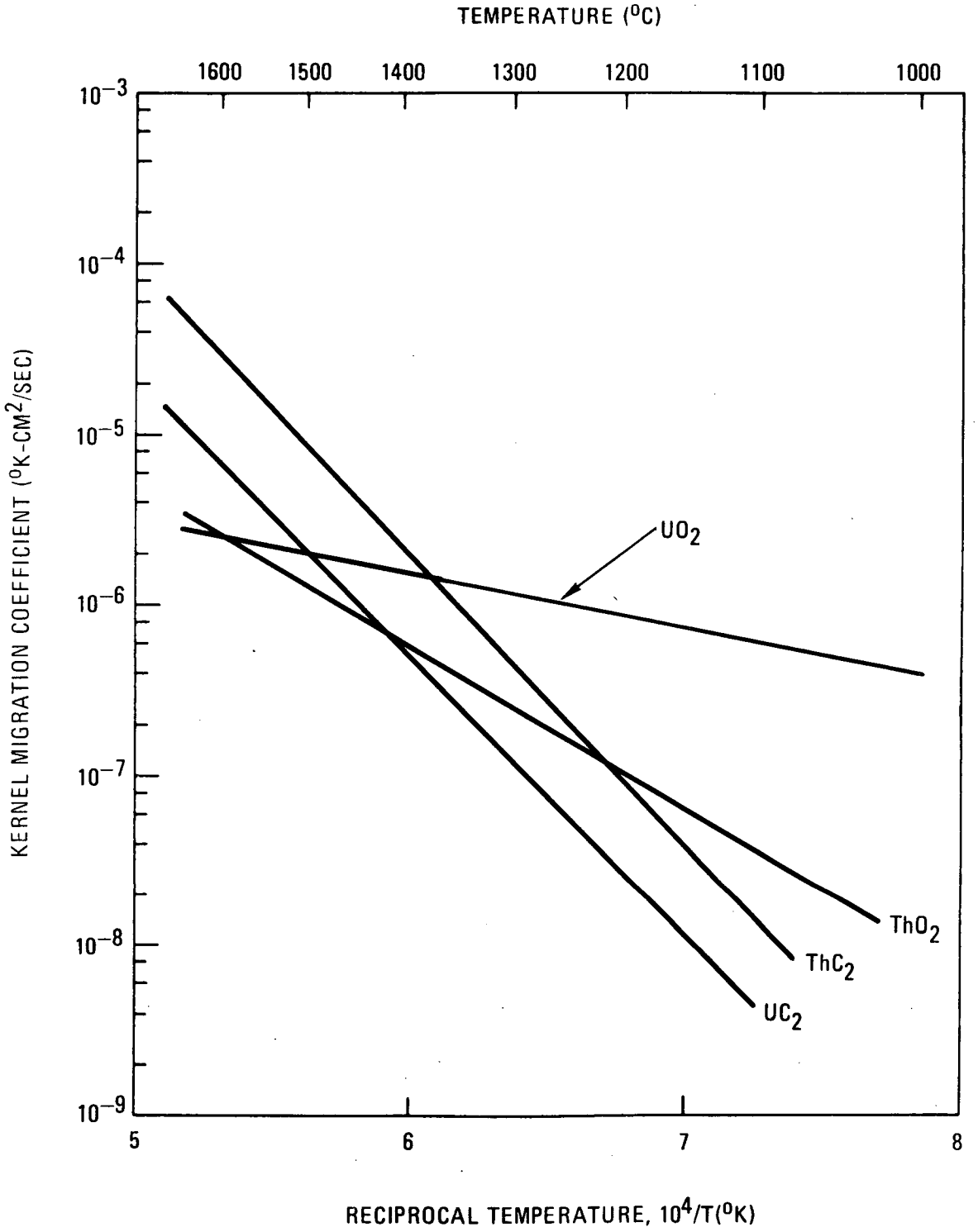

Fig. 5-18. Fuel kernel migration coefficients versus inverse temperature ($10^4/T$) determined from in- and out-of-pile experiments (Ref. 9)

Fuel performance models for the ThO_2 BISO fertile fuel are also given in Ref. 7. These have been discussed extensively in the LHTGR Safety Analysis Report for the Standard Plant (GASSAR), Ref. 8.

Coating failure assumptions for the ThO_2 TRISO particle were based on a combination of mechanisms identified for both the ThO_2 BISO and the UC_2 TRISO particles. For the first phenomenon, kernel migration for the ThO_2 TRISO was taken to be the same as the ThO_2 BISO particle based on similar kernel diameters and densities. For pressure vessel rupture, the ThO_2 BISO and TRISO are assumed to behave identically for temperatures less than 1250°C. The behavior of ThO_2 TRISO above 1250°C is assumed to follow temperature dependence relationships developed for the UC_2 TRISO fuel, which have been based on available irradiation data above this temperature level. Fission product attack of the SiC layer in the ThO_2 TRISO particle was conservatively assumed to occur in the same manner as in the UC_2 TRISO particle. Data on UC_2 SiC failure were normalized by fission product density to arrive at the ThO_2 model. Lastly, the specification limits on defective coatings for the ThO_2 TRISO particle will be the same as the ThC_2 TRISO in FSV (Table 5-9). Coating failure rate due to these defects is treated the same as the UC_2 TRISO particle and is assumed to increase linearily with burnup.

The application of the above assumptions to the test element fuel performance under FSV conditions is presented in Section 5-2.

6. SAFETY ANALYSIS

6.1. INTRODUCTION AND SUMMARY

In this section the events and accidents previously analyzed in Chapter XIV of FSV FSAR (Ref. 32) are reviewed to determine if substitution of the eight fuel test elements (FTE) in the FSV reload cores could alter the predicted event consequences. The results of an initial qualitative review are shown in Table 6-1. Those bounding case events with a potential for pertubation by the test elements were selected for further analysis. They are:

1. Reactivity accidents - rod withdrawal accident (RWA).

2. Loss of normal shutdown cooling.

3. Moisture inleakage.

4. Loss of forced cooling (LOFC).

5. Primary coolant system ruptures - design basis depressurization accident (DBDA).

These cases were analyzed with respect to (1) the behavior of the eight fuel test elements under accident conditions, and (2) the possible changes which these elements could cause in the accident conditions or consequences reported in the FSAR.

From these analyses, key factors which influence the performance of the test elements in accident situations were determined to be:

TABLE 6-1
POTENTIAL EFFECTS OF FUEL TEST ELEMENTS ON FSV FSAR ACCIDENT PREDICTIONS

FSAR Chapter XIV Event	Potential Effects on Event Analysis Due to FTEs in Core
14.1 Environmental Disturbances	
Earthquake	None - Any reactivity effect would be bounded by rod withdrawal events. (FSAR)
Wind effects Flood Fire Landslides Snow and Ice	The core is not affected by these events.
14.2 Reactivity Accidents and Transient Response	
Summary of Reactivity Sources	
Excessive removal of control poison Loss of fission product poisons Rearrangement of core components Introduction of steam into the core Sudden decrease in reactor temperature	Reactivity insertions in these events are less than rod withdrawal events. (FSAR)
Rod withdrawal accidents	Evaluation required, see Section 6.2.1.
14.3 Incidents	
Incidents Involving the Reactor Core	
Column deflection and misalignment	No change from Section 3.3.12 of Ref. 32.
Fuel element malfunctions	Discussion in Section 5, Performance Analysis.
Misplaced fuel element	Since each element represents only 0.07% of the core, any effect would be insignificant.
Blocking of coolant channel	Since FTE graphite has a higher thermal conductivity, this incident would be less severe than Section 3.6.5.2 of Ref. 32.

TABLE 6-1 (Continued)

	FSAR Chapter XIV Event	Potential Effects on Event Analysis Due to FTEs in Core
	Control rod malfunctions	No change from Section 3.8 of Ref. 32.
	Orifice malfunctions	No change from Section 3.6 and 3.9 of Ref. 32.
	Core support floor loss of cooling	No change from Section 3.3.2.2 of Ref. 32.
	Incidents involving the primary coolant system	None
	Incidents involving the control and instrumentation system	None
	Incidents involving the PCRV	None
	Incidents involving the secondary coolant and power conversion system	None
	Incidents involving the electrical system	None
	Malfunctions of the helium purification system	None
	Malfunctions of the helium storage system	None
	Malfunction of the nitrogen system	None
14.4	Loss of Normal Shutdown Cooling	Evaluation required, see Section 6.2.2.
14.5	Secondary Coolant System Leakage	
	Steam leaks outside the primary coolant system	None
	Leaks inside the primary coolant system (moisture inleakage)	Evaluation required, see Section 6.2.3.
	Steam generator leakage accident consequences	Evaluation required, see Section 6.2.3.

TABLE 6-1 (Continued)

FSAR Chapter XIV Event	Potential Effects on Event Analysis Due to FTEs in Core
14.6 Auxiliary System Leakage	
Failures involving the helium purification system	
Loss of both purification trains	Any possible effects would be much less than DBDA.
Failure of regeneration line w/simultaneous valve failure and operational error	
Accidents involving the gas waste system	
Fuel handling and storage accidents	
Fuel handling accidents	FTE decay heat and activity levels are less than the highest power core elements assumed in FSAR analysis.
Fuel storage accidents	
14.7 Primary Coolant Leakage	Less than 14.11 (DBDA).
14.8 Maximum Credible Accident	Less than 14.11 (DBDA).
14.9 Maximum Hypothetical Accident	No change from 14.11.
14.10 Design Basis Accident No. 1 "Permanent Loss of Forced Circulation (LOFC)"	Evaluation required, see Section 6.2.4.
14.11 Design Basis Accident No. 2 "Rapid Depressurization/Blowdown (DBDA)"	Evaluation required, see Section 6.2.5.

1. The test fuel utilizes the same basic fissile and fertile isotopes as standard FSV fuel.

2. The graphite used in FTE-1 through FTE-8 has better structural and thermal properties (Ref. Section 5.4) than the graphite of the standard fuel element.

3. Test elements will not be placed in any rodded columns. Rod insertion interferences, therefore, need not be considered.

4. The FTE design criteria, manufacturing process control, and quality assurance provisions are the same as or better than those used for the standard FSV elements.

5. The fraction of test fuel in the core is small (0.4%); therefore, these elements have a minor effect on the overall consequences of any accident.

From these factors and the detailed analyses performed, it is concluded that fuel test elements FTE-1 through FTE-8 will not influence the overall transient consequences, nor will use of these elements have any significant effect on the health and safety of the public.

6.2. FUEL TEST ELEMENT EFFECTS ON ACCIDENT CONSEQUENCES AND PERFORMANCE DURING ACCIDENTS

6.2.1. Reactivity Events: Rod Withdrawal Accident (RWA)

The FSV reference RWA, as discussed in Section 14.2.2 of the FSAR (Ref. 32), occurs at the end-of-cycle (EOC) of an equilibrium core. The core is assumed to be operating at 100% of rated power and at steady-state when the most reactive rod pair (worth = 0.012 Δk) is withdrawn uncontrollably. An EOC equilibrium core is assumed because temperature coefficients of reactivity are least negative at this time, owing to the high

inventory of fission products and U-233 and the depletion of lumped burnable poison and U-235.

Changes in the reactivity worth of the core, control rod worth, power distribution, and fuel failure were evaluated for the test elements against the standard elements they replace.

6.2.1.1. Reactivity Effects and Power Distributions. The FTEs are identical to the normal fuel elements neutronically except for differences in the local power density. FTE-1, which is loaded into segment 2, has a higher power density than the reference fuel element being replaced, whereas the reverse is true for FTE-2 through FTE-5. These changes negligibly decrease core reactivity because the number of FTEs is small compared with the total number of fuel elements (8 test elements of 1482 total elements).

Introducing fuel test elements into the core will not alter the worth of any control rod. Since the total number of neutrons absorbed by the fuel is independent of the power distribution in a reactor operating at constant power, the FTEs will not change the number of these absorptions. Likewise, the absorptions (more specifically, the flux) in the control rods will not change significantly because the neutron diffusion length in the core is large compared with the dimensions of a fuel element. Therefore, the fractional absorptions, or worth, of all rods will not change.

Finally, substituting a fuel test element for a normal fuel element does not alter the behavior of the core immediately surrounding any of the test elements during a RWA. The reason is that steady-state power densities for fuel elements adjacent to the FTEs do not change appreciably from the reference. Therefore, the maximum power peaking experienced by these local fuel elements will not differ from that predicted for the FSAR reference case (Ref. 32).

It is evident, therefore, that the fuel test elements will not have a discernible effect upon the overall core behavior during a rod withdrawal accident.

6.2.1.2. Fuel Failure Considerations. The most severe reactivity accident is an uncontrolled withdrawal of the most reactive rod at the end of the first reload. The potential for fuel failure during this accident is enhanced minutely by the presence of FTE-1 because it has a higher power density, hence a higher steady-state temperature, than the replaced fuel element. The other FTEs have lower power density than the element replaced, and therefore are of less concern.

Even if all the particle coatings in FTE-1 were assumed to fail, the additional failures would be insignificant overall. The fuel fraction of FTE-1 is only 0.07% of the total core. For the FSV reference RWA with failure of the primary protection, it has been determined that up to 2% of the particles in the core could fail. Thus an additional 0.07% failures will not significantly affect the consequences of the RWA. However, a quantitative evaluation described below shows that only a small fraction of the fuel particles in FTE-1 may be subject to failure during the RWA and that the FTEs actually yield less radioactive release than the replaced reference fuel.

The power density of FTE-1 is 38% higher than the replaced fuel at beginning-of-cycle (BOC) but only 14% at EOC. Assuming the BOC power density for conservatism, the operating temperature is thus calculated to be 1253°C (2282°F) or 241°C higher than the reference fuel.

For the FSAR case with an assumed concurrent failure of the 140% overpower trip, the backup high reheat steam temperature trip would shutdown the reactor. Although the maximum temperatures in the core following this assumed accident do not occur in the region containing FTE-1, a conservative estimate of the temperature and fuel damage of the region was made. The temperature of the region containing FTE-1 was assumed to be the maximum core-averaged fuel temperature during the transient. This is conservative since the radial peaking factor of this region is less than 0.6. Superimposing the estimated region temperature upon the 241°C higher steady-state temperature of FTE-1 yields 1351°C (2464°F) for the temperature of FTE-1 in the case of the high reheat steam temperature trip. At peak FIMA and fluence,

the failure rate at 1351°C is about 0.6% in the test element versus the 0.8% fuel failure which would occur in a standard FSV fuel element at the FSAR-predicted maximum temperature of 1110°C. Fission product inventory is a function of the integrated power generated by a fuel element. The highest power test element, FTE-1, produces power over its six-month cycle at an average rate of 1.2 times that of the reference element which it replaces. Since the reference elements for FTE locations 1 through 5 would have been in the core six months longer than the test elements, the FTE-1 fission product inventory at EOC will then be only 60% of its reference element inventory used in the FSAR RWA analysis. Similarly, in test elements FTE-2 through FTE-5, the cycle duration and integrated power are less than that of elements being replaced. For FTE-6, -7, and -8, the cycle duration and integrated power are unchanged.

Since for all fuel test elements the product of fission product inventory and failed fuel fraction is less than or equal to that of the reference elements, total core releasable activity would not be significantly affected by inclusion of the fuel test elements.

It is concluded that the inclusion of FTEs in the FSV core does not alter the findings of the RWA analysis described in the FSAR for the normal reload cores.

6.2.2. Loss of Normal Shutdown Cooling

This accident is defined in Section 14.4 of Ref. 32 as the unavailability of the normal number of helium circulators, the loss of normal driving power for the helium circulators, or the unavailability of the economizer-evaporator-superheater sections of one or both steam generators. Loss of the reheater sections of one or both steam generators is the same as loss of normal helium circulator driving power, since the circulators are normally driven with reheat steam.

In the FSAR analysis of this accident, the most severe case (Section 14.412.1, Case B2) was determined to be cooling with one circulator propelled by the fire water system. In this case, a peak fuel temperature of 1193°C (2180°F) can occur locally in a few channels of the core approximately 9 hours after accident initiation. This represents a 67°C (120°F) decrease from the maximum fuel temperature during operation (Section 3.6.3.3 of the FSAR), due to the flattening of the local temperature peaks after the reactor trip. Since the normal operating temperature of the hottest test element, FTE-1, is less than that of the highest temperature core elements for which the FSAR prediction was made, the maximum temperature of FTE-1 during this accident will also remain below its normal operating temperature. Therefore, inclusion of the test elements in the reactor core will have no effect upon the FSAR predictions for this event.

6.2.3. Moisture Ingress

The analysis in Section 14.5.2 of Ref. 32 considers inleakage into the primary coolant system from an economizer-evaporator-superheater subheader or tube or from the helium circulator bearing water supply. All other water-containing systems in the proximity of the primary coolant system are at a pressure less than the helium pressure during operation at power and cannot leak inward. Design of the steam generator limits the steam and water inleakage flowrate to 15.4 kg/sec (34 lbm/sec) initially and decreasing to 10 kg/sec (22 lbm/sec) in about 5 sec.

The FSAR treats several moisture ingress cases. Of these, case 5, a steam generator subheader rupture compounded by concurrent failure of the moisture monitor system and a dumping of the wrong (non-leaking) steam loop, has the most potential for graphite oxidation and fuel hydrolysis in the shortest time following the accident. To evaluate the potential effect of the fuel test elements on the analysis of case 5, the following phenomena were investigated:

1. Steam-graphite.
2. Hydrolysis of failed fuel.

3. Potential change in fission product release due to 1 and 2.

6.2.3.1. Steam-Graphite Reactions. The steam-graphite reaction is dependent on five principal variables (Ref. 32):

1. Fractional burnoff of graphite.
2. Steam partial pressure.
3. Hydrogen partial pressure.
4. Catalyst concentration (Ba and Sr).
5. Graphite temperature.

These variables apply both for the H-327 non-isotropic needle-coke graphite in the FSV standard elements and for the H-451 near-isotropic graphite in the test elements. The steam-graphite reaction rates at various temperatures of these two graphite types are equal within experimental uncertainty over the temperature range of interest, 700° to 1300°C (1292° to 2372°F) (Refs. 8 and 13). As in the FSAR analyses, fractional graphite burnoff (item 1) was conservatively assumed to be 1% at time of accident initiation in this evaluation.

With these similarities in reaction rate versus temperature and burnoff, there will be no significant change in the steam or hydrogen partial pressures (items 2 and 3) during this accident due to the test elements. For these reasons, only the effects of variations in items 4 and 5 are subjects of comparison in this report.

The FTE power peaking factors shown in Fig. 5-1 illustrate that all test elements except FTE-1 will operate at power levels lower than, or equal to, the levels in the standard element which they replace. As a result, temperatures in test elements FTE-2 through FTE-5 are no higher than those in the elements they replace, as shown in Figs. 5-4 and 5-5. This factor would tend to produce a lower amount of graphite oxidation in these cooler elements. FTE-1 is located in region 25, the coolest in the core; the steady-state graphite temperature of this region is about 649°C (1200°F). Even with the increase in power factor, the graphite surface

temperature would not exceed the 871°C (1600°F) which is conservatively assumed in determining the reaction rate throughout the core in the FSV FSAR analysis (Ref. 32). Thus, the increase in power for this element will not increase its steam-graphite reaction rate above the FSAR-calculated core average value.

The effect of the barium catalyst concentration was conservatively evaluated. Whereas the Ba concentration employed in the FSAR for the reference fuel is 0.001 mg/g C in the graphite, it is expected to be different for the test elements which employ some BISO particle coatings. Although the BISO fuel rods constitute only about 7% of the rods in FTE-2, -4, and -6 and will not all be irradiated for the full 5.5 years, a conservative estimate of the Ba concentration was made assuming the entire FTEs contain a TRISO/BISO mixture and reside in the core for the full exposure. The methods and parameters for the large HTGR fuel described in Ref. 26 were employed to obtain a Ba concentration of 0.04 mg/g C.

Using this concentration, the reaction rate for the FTEs would be about 9 times greater than that of the reference fuel at 1600°F (FSAR Section 14.6.2.2) and would yield about a twofold increase in the mass of graphite reacted relative to the reference fuel (Ref. 34). Even if all six FTEs contained TRISO/BISO fuel, the net increase in amount of graphite reacted in the entire core would be only 0.4%. Therefore, the presence of FTEs does not effectively alter the amount of reaction products or alter the transients described in the FSAR with respect to PCRV pressures and margin to relief system setpoints.

6.2.3.2. Hydrolysis of Failed Fuel. Since FTE-7 and FTE-8 have original Segment 7 fuel, these elements will not change the original calculations. The effects of FTE-1 through FTE-6, which contain experimental fuel, were considered. It was found that the failed fuel particle fraction of the experimental fuel is less than that of the standard fuel (Table 5-2). Since only failed fuel can hydrolyze, this reduction in failed fuel inventory will tend to slightly reduce the total hydrolysis in the core.

During a moisture ingress event, the rate of hydrolysis and noble gas fission product release is dependent upon local fuel temperatures. Since the reactor would be automatically shut down in the first few seconds after the initiation of this event, the local temperature peaks would flatten out and approach the coolant temperature. The operating temperature differences between the test elements and the standard elements, shown in Table 5-2, would rapidly diminish and minimize any effect on fuel hydrolysis rates.

The conclusion is that the introduction of FTE-1 through FTE-8 will not adversely affect the original analysis for the FSV FSAR for steam ingress events. The FSAR values for total amount of graphite-steam reaction, cesium and other fission products released to the primary coolant, and fuel hydrolyzed will not be exceeded for these accident conditions.

6.2.3.3. Fission Product Release. An evaluation was performed for the effect on fission products released from the oxidized graphite. A conservative estimate of the Cs-137 concentration in the graphite of the BISO-bearing FTEs gives a fourfold increase over that of the reference fuel (Ref. 33). Applying this to the conservative estimate of burnoff in FTE-1 through FTE-6 yields a potential 2% increase in radioactivity release to the primary coolant during the accident, i.e., an increase from the FSAR value of about 62 Ci to 63 Ci. Since the transients do not lead to release from the PCRV, the presence of FTEs in the core does not affect the FSAR conclusions regarding the consequences of moisture ingress events.

6.2.4. Permanent Loss of Forced Cooling (LOFC)

This hypothetical event assumes permanent loss of forced circulation of primary coolant helium. This would require the extended failure of all four helium circulators, their steam and water drives, or their multiple sources of motive power, or failure of both the main steam and reheat steam sections of both steam generators.

Analyses of this event in Section 14.10 of the FSAR estimate 95% of the fuel particles in the core will suffer failed coatings when the core heats up. The analysis shows that the maximum predicted core hot region temperature is 2980°C (5396°F) during the event. If any of the test elements or standard FSV elements were to heat to this maximum temperature, 100% of the fuel coatings in that element would be expected to fail. As the test elements are not expected to achieve the maximum temperature, the expected coating failure rate would be the same or less than the standard fuel. Since the test fuel comprises only 0.4% of the core loading, any difference in fuel failure rates is insignificant and does not alter the FSAR conclusions for off-site dose consequences for this event.

6.2.5. Primary Coolant System Ruptures: Design Basis Depressurization Accident (DBDA)

Aspects of a DBDA which were investigated in Section 14.11 of the FSAR are:

1. Integrity of reactor internals.
2. Continuation of adequate primary coolant circulation.
3. Ingress of air.
4. Effects of operator actions.
5. Vertical thrust on the PCRV.
6. Effect on building pressure.
7. Radiological consequences.

Review of these aspects shows that only item 7 has the potential to be affected by the FTEs.

The radiological release from this postulated event would consist of the release of essentially all of the circulating primary coolant activity plus a small fraction (up to 1%) of the PCRV plateout activity which is potentially releasable. Contribution of the test elements to this activity can be estimated from the comparison of FTE versus standard FSV failed fuel fractions shown in Table 5-2. This comparison predicts that test elements

FTE-1 through FTE-6 all exhibit less fuel failure potential than their reference fuel counterparts with an average failed fuel fraction 30% of that in the elements being replaced.

Failed fuel predictions for FTE-7 and -8 are the same as for the standard fuel. These predictions indicate that the total fission product release from a DBDA could be slightly less with the test elements in the core. This reduction would be insignificant due to the small fraction of test fuel in the core. Thus, the predicted doses from this event remain, as presented in the FSAR, at least an order of magnitude below 10 CFR 100 guidelines with the test elements installed in the core.

7. RESEARCH AND DEVELOPMENT

7.1. FUEL TEST ELEMENT EXPERIENCE

Experience on the Peach Bottom reactor and contributions from foreign reactor programs have contributed significantly to the FSV fuel design (Ref. 2). This experience includes irradiation of numerous test elements under actual operating conditions which has added confidence to the accelerated capsule test results. The following sections provide a brief summary of recent test element experiments in Peach Bottom and Dragon (also see Table 2-3 for a description of these reactors).

7.1.1. Peach Bottom FTEs

A total of 33 test elements have been inserted into Peach Bottom core 2 by replacing standard driver elements. Sponsors of FTEs included ERDA under the National HTGR Fuel Development Program, the United Kingdom Atomic Energy Authority (UKAEA), KFA (Germany), the Electric Power Research Institute (EPRI), and GA. Recycle test elements (RTEs) were sponsored by ERDA under the National HTGR Fuel Recycle Development Program. An irradiation schedule for all test elements is given in Fig. 7-1, which includes information about sponsor, instrumentation such as in-pile purge and temperature measurements, and postirradiation examination (PIE) plans. The 40 MW(e) Peach Bottom HTGR underwent its scheduled final shutdown on October 31, 1974, and the postirradiation examination of fuel is in progress at the GA and ORNL hot cells.

In addition to the FTE and RTE program, some driver elements, control rods, and reflector blocks have been identified for destructive PIEs in the frame of core component surveillance requirements. A summary of sponsors and plans for all test element and surveillance work completed or to be conducted is shown in Table 7-1.

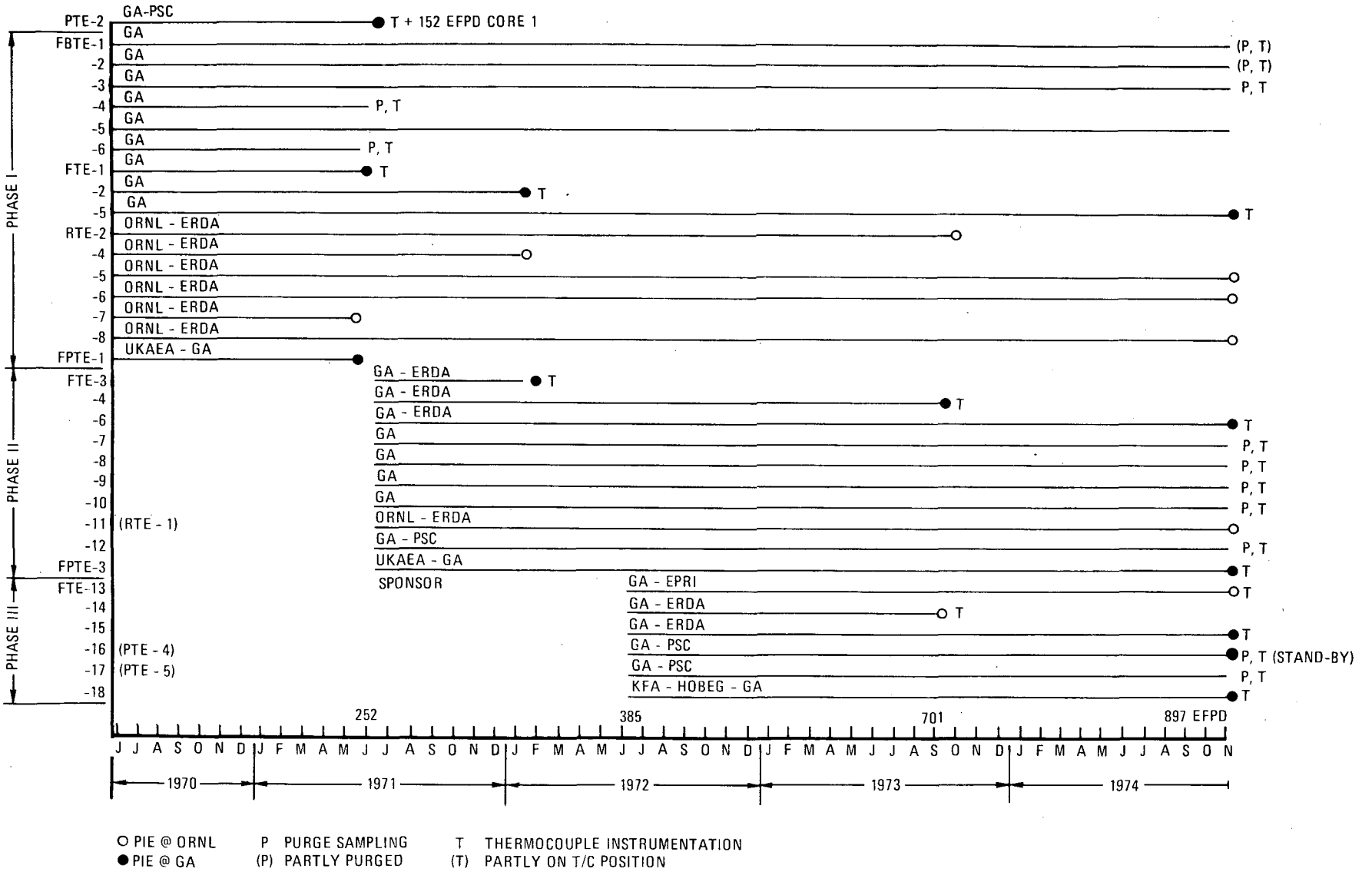

Fig. 7-1. Fuel test element irradiation schedule

TABLE 7-1
SUMMARY OF PEACH BOTTOM HTGR TEST ELEMENT AND SURVEILLANCE WORK ITEMS FOR CORES 1 AND 2

	Main Sponsor ERDA	Main Sponsor Private	Total Number
Fuel and recycle test elements			
Destructive PIEs (12 at GA, 8 at ORNL)	12	8	
In-pile montiored test elements (one standby for PIE)	--	12	
Element for gamma-scan only		1	
Total number of test elements under surveillance (26 FTEs, 7 RTEs)	12	21	33
Driver elements[a] for destructive PIE	2 + 5 with EOL γ scan	2 + 1[b]	
Driver elements[a] for gamma-scan only	30 (Phase II)	20 (Phase I)	
Total number of driver elements under surveillance	37	24	61
Control rods for destructive PIE	--	1 + 1[b]	2
Reflector elements for destructive PIE	1	2[b]	3
Reflector elements for gamma-scan only	--	2	2
Total number of integral core components under surveillance	50	51	101

[a] Seventeen driver elements have been instrumented; seven driver elements have undergone preirradiation metrology.

[b] Core 1 components; all other elements are core 2 related.

7.1.2. Dragon Reactor Large Block Experiments

Dragon is a 20-MW(t) high-temperature gas-cooled test reactor which first became critical in August 1964 (Table 2-3 and 2-4). The Dragon reactor consists of 37 replaceable assemblies, each of which can be further divided into seven hexagons (a central channel surrounded by six driver elements) with a nominal pitch of 6.35 cm and a total cross flat width (three hexagons) of 19.05 cm. Designed solely for experimental purposes, the reactor has irradiated approximately 250 fuel elements. A comparison of Dragon fuel with other HTGR Projects was given in Table 2-4. Other features of the reactor are discussed in Ref. 3.

Large block experiments and supporting center channel experiments in the Dragon reactor are summarized in Table 7-2. The tests include graphite block tests which are pursued by France (CEA), Germany (KFA), and British (UKAEA) sponsors, and molded-block tests sponsored by Germany. Figure 7-2 compares the four different integral block geometries referred in Table 7-2. The objectives of these tests and other supporting experiments on various graphite types are further discussed in Ref. 3.

Unfortunately, the Dragon Project terminated March 31, 1976 and with it all irradiation experiments listed in Table 7-2. All experiments are now scheduled for postirradiation examinations.

7.2. GRAPHITE DEVELOPMENT PROGRAM

Development and qualification of graphite materials for use in the HTGR is presently being performed under the ERDA-sponsored Graphite Development Program.

Results obtained to date on the graphite characterization program are presented in Refs. 10, 11, and 12, which include extensive irradiation data on the OG-1 and OG-2 graphite irradiation capsules. Table 7-3 shows the scope of the irradiation program for the most recently completed capsule test. Table 7-4 summarizes mechanical property data obtained on H-451 and other candidate fuel element graphites (Ref. 10).

TABLE 7-2
SUMMARY OF INTEGRAL BLOCK IRRADIATIONS IN DRAGON REACTOR

Experiment Designation	Sponsor	Sponsors Designation	Irradiation Period						Target Peak Fluence x 10^{21} (E > 0.18 MeV)	Design Temp. Peak in Time (°C)		Graphite Type	Reference Geometry
			Start			End				Fuel	Graphite		
			Charge	Core	Date	Charge	Core	Date					
MHGB-1A	CEA/BN	MHGB-1A	IV	6	6/73	V	11	1976	6.8	1100	980	P_3JHAN	FSV
MHGB-2A	CEA/BN	MHGB-2A	V	2	2/74	V	4	1974	1.3	1250	1100	P_3JHAN IE1-24	FSV
IB-1	KFA	DR-GB1	V	2	2/74	V	5	1975	2.0	1350	1150	AS2-500	1160 MW
IB-2	KFA	DR-GB2	V	6	4/75	V	21	1978	8.5	1300	950	AS2-500	1160 MW
IB-3	CEA	MHGB-3	V	8	12/75	V	23	1979	9.4	1350	1150	P_3JHA_2N	1160 MW
IB-4	UKAEA	IE 573	V	4	7/74	V	7	1975	2.0	1400	1090	SM2-24	UK MK III
IB-5	UKAEA	IE 574	V	8	12/75	V	19	1978	7.1				UK MK III
IB-6	KFA	DR-GB3	V	10	4/76	V	25	1980	8.5	1300	1100	AS2, ASI H-451	FSV
MB-1	KFA	DR-B1	IV	6	6/73	V	7	1975	3.4	1300	1000	Moulded Block	Block in carrier
MB-2	KFA	DR-B2	V	1	11/73	V	3	1974	1.5	1300	1000		
MB-3	KFA	DR-B3	V	2	2/74	V	15	1977	8.5	1300	1000		
MB-4	KFA	DR-B4	V	8	12/75	V	21	1978	8.5	1200	1150		FSV fuel element section
MB-5	KFA	DR-B5	V	8	12/75	V	11	1976	2.0	1200	1150		

Note: Because of the unexpected termination of the Dragon Project by March 31, 1976 all experiments with longer irradiation plans terminated at less than their target fluence.

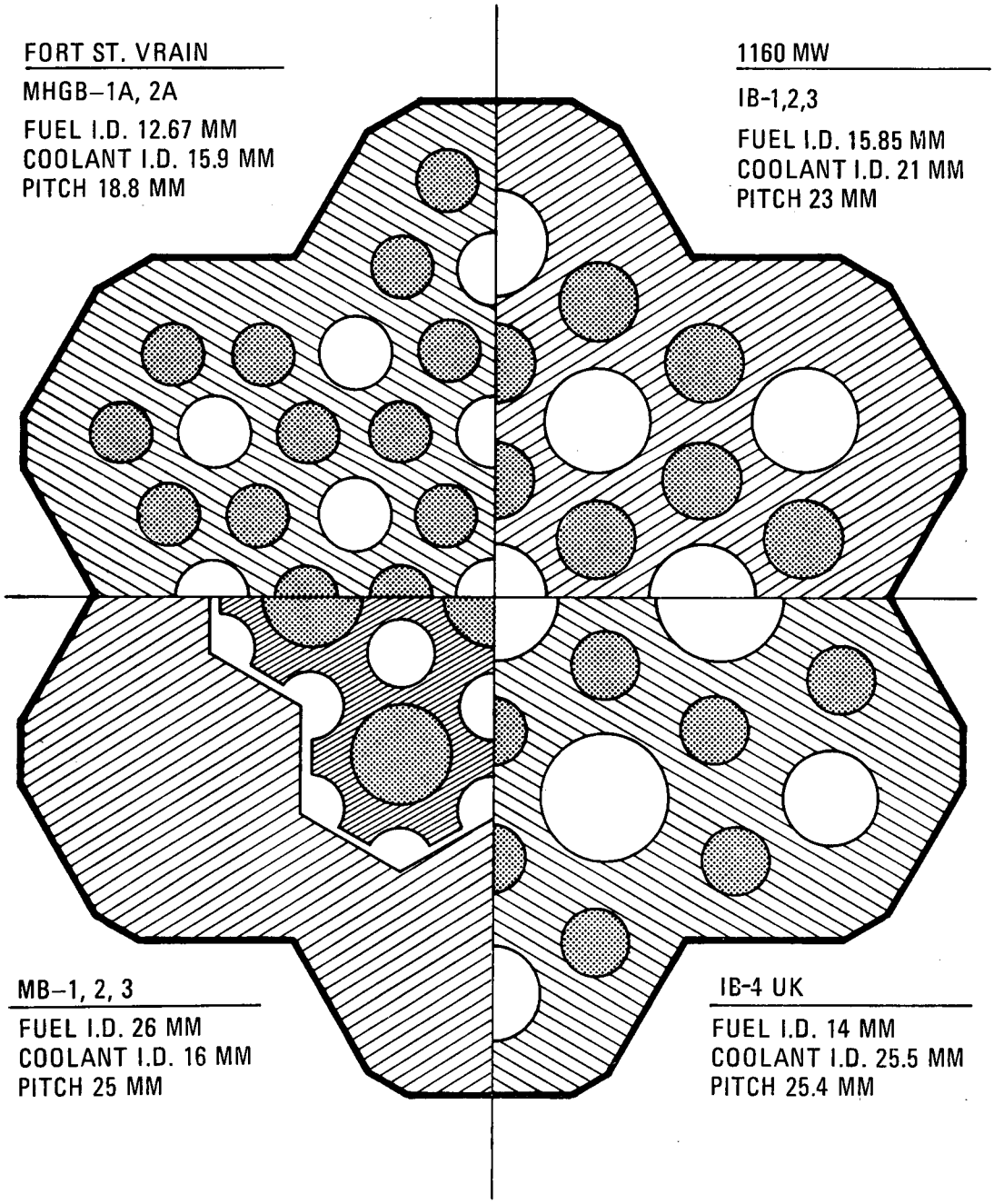

Fig. 7-2. Comparison of integral block test geometries in Dragon reactor

TABLE 7-3
GRAPHITES AND OTHER MATERIALS IRRADIATED IN CAPSULE OG-2

Designation	No. of Specimens	Type	GA Log Book Number	Form & Dimensions of Parent Sample	Source[a]	Raw Materials		
						Filler	Binder	Impregnant
Graphite H-451	428	Extruded, near isotropic	5651-28 5651-86	45 x 7.2-mm-diam x 86 x 3.6-mm-long (18-in.-diam x 34-in.-long) log	GLCC	Near-isotropic petroleum coke	Coal tar pitch	Petroleum pitch
H-429	69	Extruded, near isotropic	4974-104-A	22 x 8.6-mm-diam x 20 x 3.2-mm-long (9-in.-diam x 8-in.-long) log	GLCC	Near-isotropic petroleum coke	Coal tar pitch	Coal tar pitch
TS-1240	134	Extruded, near isotropic	5651-73	45 x 7.7-mm-diam x 86 x 3.6-mm-long (18-in.-diam x 34-in.-long) log	UCC	Near-isotropic petroleum coke		
H-327	204	Extruded, anisotropic	4974-3	(18-in.-diam x 34-in.-long) log	GLCC	Needle coke	Coal tar pitch	Coal tar pitch
P_3JHAN	66	Extruded, near isotropic	5651-53	20 x 3.2-mm x 20 x 3.2-mm x 20 x 3.2-mm (8-in. x 8-in. x 8-in.) cube	Pechiney	Near-isotropic coal tar pitch coke	Coal tar pitch	Coal tar pitch
2020	120	Isostatic molded, fine grained	5651-56	45 x 7.2-mm-diam x 15 x 2.4-mm-long (18-in.-diam x 6-in.-long) slab	SCC	Petroleum coke	(b)	(b)
H-328	1	Molded, near isotropic	--	43 x 1.8-mm-diam x 86 x 3.6-mm-long (17-in.-diam x 34-in.-long) log	GLCC	Gilso coke	Coal tar pitch	Coal tar pitch
H-430	1	Molded, near isotropic	--	21 x 8.4-mm-diam x 19 x 0.5-mm-long (8.6-in.-diam x 7.5-in.-long) log	GLCC	Near-isotropic petroleum coke	Coal tar pitch	(b)
IH-451	14	Extruded, near isotropic	5948-101	45 x 7.2-mm-diam x 86 x 3.6-mm-long (18-in.-diam x 34-in.-long) log	GLCC/GA	Near-isotropic petroleum coke	Coal tar pitch	Additional impregnation done at GA
H-451C	12	Extruded, near isotropic	5948-14	45 x 7.2-mm-diam x 86 x 3.6-mm-long (18-in.-diam x 34-in.-long) log	GLCC/GA	Near-isotropic petroleum coke	Coal tar pitch	Samples taken from cure-in-place experiments
565161	16	Experimental	5651-61	(b)	ORNL	(b)	(b)	(b)

TABLE 7-3 (Continued)

Designation	No. of Specimens	Type	GA Log Book Number	Form & Dimensions of Parent Sample	Source[a]	Description
Other Materials						
B_4C-G	18	Extruded boronated graphite	5646-13	7.6-mm o.d. x 254-mm-long (0.30-in. o.d. x 10-in.-long) rods	GLCC	FSV lumped burnable poison
			5646-91	6.3-mm o.d. x 229-mm-long (0.25-in. o.d. x 0.9-in.-long) rods	(c)	Oxidation-resistant shield compacts
MATRIX	4	Binder residue	--	(b)	GA	Coke residue from pitch binder in large HTGR fuel rod matrix
IMPCBN	1	Impregnant carbon	--	(b)	GA	Carbon residue from impregnant
GLSYCN	18	Glassy carbons	--	(b)	GA	Model carbons
PyC	13	Pyrolytic carbon	--	(b)	GA	Fuel particle coating material
SiC	4	SiC coatings	6041-7	(b)	GA	Fuel particle coating material
PALAR	1	Insulation	--	(b)	(b)	Palarite insulation
FPA	1	Insulation	--	(b)	(b)	Carbon foam insulation

[a] Great Lakes Carbon Company (GLCC); Union Carbide Corporation (UCC); Stackpole Carbon Company (SCC); Pechiney (France); General Atomic Company (GA); Oak Ridge National Laboratory (ORNL).

[b] Unknown.

[c] Rods fabricated by GLCC, GA, Norton Company, Carborundum Company.

TABLE 7-4
SUMMARY OF MECHANICAL PROPERTY DATA FOR GRAPHITES IRRADIATED IN CAPSULES OG-1 AND OG-2

Material	Orientation	Location in Log	Mean Irradiation Temperature (°C)	Fluence x 10^{-21} (n/cm^2) ($E > 0.18$ MeV)$_{HTGR}$	Ultimate Tensile Strength (Pa x 10^{-3}) Observed (± Std Dev)	Ultimate Tensile Strength (Pa x 10^{-3}) Predicted	Ultimate Tensile Strength (psi) Observed (± Std Dev)	Ultimate Tensile Strength (psi) Predicted	Young's Modulus (Pa x 10^{9}) Observed (± Std Dev)	Young's Modulus (Pa x 10^{9}) Predicted	Young's Modulus (10^{6} psi) Observed (± Std Dev)	Young's Modulus (10^{6} psi) Predicted
H-451	Axial	Midlength-center	--	0	10783 ± 931	--	1564 ± 135	--	7.86 ± 0.62	--	1.14 ± 0.09	--
			580-630	1.4	16713 ± 1827	14755	2424 ± 265	2140	18.13 ± 1.38	15.17	2.63 ± 0.20	2.2
			580-630	2.0	17134 ± 1220	14893	2485 ± 177	2160	15.31 ± 0.76	15.17	2.22 ± 0.11	2.2
			580-630	2.6	17106 ± 2220	15031	2481 ± 322	2180	17.51 ± 1.38	15.17	2.54 ± 0.20	2.2
			910-950	3.0	16348 ± 1868	14065	1271 ± 271	2040	14.20 ± 1.65	13.79	2.06 ± 0.24	2.0
			890-970	5.3	19147 ± 1800	15169	2777 ± 261	2200	17.58 ± 1.03	16.55	2.55 ± 0.15	2.4
			1340-1370	3.2	15396 ± 793	13790	2233 ± 115	2000	12.34 ± 0.55	13.10	1.79 ± 0.08	1.9
	Radial		--	0	11521 ± 1669	--	1671 ± 242	--	6.89 ± 0.34	--	1.00 ± 0.05	--
	Radial		900-950	2.8	18257 ± 1862	15100	2648 ± 270	2190	12.96 ± 0.90	12.41	1.88 ± 0.13	1.8
TS-1240	Axial	Midlength-center	--	0	10832 ± 1737	--	1571 ± 252	--	6.21 ± 0.69	--	0.90 ± 0.10	--
			620	1.2	12714 ± 3116	14755	1844 ± 452	2140	11.86 ± 2.21	11.72	1.72 ± 0.32	1.7
			765	1.7	14272 ± 2654	14479	2070 ± 385	2100	11.86 ± 1.17	11.03	1.72 ± 0.17	1.6
			920	2.5	14638 ± 1786	14272	2123 ± 259	2070	11.45 ± 0.90	11.03	1.66 ± 0.13	1.6
			1105	2.9	13093 ± 3723	14134	1899 ± 540	2050	11.65 ± 1.45	11.03	1.69 ± 0.21	1.6
	Radial		--	0	9536 ± 2055	--	1383 ± 298	--	6.21 ± 0.76	--	0.90 ± 0.11	--
	Radial		805	1.7	13452 ± 2255	12755	1951 ± 327	1850	10.34 ± 1.79	11.03	1.50 ± 0.26	1.6
H-327	Axial	Midlength-center	--	0	9108 ± 1089	--	1321 ± 158	--	8.96 ± 0.83	--	1.30 ± 0.12	--
			740	2.2	13403 ± 2600	12342	1944 ± 377	1790	15.51 ± 2.76	16.55	2.25 ± 0.40	2.4
			750-810	3.6	16706 ± 2351	12411	2423 ± 341	1800	19.10 ± 3.38	16.55	2.77 ± 0.49	2.4
			835-850	4.5	16789 ± 2489	12480	2435 ± 361	1810	17.58 ± 2.21	17.24	2.55 ± 0.32	2.5
			860-900	2.3	14665 ± 1937	11997	2127 ± 281	1740	20.82 ± 1.86	15.86	3.02 ± 0.27	2.3
			960-1035	2.7	13376 ± 2282	11928	1940 ± 331	1730	17.10 ± 2.76	15.86	2.48 ± 0.40	2.3
			940-1035	5.7	15320 ± 3227	13031	2222 ± 468	1890	16.00 ± 2.14	17.93	2.32 ± 0.31	2.6
			1040-1200	6.3	13810 ± 4033	12755	2003 ± 585	1850	16.00 ± 2.07	17.24	2.32 ± 0.30	2.5
			--	0	15072 ± 2020	--	2186 ± 293	--	13.31 ± 1.72	--	1.93 ± 0.25	--
			640-700	2.6	21732 ± 1917	20684	3152 ± 278	3000	26.54 ± 2.28	25.51	3.85 ± 0.33	3.7
			770-810	1.9	19216 ± 1717	20202	2787 ± 249	2930	21.37 ± 1.79	24.13	3.10 ± 0.26	3.5
			1050-1100	3.3	19457 ± 1751	19719	2822 ± 254	2860	22.27 ± 1.31	23.44	3.23 ± 0.19	3.4
	Radial		--	0	5654 ± 1972	--	820 ± 286	--	4.41 ± 0.55	--	0.64 ± 0.08	--
	Radial		960-1020	3.0	6633 ± 1365	7377	962 ± 198	1070	8.48 ± 1.38	7.58	1.23 ± 0.20	1.1

7.3. FUEL DEVELOPMENT

7.3.1. Introduction

The fuel irradiation program includes both accelerated tests in high flux reactors and non-accelerated tests in operating HTGRs. The accelerated tests typically contain 18 to 36 fuel rods in a simulated fuel rod hole, while non-accelerated tests are carried out in full-sized fuel elements with much larger numbers of rods of each fuel variety. Results of accelerated irradiation tests are normally conservative because they subject fuel to conditions of temperature neutron flux and particle power rating more severe than in an operating HTGR. Because of their conservative nature and timely production of data, the results of accelerated tests provide the primary basis for the fuel specification. On the other hand, non-accelerated tests such as FTE-1 through FTE-8 are utilized to demonstrate the adequacy of core design methods and satisfactory performance of the full-scale integral fuel systems after accelerated tests have provided confidence that the fuel specification is adequate to ensure satisfactory performance with minimum risk. The following discusses the results of the fuel development program relative to FTE-1 through FTE-8 fuel types in order to provide a measure of the large technical basis for current fuel specification and performance predictions.

7.3.2. Fuel Particles

The HTGR coated particle concept is very flexible and lends itself to an orderly development program leading to process improvements, greater performance potential, and fuel cycle economy. The fuel particle designs which will be included in the FTE-1 through FTE-8 series are shown in Table 7-5. All of these particle types are of the generic TRISO or BISO coating designs which have been included in numerous irradiation tests conducted over the last 12 years, as shown in Table 7-6. Almost 600 coated particle samples, 289 TRISO and 243 BISO, have been irradiated in 40 accelerated capsule experiments. Each sample contained between 300 and 5000 coated particles, all of which were examined before and after

TABLE 7-5
NOMINAL FUEL PARTICLE DESIGNS IN FSV FTE-1 THROUGH FTE-8

Particle Type	Kernel Material	Coating Type	Nominal Dimensions (μm)				
			Kernel Diameter	Buffer Thickness	IPyC Thickness	SiC Thickness	OPyC Thickness
Fissile	UC_2	TRISO	195	110	35	35	40
Fissile	WAR $U{\cdot}C_X{\cdot}O_Y$ [a]	TRISO	305-365	60	35	35	40
Fissile	$(3.6\ Th,U)C_2$	TRISO	150-250	50	20	20	40
Fertile	ThC_2	TRISO	350-450	50	20	20	50
Fertile	ThO_2	BISO	500	95	--	--	85
Fertile	ThO_2	TRISO	450	60	35	35	45

[a] Nominal value of X = 4.0 and Y = 1.0.

TABLE 7-6
COMPLETED GA IRRADIATION TESTS OF COATED PARTICLES

Test Number	Coated Particle Type(s)	Number of Samples			Peak Irradiation Test Conditions			Results	
								Samples Demonstrating Successful Performance[b,c]	
		TRISO[a]	BISO[a]	Total	Temperature (°C)	Burnup (% FIMA)	Fast Fluence E > 0.18 MeV (10^{21} n/cm^2)	TRISO	BISO
P13E to P13J	TRISO,BISO,other	34	27	70	900 to 1350	4 to 22	0.6 to 4.3	31	23
P13K	BISO,other		15	15	900,1300	59	2.9		10
P13L	TRISO,BISO	15	15	30	900,1300, 1500	75	7.8	4	3
P13M	TRISO,BISO	10	5	15	1350	70	6.9	9	3
P13N	TRISO,BISO	15	9	24	1350,1500	68	5.2	10	5
P13P	TRISO,BISO	20	12	32	1050,1350	70	8.5	17	0
P13R[d]	TRISO,BISO	9	12	21	1075	75	12.1	3	8
P13S[d]	TRISO,BISO	9	11	21	1075	75	11.8	5	9
P6 to P14	BISO,other		57	111	600 to 1450	7 to 18	0.1 to 5.6		29
P15	BISO		14	14	1200	24	3.8		11
P16	BISO		13	13	1300	15	2.5		10
P17	BISO		15	15	1175	27	4.8		15
P18	BISO		15	15	1125	26	8.4		15
P19	BISO		14	15	900,1100	23	6.7		14
P20	TRISO	15		15	900,1150	27	8.7	10	
P21	TRISO	15		15	900,1200	17	4.3	11	
P22	TRISO	30		30	900,1100	~23	7.7	13	
P23	TRISO,BISO	20	6	26	900,1250	13	2.3	18	6
F-25	TRISO	9		9	1250	~15	4.3	7	
F-26	TRISO	9		9	1200	20	7.0	5	
F-27	TRISO,BISO	7	3	10	1250	17	5.7	4	3
F-28	TRISO	9		9	1250	~15	4.0	6	
F-29	TRISO	9		9	1150	24	8.5	5	
F-30	TRISO	16		16	1250	20	10.6	9	
FR-1	TRISO	10		10	550,875	22	5.3	5	
FR-2	TRISO	10		10	550,1200	7	1.0	10	
FR-3	TRISO	10		10	600,1200	7	1.3	10	
HRB-2[e]	TRISO	8		8	750,1100	11	7.9	8	
Total tests		289	243	597	Successful tests to 1500°C	Successful tests to 75% FIMA	Successful tests to 12.1	197	164

[a] Samples with round, dense kernels, 150- to 500-micrometer nominal diameter.

[b] Less than 1% failure.

[c] A number of experimental particle batches designed to test the limits of coating parameters or particle performance have shown varying degrees of failure. No failures have been observed in samples containing particles designed to current specifications.

[d] Preliminary results, postirradiation examination in progress.

[e] Cooperative ORNL-GA irradiation experiment in HFIR.

irradiation. Of these, 197 TRISO and 164 BISO samples demonstrated successful irradiation performance (>99% survival) under conditions which covered the entire range of anticipated service conditions as shown in Table 7-7. A number of samples designed to test the limits of coating design and particle performance showed varying degrees of failure. These tests provide confidence in the performance models used to predict performance, and they form the basis for the fuel product specifications for coated particle fuels.

The discussion above indicates the depth of experience with the generic fuel designs. The technical status of the six specific particle types included in the FSV FTEs is discussed in the following text.

7.3.2.1. TRISO UC_2. The initial irradiation test of the reference LHTGR fissile particle, UC_2 TRISO, was conducted in capsule P13L. Fuel particles in this test exhibited satisfactory performance to exposures of 1250°C and 7.8×10^{21} n/cm^2 $(E > 0.18 \text{ MeV})_{HTGR}$ with fuel burnups of 75% FIMA. These data provide the primary basis for the current fissile particle design. Early in the test program a very conservative approach to the all-uranium fissile particle design was taken because of lack of experience with the extremely high burnups. Therefore, fuel kernels of 100 μm diameter and thus relatively low power and fission product inventories per particle were investigated. Larger diameter fissile particles were irradiated in capsules P13N (150 μm UC_2) and P13P (200 μm UC_2). In the latter test, LHTGR reference size particles (200 μm UC_2 TRISO) exhibited satisfactory performance to neutron exposures of 8.5×10^{21} n/cm^2 at 1350°C (Ref. 9). A recently completed series of tests now undergoing postirradiation examination (capsules P13R and P13S) has demonstrated survival of TRISO UC_2 reference design fissile particles from five different manufacturing batches to 12.1×10^{21} n/cm^2 at 1075°C (design) and ≥75% FIMA (Ref. 31). This fluence is more than 50% beyond the expected peak exposure in commercial reactors and provides high confidence that the UC_2 TRISO fuel in FTE-1 through FTE-8 will perform satisfactorily. A summary of the results of primary irradiation tests of UC_2 TRISO fuel is shown in Table 7-8.

TABLE 7-7
NUMBER OF COATED PARTICLE SAMPLES SUCCESSFULLY TESTED TO INDICATED EXPOSURE

	Fast Fluence (10^{25} n/m^2)							
Type	1	2	3	4	5	6	7	≥8
BISO	31	18	31	19	15	15	8	31
TRISO	21	21	19	38	29	9	23	38

	Burnup (% FIMA)												
Type	≤2	4	6	8	10	12	14	16	18	20	21-49	50-69	70-75
BISO	14	13	39	9	7	8	9	7	12	6	36	5	3
TRISO	15	2	13	7	9	27	9	25	11	6	37	22	15

	Temperature (°C)									
Type	500	600	700	800	900	1000	1100	1200	1300	≥1400
BISO		1		6	12	11	22	22	71	23
TRISO	6	3	7	1	24	30	36	29	63	

TABLE 7-8
PRIMARY IRRADIATION TESTS OF UC_2 TRISO FUEL

Test Number	Number of Samples	Peak Irradiation Test Conditions			Samples Demonstrating Successful Performance[a]
		Temp (°C)	Burnup (% FIMA)	Fast Fluence ($E > 0.18$ MeV)$_{HTGR}$ (10^{25} n/m^2)	
P13L	15	1400	75	7.8	4
P13M	10	1350	70	6.9	5
P13N	15	1350	68	5.2	5
P13P	18	1350	70	8.5	12
P13R	9	1075	75	12.1	3
P13S	9	1075	75	11.8	4

[a] Less than 1% failure of OPyC.

7.3.2.2. TRISO WAR. The fabrication of fuel from ion exchange resins consists of contacting a weak-acid (carboylic) resin (WAR) with uranyl nitrate solutions until all the active sites in the resin are filled. A de-oxygenation and conversion heat treatment follows the loading process in order to produce the final fuel kernel which consists of UO_2, UC_2, or $U{\cdot}C_x{\cdot}O_y$ dispersed in a glassy carbon matrix. On the basis of potential economic and performance advantages, the TRISO WAR fissile particle displaced BISO $(4Th,U)O_2$ as the reference recycle particle early in 1974 (Ref. 35). The relatively long lead time remaining to qualify the recycle particle permitted selection of the WAR of that time with the recognition that additional performance tests were needed. The TRISO UC_2 which had already demonstrated satisfactory performance was retained as the reference fresh fissile kernel. However, qualification of TRISO WAR for fresh fuel application was of immediate interest in order to maximize commonality between recycle and fresh fuel designs and processes. Consequently, WAR particles are being included in all current irradiation tests including the FSV FTEs.

Irradiation tests of TRISO WAR with O/U ratios in the range 0.6 to 1.4 have shown excellent irradiation performance, and the results are summarized in Table 7-9. The lanthanide fission products are effectively immobilized in the kernel by the formation of stable oxides so that SiC attack, which can be performance-limiting in TRISO UC_2 at high temperature (Section 5.7), is minimized (Ref. 36). Kernel migration, which represents a potential failure mechanism, is also reduced in WAR fuel relative to the TRISO UC_2. In view of these results, excellent performance during irradiation in the FSV FTEs is predicted.

7.3.2.3. $(Th,U)C_2$ TRISO/ThC_2 TRISO. The $(Th,U)C_2$ TRISO and ThC_2 TRISO particles are the reference fissile and fertile particle which were qualified for the FSV HTGR. The $(Th,U)C_2$ TRISO/ThC_2 TRISO fuel system has demonstrated satisfactory performance under conditions exceeding the most severe combinations of temperatures, burnup, and fluence experienced in FSV. The final development of these particles took place in a qualification capsule

TABLE 7-9
SUMMARY OF WAR TRISO IRRADIATION EXPERIENCE

Capsule	Number of Samples	Peak Irradiation Test Conditions			Samples Showing Successful Performance[a]
		Temp (°C)	Burnup (% FIMA)	Fast Fluence ($E > 0.18$ MeV)$_{HTGR}$ (10^{25} n/m^2)	
HRB-4	7	1250	16	4.5	No failures caused by WAR
HRB-5	7	1250	29	10.3	No failures caused by WAR
HRB-7	4	1500	80	5.9	3
HRB-8	4	1250	80	7.7	3
HRB-9	17	1250	80	7.9	8
HRB-10	17	1500	80	5.0	5
P13P	2	1050	60	6.4	2

[a] Less than 1% failure of all coatings.

series followed by a proof test of production fuel which was carried out successfully in capsule F-30 (Ref. 37). A brief summary of results from the most important capsules contributing to qualification of this fuel is shown in Table 7-10. Excellent performance during irradiation in the FSV FTEs can be assured.

7.3.2.4. BISO ThO_2. The design of the reference fertile ThO_2 BISO particles is based primarily on empirical irradiation results and dimensional change considerations. Initial design studies indicated that BISO fertile particles having very thick coatings exhibit large shrinkages, particularly early in life, while particles with thin coatings may experience net expansion at high burnups. These considerations have led to the selection of the current nominal coating thicknesses; i.e., 95-μm buffer and 85-μm outer pyrocarbon layers. In a series of ThO_2 BISO design screening tests, it was demonstrated that many BISO particle designs exhibit satisfactory performance, providing the anisotropy of the dense outer pyrocarbon layer is sufficiently low. More recent results from unbonded particle tests conducted in capsules P13R and P13S have shown that the 11 different ThO_2 BISO batches meeting current LHTGR design specifications had a 99.93% survival at 12.1×10^{21} n/cm^2, 1075°C, and 5.6% FIMA (Ref. 38). A summary of irradiation tests containing ThO_2 BISO particles is shown in Table 7-11.

A wide range of coated-particle microstructural and geometrical designs have been successful in these experiments, indicating that considerable latitude is available in fertile particle designs. Some samples were deliberately under-designed or had other properties leading to failure. These samples were important to the establishment of failure criteria and fuel specification limits.

Performance of the BISO ThO_2 particles under high-temperature conditions such as those produced by a loss of forced circulation of coolant has been predicted based on existing data (Ref. 38). Results of that work and the ongoing development provide confidence that the ThO_2 BISO particle will perform in an adequate and predictable manner during irradiation in FSV FTE-1 through FTE-8.

TABLE 7-10
PRIMARY IRRADIATION TESTS OF $(Th,U)C_2$ TRISO, ThC_2 TRISO FUEL

Test Number	Number of Samples	Peak Irradiations Test Conditions			Samples Demonstrating Successful Performance[a]
		Temp (°C)	Burnup (% FIMA)	Fast Fluence $(E > 0.18\ MeV)_{HTGR}$ $(10^{25}\ n/m^2)$	
F-25	9	1250	15	4.3	7
F-26	9	1200	20	7.0	5
F-27	7	1250	17	5.7	4
F-28	9	1250	15	4.0	6
F-29	9	1150	24	8.5	5
F-30	16	1250	20	10.6	9

[a] Less than 1% failure of OPyC.

TABLE 7-11
PRIMARY IRRADIATION TESTS OF ThO_2 BISO FUEL

Test Number	Number of Samples	Peak Irradiation Test Conditions			Samples Demonstrating Successful Performance[a]
		Temp (°C)	Burnup (% FIMA)	Fast Fluence $(E > 0.18\ MeV)_{HTGR}$ $(10^{25}\ n/m^2)$	
P13L	15	900-1300	4	7.8	3
P13M	5	1350	4	6.9	3
P13N	9	1350-1500	3	5.2	5
P13P	12	1050-1350	4	8.5	0
P13R	12	1075	5.5	12.1	8
P13S	11	1075	5.5	11.8	9

[a] Less than 1% failure of OPyC.

7.3.2.5. TRISO ThO_2. Qualifications of the TRISO coating concept have been completed utilizing a wide variety of design and kernel types (Refs. 9, 37). The FSV initial core has TRISO ThC_2 with essentially the same kernel size as the proposed ThO_2 TRISO. To accommodate CO pressure buildup during irradiation and to provide an additional performance margin, the coatings on the ThO_2 TRISO particles have been made substantially thicker.

The TRISO ThO_2 design is a primary candidate for future reload segments of FSV. Incorporation of this design into FTE-1 through FTE-6 test arrays will provide an excellent demonstration of performance in an operating reactor and confirmation of prediction based on accelerated capsule tests. A summary of accelerated irradiation tests for large- (>750 μm) diameter TRISO particles illustrating the depth of experience with this particle is given in Table 7-12. The substantial data based on the thermo/chemical performance of the ThO_2 BISO particles is also relevant to the ThO_2 TRISO (Ref. 16).

Prior to incorporation of TRISO ThO_2 into FSV FTE-1 through FTE-8, additional data demonstrating satisfactory TRISO ThO_2 performance will be available from capsules now under irradiation (GF-4/GF-5, HT-31, HT-33) and postirradiation tests being conducted in fuel development programs at GA. This work provides confidence that the expected satisfactory performance of the TRISO ThO_2 particle in FSV FTE-1 through FTE-8 is therefore assured.

7.3.3. Fuel Rods

The fuel rods for the LHTGR are fabricated by injecting molten pitch into a mold containing coated fuel particles and graphite granules (shim particles) which are used to adjust fuel loading in the rods. The green fuel rods are then placed in the graphite fuel block, carbonized, and then heated to 1600°-1800°C to outgas the binder materials. The process of curing and firing the rods in the fuel block is known as "cure-in-place." Cure-in-place represents a process simplification relative to curing in Al_2O_3 powder beds as done in the production of standard fuel for the FSV HTGR. A number of irradiation tests have demonstrated the satisfactory performance of fuel rods made by this improved process.

TABLE 7-12
PRIMARY IRRADIATION TESTS OF LARGE DIAMETER (750 μm TO 900 μm) TRISO FUEL

Test Number	Number of Samples	Peak Irradiation Test Conditions			Samples Demonstrating Successful Performance[a]
		Temp (°C)	Burnup (% FIMA)	Fast Fluence ($E > 0.18$ MeV)$_{HTGR}$ (10^{25} n/m^2)	
F-30	4	1050-1400	4.7	10.2	4
P13S	2	1050	11	11.6	1
GF-1	3	1250	8	4.4	2
GF-2	4	1250	0.7-8	3	4
GF-3	7	1050	5-11	12.8	5

[a] Less than 1% failure of OPyC.

Modest evolutionary changes in the LHTGR fuel rod manufacture, in addition to cure-in-place, have been introduced into the fuels which will be tested in the FSV FTE-1 through FTE-8 series. These changes are primarily directed toward process simplification and improvement of the uniformity of the fuel as summarized in Table 7-13. The fuel research and development program has been structured to qualify the fuel rod process by demonstrating that performance criteria are met. The criteria for satisfactory fuel rod performance are:

1. Maintain integrity to peak exposure.

2. Exhibit shrinkage behavior compatible with moderator graphite.

3. No detrimental interaction between fuel rod matrices and particles.

Successful performance of fuel rods has been demonstrated beyond peak HTGR conditions in accelerated irradiation tests.

A total of 171 pitch-bonded fuel rods fabricated by GA have been irradiated in 16 high-exposure, instrumented, capsule experiments. As shown in Table 7-14, more than 110 of these rods have demonstrated successful performance independent of the particle types combined in the rods (TRISO/BISO, TRISO/TRISO). A number of rods have been designed for failure to study the effects of particle, matrix, and process variables on irradiation performance. The results of these tests provide a firm basis for specifications of fuel rod properties and processes.

Capsule tests most important to demonstrating the high exposure performance of LHTGR (cured-in-place) fuel rods are HRB-4, HRB-5, HRB-6 (Ref. 28), P13Q, P13R, and P13S. The latter three capsules are now undergoing postirradiation examination. However, in-pile fission gas measurements have shown that the fuel performed satisfactorily well beyond expected peak LHTGR fluences. Capsule P13Q was an integral body test of cure-in-place rods containing reference fissile and fertile particles irradiated to a

TABLE 7-13
EVOLUTIONARY CHANGES IN HTGR FUEL ROD FABRICATION PROCESSES

Parameter	Fort St. Vrain	Large HTGR	Purpose of Change
Carbonizing	In packed Al_2O_3 bed	In block	Simplify process
Heat treat	Free standing, 1800°C	In block, 1800°C	Simplify process
Shimming	Particle size - blending	Graphite particles	Simplify process
Binder type	Coal tar pitch (ISV)	Petroleum pitch	Improve uniformity
Filler	Natural flake graphite	Petroleum-derived flake graphite	Improve uniformity

TABLE 7-14
COMPLETED GA IRRADIATION TESTS OF FUEL RODS

Capsule Number	Peak Irradiation Test Conditions		Results	
	Temperature (°C)	Fast Fluence (10^{25} n/m^2)	No. of Rods Tested	No. of Rods Demonstrating Successful Performance[a]
F-25	1150-1300	3.3-4.8	12	10
F-26	1250-1300	5.1-7.0	8	5
F-27	700	3.7-4.0	2	1
	1250-1350	4.8-5.7	5	3
F-28	700-900	1.8-2.5	2	2
	1200-1250	3.2-3.7	4	3
F-29	750	3.4-5.0	2	2
	1200	6.8-7.8	4	0
F-30	1050	5.3-10.6	10	10
	1250	4.1-6.5	3	3
HRB-2[b]	750	4.6-6.2	3	3
	1100	7.5-7.9	2	3
HRB-3[b]	1150	5.9	2	1
HRB-4[b]	1250	4-10.5	6	6
HRB-5[b]	1250	2-4.5	6	6
HRB-6[b]	1250	5-9	6	6
P13M	1050	8.1-8.4	6	6
	1350	2.8-4.8	6	6
P13N	1350	1.6-5.4	16	14
	1560	4.2-4.7	4	2
P13P	1050	5.0-7.5	8	8
	1350	2.5-8.5	13	8
P13R	1075	3.7-12.4	15	(c)
	1300	7.9-9.5	5	(c)
P13S	1075	3.5-12.1	15	(c)
	1500	7.5-9.1	5	(c)
	Successful tests to 1500°C	Successful tests to 10.6 x 10^{25} n/m^2	171	>110[c]

[a] Criteria are good rod integrity and dimensional shrinkage compatible with moderator or graphite.

[b] Excludes ORNL rods (Ref. 28).

[c] All rods irradiated in capsules P13R and P13S were intact and in very good condition; however, results are not included because postirradiation examination is still in progress (Ref. 31).

peak exposure of 9.9×10^{25} n/m^2. It had a low and nearly constant in-pile release (R/B Kr-85m $\sim 1 \times 10^{-6}$) throughout its operation, indicating little or no coated particle failure occurred.

The three HRB capsules (HRB-4, -5, and -6) were the first test of TRISO/BISO fuel rods that were cured in place and that contained isotropic graphite shim particles (Ref. 28). They were irradiated to a peak exposure of 10.5×10^{25} n/m^2 $(E > 0.18 \text{ MeV})_{HTGR}$ at 1250°C. All rods were found to be in excellent condition after irradiation. Dimensional change measurements showed all rods exhibited both radial and axial shrinkage, and the dimensional change profiles were compatible with those of moderator graphite fuel elements. This is an important measure of fuel rod performance since net shrinkage is necessary to avoid mechanical interactions with the moderator block, but excessive shrinkage is undesirable because of its effect on fuel temperatures. Some matrix-coating interactions were observed in these rods as a result of a high matrix binder phase content; however, slight modifications in the matrix composition have eliminated this condition in rods fabricated subsequent to these tests.

The F-30 capsule was the FSV fuel proof test which contained FSV production material and irradiated to about 20% beyond expected peak exposure (Ref. 37). All fuel rods were in very good condition after irradiation and exhibited dimensional changes that were in excellent agreement with model predictions. The excellent irradiation performance of fuel rods in capsule F-30 gives a high degree of confidence in the performance of close-packed TRISO/TRISO fuel rods.

As mentioned in Section 7.1.1, large numbers of fuel rods have been successfully irradiated under representative HTGR conditions in test elements in the Peach Bottom reactor (Ref. 39 and 40). Irradiation data obtained from these tests substantiate the performance predictions based on accelerated capsule tests and provide confidence that satisfactory performance will be exhibited in FSV FTE-1 through FTE-8.

7.4. FISSION PRODUCT AND COOLANT CHEMISTRY

7.4.1. Current Programs

Research and development work on fission product behavior and interactions involving coolant impurities and core materials in the HTGR is presently in progress at GA and ORNL and is described in Ref. 18. This work is directed toward improved prediction of:

1. Circulating and plateout inventories in the primary circuit.

2. Fission product release to the environment under normal and accident conditions.

3. Consequences of steam in-leakage into the primary circuit.

4. Acceptable levels of steam in-leakage under normal and accident conditions.

Other programs which are related to the HTGR chemistry work include:

1. Accident initiation and progression analysis (AIPA) study being carried out be GA under the ERDA sponsorship for a probabilistic assessment of HTGR accidents.

2. Fission product plateout studies on the direct (gas turbine) HTGR program being performed by GA to provide information on fission product plateout and decontamination.

3. HTGR safety studies at ORNL under the ERDA safety program to review fission product and primary coolant technology.

4. HTGR safety program studies at GA directed towards investigation of fission product plateout.

5. Foreign programs including in-pile and out-of-pile integral loop experiments (CPL and SSL) under a cooperative agreement between GA and CEA.

The Fort St. Vrain fission product surveillance program has been included in the HTGR chemistry national program. This program includes the measurement and evaluation of circulating activity in the FSV primary circuit, determination of iodine plateout levels, analysis of coolant impurity levels, and other fission product behavior studies. A cooperative arrangement with PSC is planned for the performance of this work.

The FSV test elements will be an important source of data for verifying fission product diffusion coefficients in graphite, the effect of coolant impurities on the graphite and fuel rods, and the effect of fission product migration on these interactions. The elements will also contribute significantly to the validation of computer codes such as FIPER and RAD used to predict fission product behavior under integral test conditions in an operating HTGR environment.

7.4.2. Oxidation of Graphite Element

The potential effects of steam ingress on the test element materials have been considered extensively in the design of the LHTGR and are discussed in Ref. 8. The near-isotropic graphite has been shown to oxidize in the same manner as H-327 graphite. From studies on H-327, it is estimated that the loss of strength due to 1% burnoff at temperatures above 900°C will be less than 5% in near-isotropic graphite. Work at ORNL has shown that 1% burnoff increases helium permeability of H-327 graphite by only about 10%. Data on permeability changes in H-451 graphite will be obtained.

7.4.3. Hydrolysis of Exposed Fissile Particles

Another chemical reaction affecting the fuel particles is hydrolysis or oxidation of exposed carbide fuel (UC_2). This can occur if oxidant

impurities (H_2O, CO_2, CO) contact the fuel material as a result of coating failure and diffusion or permeation flow through the fuel block graphite. Hydrolysis is expected to increase the steady-state fission gas release (R/B) from particles with failed coatings, and experiments are under way to determine the extent of the increase.

Oxidation of exposed UC_2 can occur via the reactions with CO. The CO reaction is much slower than the reactions involving H_2O or CO_2, and in fact may not occur at all in the reactor, as experience at the Peach Bottom HTGR has shown. In Peach Bottom core 1, large (approximately 80%) failed fuel fractions existed throughout most of the core life. The CO concentration was always 0.5 to 1.0 ppmv, yet virtually no fuel oxidation was observed in the irradiated fuel. Investigation of CO oxidation of carbide fuels at higher CO concentrations is being done.

8. REFERENCES

1. Hudritsch, W. W., et al., "Preirradiation Characterization of Material for the Fort St. Vrain HTGR Core Surveillance Program," General Atomic Report GA-A12455, June 30, 1975.
2. "Fuel Development Program Plan for the Steam-Cycle HTGR," General Atomic, to be published.
3. Wallroth, C. F., "Feasibility Study of the Dragon Reactor for HTGR Fuel Testing," ERDA Report GA-A13333, General Atomic, March 3, 1975.
4. "Test Plan for Fort St. Vrain Test Elements FTE-1 through FTE-8," General Atomic, March 5, 1976, unpublished data.
5. Doll, D. W., "Specifications for Machining FSV Test Element Blocks," General Atomic, April 15, 1976, unpublished data.
6. "HTGR Fuel Specifications," General Atomic, October 14, 1975, unpublished data.
7. "Fuel Design Data Manual," General Atomic, December 17, 1975, unpublished data.
8. "GASSAR-6, General Atomic Standard Safety Analysis Report," February 5, 1975 (NRC Docket STN 50-535), and all current amendments.
9. Harmon, D. P., and C. B. Scott, "Development and Irradiation Performance of LHTGR Fuel," ERDA Report GA-A13173, General Atomic, October 31, 1975.
10. Johnson, W. R., and G. B. Engle, "Properties of Unirradiated Fuel Element Graphites H-451 and TS-1240," ERDA Report GA-A13752, General Atomic, January 31, 1976.
11. Price, R. J., and L. A. Beavan, "Final Report on Graphite Irradiation Test OG-1," ERDA Report GA-A13089, General Atomic, August 1, 1974.
12. Price, R. J., and L. A. Beavan, "Final Report on Graphite Irradiation Test OG-2," ERDA Report GA-A13556, General Atomic, December 15, 1975.

12a. "Revisions to H-327 Design Data," General Atomic unpublished data, July 28, 1976.

13. Engle, G. B., et al., "Development Status of Near-Isotropic Graphites for Large HTGRs," USAEC Report GA-A12944, General Atomic, June 1, 1974.

13a. Merrill, M. H., "Nuclear Design Methods and Experimental Data in Use at Gulf General Atomic," Gulf General Atomic Report Gulf-GA-12652 (GA-LTR-2), July 1973.

14. Shenoy, A. S., and D. W. McEachern, "HTGR Core Thermal Design Methods and Analysis," General Atomic Report GA-A12985, December 31, 1974.

15. Smith, C. L., "FSV Fuel Performance Models for TRISO $(Th/U)C_2$ - TRISO ThC_2 Fuel," General Atomic, May 6, 1975, unpublished data.

16. Smith, C. L., "Fuel Particle Behavior Under Normal and Transient Conditions," ERDA Report GA-A12971, General Atomic, October 1, 1974.

17. Smith, C. L., "Fuel Performance Models for Fuel Particles Proposed for FSV Test Elements FTE-1 and FTE-2," General Atomic, May 27, 1975, unpublished data.

18. Baldwin, N. L., et al., "The Behavior of Fission Product Gases in HTGR Fuel Material," December 1975, unpublished data.

19. Haire, J., "Calculations in Support of Fort St. Vrain FTE-1 through FTE-8," General Atomic, March 1976, unpublished data.

20. Stansfield, O. M., "Summary of WAR Kernel Development Status Meeting June 11, 1975," General Atomic, June 1975, unpublished data.

21. Haire, M. J., and D. W. McEachern, "Gaseous Radioactivity Levels in the Primary Coolant of an HTGR," General Atomic Report GA-A12946, October 1, 1974.

22. Alberstein, D., et al., "Metallic Fission Product Release from the HTGR Core," General Atomic Report GA-A13258, May 15, 1975.

23. Myers, B. F., and W. E. Bell, "Strontium Transport Data for HTGR Systems," USAEC Report GA-A13168, General Atomic, December 6, 1974.

24. Luby, C. S., D. P. Harmon, and W. V. Goeddel, "HTGR Fuel Design and Irradiation Performance," Trans. Am. Nucl. Soc. 13, 580 (1970).

25. "Public Service Company of Colorado 330-MW(e) High-Temperature Gas-Cooled Reactor Research and Development Program - Quarterly Progress Report for Period Ending September 30, 1970," USAEC Report GA-10313, Gulf General Atomic, October 30, 1970.

26. Scott, C. B., and D. P. Harmon, "Postirradiation Examination of Capsule F-30," General Atomic Report GA-A13208, April 1, 1975.

27. Young, C. A., and D. P. Harmon, "Preirradiation Report: Fuel Materials for P13R and P13S Irradiation Capsules," ERDA Report GA-A13026, General Atomic, November 1974.

28. Scott, C. B., and D. P. Harmon, "Postirradiation Examination of Capsules HRB-4, HRB-5, and HRB-6," ERDA Report GA-A13267, General Atomic, November 28, 1975.

29. Johnson, W. R., et al., "Postirradiation Examination of Capsules HT-24 and HT-25," ERDA Report GA-A13486, General Atomic, September 15, 1975.

30. Johnson, W. R., "Thermal Conductivity of Large HTGR Fuel Rods, ERDA Report GA-A12910A, General Atomic, January 1976.

31. "HTGR Fuels and Core Development Program, Quarterly Progress Report for the Period Ending May 31, 1975," ERDA Report GA-A13444, General Atomic, June 30, 1975.

32. "Fort St. Vrain Nuclear Generating Station - Final Safety Analysis Report," Public Service Company of Colorado, Docket No. 50-267.

33. Peroomian, M. B., A. W. Barsell, and J. C. Saeger, "Oxide-3: A Computer Code for Analysis of HTGR Steam or Air Ingress Accidents," General Atomic Report GA-A12493, January 1974.

34. Barsell, A. W., and M. B. Peroomian, "Consequences of Water Ingress into the HTGR Primary Coolant," General Atomic Report GA-A13171, April 15, 1975.

35. Hansen, F. J., et al., "Reference Fissile Particles for Recycle HTGR Fuel Elements," unpublished data.

36. "HTGR Fuels and Core Development Program Quarterly Progress Report for the Period Ending February 29, 1976," ERDA Report GA-A13804, General Atomic, March 31, 1976.

37. Scott, C. B., and D. P. Harmon, "Postirradiation Examination of Capsule F-30," General Atomic Report GA-A13208, April 1, 1975.

38. "HTGR Fuels and Core Development Program Quarterly Progress Report for the Period Ending November 30, 1975," ERDA Report GA-A13737, General Atomic, December 31, 1975.

39. Wallroth, C. F., et al., "Postirradiation Examination of Peach Bottom Fuel Test Element FTE-3," USAEC Report GA-A13004, General Atomic, August 15, 1974.

40. Wallroth, C. F., et al., "Postirradiation Examination of Peach Bottom Fuel Test Element FTE-4," General Atomic, to be published.

9. ACKNOWLEDGMENTS

This report represents a compilation of contributions from many contributors. The following personal contributions highlight the effort which went into this report:

Safety Analysis - G. T. Cramer, A. W. Barsell, D. D. Orvis, and J. P. Walkush.

Performance Analysis - M. J. Haire, A. C. Marshall, G. Reich, B. I. Shamasundar, C. L. Smith, and A. S. Shenoy.

Research and Development - G. B. Engle and O. M. Stansfield.